THE POTENTIAL ROLE OF MEGAKARYOCYTES IN MECHANICALLY MEDIATED BONE ADAPTATION

by

Constance Pagedas Soves

A dissertation submitted in partial fulfillment
of the requirements for the degree of
Doctor of Philosophy
(Biomedical Engineering)
in The University of Michigan
2010

Doctoral Committee:

Professor Steven A. Goldstein, Chair
Professor Paul H. Krebsbach
Professor Russell S. Taichman
Assistant Professor Joshua D. Miller
Assistant Professor Kurt D. Hankenson, University of Pennsylvania

Τίς Θεὸς μέγας, ὡς ὁ Θεὸς ἡμῶν;

σὺ εἶ ὁ Θεός, ὁ ποιῶν θαυμάσια μόνος.

To Xp:

“Some people get squashed crossing the tracks
Some people got high rises on their backs
I'm not broke but you can see the cracks
You can make me perfect again”
-Bono

ACKNOWLEDGEMENTS

In the immortal words of Jerry Garcia, "what a long, strange trip it's been." And long, indeed. And so many people to thank for their help in this journey.

My primary mentor, Steve Goldstein, has always been willing to support (both intellectually and financially) my ventures into an awful lot of unknown territories. Though oftentimes these ended up in months (years?) of heartache and frustration, the lessons learned from these experiences far outweigh any *Nature* paper that could have come from this work. For his support and insights, I am extremely grateful.

I also express my gratitude to the rest of my committee, Josh Miller, Kurt Hankenson, Paul Krebsbach, and Russ Taichman, for their insights and contributions along the way. Their support through this process has been invaluable.

I owe a tremendous amount to my "unofficial" mentors. Josh Miller has been unbelievably generous with his (albeit limited) time and has always been willing to help me, no matter how stupid my question or irrational my carcinogen-related fear (and has introduced me to some kickin' tunes, too). A special thank you as well to Kurt Hankenson, who continues to be a trusted mentor even after becoming a Quaker, and Andrea Alford and Amanda Thornton who have both been my "life/science coaches" through the past few years. I would be remiss not to also acknowledge Richard Hughes who, on the fateful night of April 14, 2000, had convinced me that I had just made a mistake in accepting an offer to attend UC Berkeley for graduate school. It is a decision

that has shaped me in so many ways, and I truly owe so much to him and the support he has given me over the last 8 years.

The graduate experience is so largely shaped by one's colleagues, and I really could not have asked for a better coworkers and friends. From the "oldest" guard (Janet Blumenfeld Goldenstein, Cari Bryant Arnold, Mike Ominsky, Ken Kozloff, Ed Hoffler) to the "old" guard (Sylva Krizan Nagy, Jessica Knowlton, Aaron Weaver, Mike Paschke, Jason "Puffy" Combs, Mike Friedman, Doug Taylor) to the "new" guard I have spent 8 years surrounded by a fantastic group of individuals who have made even the worst possible moments of grad school bearable and, dare I say, fun. There are so many more to acknowledge, but in the interest of conciseness, I will extend a special thanks to Dana Begun, without whom this work would not have been complete and Jaclynn Kreider, who always went above and beyond to lend a hand when needed. Jeff Meganck and Danese Joiner, my "co-defenders", have been a constant source of support and friendship throughout this wacky process, and Erik Waldorff, Riyad Tayim, Ethan Daley, and Jason Long have all been instrumental in helping me keep my head screwed on straight.

I am indebted to the many ORL staff members who were an integral part of this work - John Baker and Rochelle Uptergrove for their histology expertise, Xixi Wang, Sharon Reske, Bonnie Nolan, and Kathy Sweet for their assistance with animal studies, and Charles Roehm and Dennis Kayner for being the "brains and brawn" behind so much of our equipment. Without Anita Reddy and Jake Brunner, the molecular lab is lost. And without technical assistance from Edward Sihler and administrative support from Sharon Vaassen and Peggy Piech, the ORL would implode.

I would also like to acknowledge those outside of the lab who have provided

technical assistance. Laurie McCauley and her post-docs, Xin Li and Flavia Pirih, have provided critical resources (namely the GATA-1^{low} mice and K562 cells) and invaluable guidance. Joe Washburn at the University of Michigan Microarray Core facility has been extremely helpful in my struggles dealing with degraded RNA.

Of course, none of this would have been possible without funding from an NSF Graduate Research Fellowship, the Regenerative Sciences Training Grant (NIH-T90 DK070071), and a grant from the NIH (R01-AR051504).

And last, but certainly not least, I must acknowledge those in my personal life who have been unconditionally loving and supportive throughout this whole process. During 8 years, I have leaned upon and gained so much from the "families" I've acquired in Ann Arbor - St. Catherine's, OCF, the UMS Choral Union, the Screaming Banshees, all of whom have made my tenure as a graduate student so colorful. I am forever indebted to Vasiliki Stamoulis for keeping my life full of Vitamins L and P. My mother-in-law Eleanora Soves has been a constant source of encouragement. My parents, Tom and Elaine Pagedas, and siblings Elizabeth and Michael – at the risk of sounding like a clichéd Academy Award acceptance speech, I just couldn't have gotten through this without them (and Sprint's unlimited nights and weekends plan). And of course, my husband, Chris, has put up with an exceptional amount over the last few years and has constantly given me the strength to persevere. I just hope I'll remember what he looks like when I actually see him again.

TABLE OF CONTENTS

LIST OF FIGURES

LIST OF TABLES

LIST OF ABBREVIATIONS

β2m	Beta-2-microglobulin
BFR	Bone formation rate
BSP	Bone sialoprotein
BV/TV	Bone volume fraction
ImP	Intramedullary pressure
MAR	Mineral apposition rate
MGDF	Megakaryocyte growth and development factor
MK	Megakaryocyte
MS/BS	Mineralizing surface per total bone surface
MSC	Mesenchymal stem cell
OCN	Osteocalcin
Osx	Osterix
PMA	Phorbol 12-myristate 13-acetate
Tb.N.	Trabecular number
Tb.Sp.	Trabecular spacing
Tb.Th.	Trabecular thickness
TMD	Tissue mineral density
TPO	Thrombopoietin
UT	Untouched
WT	Wild-type

ABSTRACT

Maintenance of bone mass and geometry is heavily dependent upon mechanical stimuli. Current paradigms suggest that osteocytes embedded within the mineralized matrix and osteoblasts on the bone surfaces are the primary responders to physical forces. However, other cells within the marrow cavity are also subject to a mechanically active environment. Megakaryocytes (MKs), cells which produce platelets, may physiologically be exposed to fluid shear forces. Recent studies have highlighted the potent effects MKs have on osteoblast proliferation as well as bone formation *in vivo*. We hypothesize that MKs are capable of responding to physical forces and that the interactions between these cells and osteoblasts can be influenced by mechanical stimulation.

We have demonstrated that two MK cell lines respond to fluid shear stress in culture. Furthermore, we isolated MKs from histologic sections of murine tibiae that were exposed to compressive loads *in vivo* using laser capture microdissection. C-fos, a transcription factor shown to be upregulated in response to load in various tissue types, was increased in MKs from loaded relative to non-loaded limbs at a level comparable to that of osteocytes from the same limbs.

To assess the functional outcomes of this mechanoresponsiveness, we first set out to determine whether animals with elevated numbers of MKs demonstrated altered adaptation to mechanical loading. GATA-1^{low} mice, a transgenic mouse model with

arrested MK maturation leading to an elevated number of immature MKs within the marrow, were shown to have a minimally altered response to load compared to wild-type littermates. Mice injected with thrombopoietin, a potent inducer of MK proliferation and differentiation, showed no difference in response to load compared with vehicle-injected mice.

Finally, we developed a co-culture system to address whether mechanical stimulation of MKs in culture would impact osteoblast proliferation and differentiation. The presence of MKs in culture, but not conditioned media, has dramatic effects on osteoblast proliferation. Our data suggests a minimal, but non-significant, decrease in proliferation as well as an increase in mineralization capacity of osteoblasts co-cultured with MKs exposed to shear compared to co-cultures with unstimulated MKs. Further studies are necessary to investigate the mechanism driving this phenomenon.

CHAPTER I

INTRODUCTION

The regulation of the skeletal system is heavily dependent on mechanical cues. This has been hypothesized since the mid-1800's when German scientists observed that trabecular bone within the femoral head appeared to be oriented in the direction of stress trajectories. These observations led to Wolff's Law, which states that bone architecture adapts to accommodate changes in externally applied physical forces. Over time, the basic concept of "form follows function" has been supported by numerous *in vivo* studies which have demonstrated an adaptive response of bone to applied forces (1-5).

Mechanotransduction in Bone

Most investigations of mechanotransduction, or the cellular conversion of mechanical information to biochemical signaling, have focused primarily on osteocytes, bone cells which are embedded in mature matrix, and osteoblasts, or bone forming cells. Osteocytes are thought to be key players in bone mechanotransduction because of their strategic location within the bone matrix. These cells are housed in lacunae, small cavities within the mineralized matrix, which are connected to one another by a network

of canaliculi. This so-called "lacuno-canalicular network" is filled with interstitial fluid which flows through the system when the surrounding matrix deforms. Thus the osteocytes are prime targets for being subjected to fluid shear. *In vitro* studies have demonstrated osteocyte-like cell lines to be mechanoresponsive (6-8). *In vivo* systems have also been developed to characterize the mechanical environment of osteocytes in living tissue (9), however very limited *in vivo* data exists to support the role of these cells in mechanical adaptation. Perhaps some of the most compelling evidence stems from a mouse model in which osteocytes are selectively ablated by driving expression of diphtheria toxin receptor off of a promoter encoding DMP-1, a gene that is highly expressed in osteocytes but not expressed in less mature osteoblasts. With the administration of diphtheria toxin, the osteocytes apoptose and, importantly, these mice are resistant to bone loss associated with hindlimb-unloading (10).

Osteoblasts reside on bone surfaces and secrete matrix proteins, including type I collagen. Their attachment to the extracellular matrix via integrins make them likely candidates for being able to sense changes in matrix strain and convert mechanical cues into a cellular response through their integrin connections. Furthermore, they are also exposed to the marrow cavity, a pressurized, fluid-filled environment which might impart other types of load on these cells. *In vitro* experiments have demonstrated that osteoblastic cell lines have been shown to be responsive to hydrostatic pressure, biaxial strain, and fluid shear (11-14).

Mechanical Environment of the Marrow Cavity

Though osteocytes and osteoblasts are ideally situated for exposure to a variety of physical forces, there are several other cell types within bone that could be subject to mechanical perturbations as well. The marrow cavity itself is pressurized (~3 kPa) due to downstream venous resistance (15). Studies in sheep tibia reveal that impact loads of up to 2 kN yield increases in marrow pressures of between 15 kPa in the epiphysis, 35 kPa in the metaphysis, and 40 kPa in the diaphysis (16). Similar experiments in the human radius demonstrate a 280 kPa increase in pressure for the same applied load (17). Other researchers have calculated roughly 15 kPa increases in pressure within a pig mandible upon masseter contraction (18). Externally applied loads transverse to the knee were shown to elicit detectable, though small, changes in ImP within the femoral cavity (19).

The potent anabolic effects of intramedullary pressure (ImP) variations have been proven through the use of an *in vivo* system which allows ImP to be experimentally controlled within a functionally-isolated turkey ulna. Qin, et al. demonstrated that imposing low magnitude (~8 kPa), high frequency oscillatory pressures not only prevented disuse-associated bone loss but also led to an 18% increase in cortical bone formation compared to the contralateral control (20). These changes in ImP can also be driven by muscular contraction, and can lead to prevention of disuse osteopenia in the trabecular compartment as well (21). Other models of alterations in ImP have elicited similar results. Increase in venous pressure by use of venous tourniquets can lead to increase in periosteal bone formation (22).

Venous ligation has been shown to not only prevent disuse-associated bone loss but can engender an increase in bone mass in hindlimb suspended animals (23).

Blood flow is another important component to the complex mechanical environment of the marrow cavity. Studies in anesthetized dogs using radiolabelled microspheres as tracers in blood flow demonstrate that approximately 11% of the total cardiac output is directed to the skeleton (24). Medullary blood flow can be directly increased by muscular stimulation (25). Reported changes in blood flow as a result of exercise, however, are less striking. Though blood flow to musculature increases significantly in treadmill running dogs, the blood flow in bone does not change significantly. However, the vascular resistance within bone increases dramatically as a result of exercise (24). In another canine study, the blood flow to cortical bone was calculated to increase by 60% following 1 hour of treadmill running. A non-statistically significant increase was also noted in blood flow to cancellous bone as well (26).

The marrow itself is also a fluid, with a calculated viscosity of approximately $67x10^{-3}$ Pa-s, approximately 10 times the viscosity of water (17). Though difficult to determine experimentally, it is possible that marrow fluid flow can be altered with mechanical stimulus. Computationally, marrow viscosity has been shown to be a critical factor in the shear stresses that develop within vertebral trabecular bone subject to high frequency vibrations (27).

Mechanosensors in the Marrow?

Preliminary findings using a unique *in vivo* model of mechanically stimulated bone regeneration in our laboratory demonstrated that phosphorylation of focal adhesion kinase, a key regulator in the integrin-mediated signaling pathway, was primarily localized in the marrow compartment as evidenced by immunohistochemistry (28). This might indicate that cells responsive to controlled mechanical loading may reside within the marrow cavity. Consequently, micro-computed tomography voxel-based finite element models were developed to compare the local mechanical environments of regenerating and well-connected bone. The results highlighted the drastic differences in the marrow environment, as expressed in terms of strain energy density and principal strains, with changes in bone architecture and morphology and suggested that it was feasible that cells within the marrow may experience sufficient load to elicit a mechanically-mediated response (29). However, there is limited understanding of which cells within the marrow might be responsive to these stimuli, as well as whether or not they may impact the global adaptive response to load.

The orthopaedic community has recently begun to expand studies of mechanotransduction to include marrow stromal cells (MSCs), the marrow-derived bone precursor cells. This line of study has evolved from early findings that marrow stromal cells from animal models of disuse have reduced osteogenic capacity compared to the cells from weight-bearing animals. Keila, et al. isolated adherent marrow cells from unloaded hindlimbs of rats and demonstrated these cells lead to a decrease in number of "bone-like" nodules formed compared to weight-bearing

counterparts and speculated that the unloading causes a decrease in number of osteoprogenitor cells (30). Machwate, et al. demonstrated that the number of MSC that express alkaline phosphatase, a common marker of bone formation, decreases with unloading (31). Various groups have thus tried to determine the specific effects of load on MSC behavior. It has been shown that subjecting MSC to oscillatory fluid shear increases the proliferation capacity of these cells (32), and furthermore they, like osteocytes and osteoblasts, respond to shear via intracellular calcium signaling and phophorylation of ERK (32,33). Rubin, et al. further showed that MSCs subject to strain decrease their production of RANKL, a factor required for the differentiation of osteoclasts, or bone resorbing cells (34).

In addition, osteoclasts have been shown to respond to physical stimuli directly. The expression of carbonic anhydrase II, a metalloprotease that is critical to the cells' resorptive function, is attenuated in mature osteoclasts subject to fluid shear (35). Osteoclast precursors have also been shown to respond to fluid shear stresses in a similar manner as other mechanosenstive cells, namely through the production of nitric oxide and prostaglandin E2 (36).

Though often not addressed in orthopaedic literature, various other cell types found in the marrow cavity have also been shown to be mechanoresponsive. Deformation of neutrophils enhanced expression of CD11b/CD18, an adhesion molecule that allows these cells to adhere to vascular walls via intercellular adhesion molecule-1 (ICAM-1) (37). Similarly, the expression of adhesion molecules in monocytes, neutrophils, and hematopoietic stem cells increases in response to flow (38-40).

The role of "accessory" cells

Studies have begun to highlight the importance of communication between bone-related cells and cells within the marrow milieu. The role of osteoblasts in the regulation of the hematopoietic environment has been studied extensively (41,42). Reciprocal relationships also exist, indicating that these so-called accessory cells have the potential to impact bone formation and maintenance. For instance, osteoprogenitor cells, when cultured with accessory non-adherent cells (and similarly with the conditioned media of the non-adherent cells), demonstrate enhanced osteogenic potential (43,44). Eipers, et al. further isolated a sub-population of marrow cells that enhance the osteogenic capacity of bone precursor cells (45).

This milieu of accessory cells is comprised of a variety of cell types. However, recent studies have begun to specifically investigate the effects that megakaryocytes (MKs), most commonly thought of in the context of platelet production, can exert on bone-lineage cell behavior. Some of the earliest studies targeting these roles for MKs stemmed from observations that patients suffering from myelofibrosis, or development of fibrous tissue within the bone marrow cavity, demonstrated abnormally high numbers of MKs in bone marrow samples (46). In conjunction with this clinical findings, *in vitro* experiments have highlighted the interactions between MKs and stromal fibroblasts - namely that the secretion of platelet-derived growth factor (PDGF) and transforming growth factor-β (TGF-β) by MKs induces fibroblast proliferation as well as secretion of collagen and fibronectin (47,48). Furthermore, these interactions between MKs and fibroblasts require cell-

cell contact, mediated by α5β1 integrin engagement (48,49). Additionally, MKs express c-kit, a surface receptor for stem cell factor (SCF) which is expressed by marrow stromal fibroblasts. This interaction also induces fibroblast proliferation (50).

Though MK-stromal fibroblast interactions have been well-documented, other studies have begun to implicate more specific roles of MKs in bone maintenance. Supporting evidence for the potential impact of MKs on bone arose from studies of myelofibrosis patients who typically demonstrated osteosclerosis (or abnormal hardening) of trabecular tissue. This implies some defect in bone resorption, which would allow for new, less mineralized bone to replace the excessively mineralized tissue. This could in part be a result of elevated MK levels, which have been shown to express osteoprotegerin, a soluble protein which inhibits osteoclastogenesis (51). Wakikawa, et al. also observed that bone marrow culture treated with thrombopoietin (TPO), a known stimulator of megakaryocytopoiesis, demonstrated decreases in the numbers of TRAP+- multinucleated cells, reflecting a decrease in osteoclast number (52). This phenomenon was enhanced by the presence of MK-secreted factors, PDGF and TGF- β. The most direct evidence has been established by both Beeton, et al. (53) and Kacena, et al. (54) who independently determined that the addition of MKs to pre-osteoclast culture has inhibitory effects on osteoclast formation. Furthermore, the presence of MKs can also impair the bone-resorbing function of osteoclasts (53).

Not only are MKs suspected as having a role in inhibiting bone resorption, but have also been shown to positively impact bone formation as well. Some of the most compelling *in vivo* evidence is demonstrated through two transgenic mouse models,

each lacking a transcription factor (NF-E2, GATA-1) necessary for full MK maturation, and resulting in the accumulation of immature MKs in the marrow. With time, both strains of mice develop a dramatically high bone mass phenotype (55). Furthermore, in culture conditions, osteoblast proliferation is enhanced by the presence of MKs, but this result is dependent upon cell-cell contact. In addition, this communication may be mediated by gap junctions (56). Another study by Miao, et al. demonstrates that the presence of MKs greatly enhances MSC ability to form colonies and express alkaline phosphatase in culture (57).

MKs also express proteins that could have implications for bone matrix production. Estrogen treatment, known to initiate anabolic effects in postmenopausal women, has been shown to lead to increased numbers of MKs within marrow (58,59). Bord, et al. also demonstrated basal expression of estrogen receptors α and β in MKs, and confirmed expression of TGF-β family members, which are known to impact osteoblast development (60). MKs also express BMP-2, BMP-4, and BMP-6 (61). They have been shown to secrete matrix proteins, including osteonectin (62), and are also the only cell type not directly associated with bone that expresses osteocalcin (63). Studies have also demonstrated that factor XIII, secreted by MKs and commonly thought of as the crosslinker of fibrin clots during blood coagulation, may also play a role in the crosslinking of bone matrix proteins, including osteonectin, osteopontin, and fibronectin (64). Though the mechanism by which MKs might impact bone remodeling is ill-defined, it is apparent that the function of MKs extends beyond platelet formation and has potent effects on cells that directly regulate bone

homeostasis. The question remains as to whether or not these interactions can be mediated by the presence of load.

Mechanical Environment of MKs

The location of megakaryocytes within the marrow, and subsequently the mechanical cues that they my be subject to physiologically, depends upon the differentiation state of the cell. Hematopoietic stem cells, from which MKs are derived, reside at osteoblast surfaces (41,65). Immature MKs are localized to the marrow stroma, however mature MKs are most frequently observed at the abluminal aspect of sinusoids (66). The spatial distribution could in part be regulated by chemokine signaling. MKs at all stages of differentiation express CXCR4, a cell-surface receptor that interacts directly with SDF-1, produced by osteoblasts and stromal cells (67). Interestingly, however, there is evidence that mature MKs and platelets have a diminished response to SDF-1 in chemotactic assays compared to immature MKs (68). This suggests a possible role for SDF-1 in the retention of immature MKs in the marrow stroma, while allowing mature MKs to migrate to the vasculature, where platelets will subsequently be released.

Adhesion and fluid shear on MKs are potentially complex regulators of cell function. The adhesion of MKs to the extracellular matrix within marrow can have dramatic effects on cell behavior, but these effects also depend greatly on the differentiation state of the cell as well as the matrix protein with which these cells are in contact. Early MK precursors are primarily found in the adherent population of hematopoietic stem cells, but the adherence of these precursor cells also impairs their

capacity to differentiate (69). Plating mature MK, however, onto extracellular matrix-coated substrates can lead to the spontaneous formation of proplatelets. Importantly, this effect is only seen when cells are plated onto fibrinogen, laminin, and von Willebrand factor, but not on collagen (70). Similarly, by blocking α4 integrin, which engages fibronectin, thrombopoietin-induced MK differentiation is attenuated (71). The adhesion of MKs to collagen I, found predominantly in bone and in the endosteal regions of marrow but absent on vascular walls (72), has been shown to inhibit proplatelet formation (73).

The understanding of how these cells respond to fluid shear is still limited. Eldor, et al. demonstrated that, like other marrow constituents, MKs will adhere more readily to an ECM-coated slide in the presence of shear than in quiescent conditions (74). De Bruyn, et al. similarly demonstrated that, under turbulent fluid conditions, Rap1 (a small GTPase) is activated, which facilitates the adhesion of MKs to fibrinogen via aIIbb3 integrin (75). Mature MKs in contact with sinus endothelial cells are exposed to low but constant levels of shear from blood flow, estimated to be approximately 0.13-0.41 Pa (76). Shear forces on these mature cells in contact with collagen-IV-rich vascular matrix are thought to trigger the formation of platelets (76,77).

Global Hypothesis

Based on these observations, we hypothesize that megakaryocytes (MKs) respond to the mechanical environment induced by physiologic loading of bone and,

furthermore, this response can impact the downstream effects that MKs can have on bone homeostasis.

Chapter Overview

Chapter 2 will describe our efforts to assess the responsiveness of MKs to controlled mechanical stimuli both in culture as well as in an *in vivo* model. Subsequently, we will address the functional implications of MK mechanosensitivity. In chapter 3, we will study the long-term adaptation of two mouse models with elevated numbers of MKs. Chapter 4 will specifically address whether physical stimulation of MKs in culture can directly impact their effects on osteoblast proliferation and differentiation.

CHAPTER II

ASSESSMENT OF MEGAKARYOCYTE MECHANORESPONSIVENESS *IN VITRO* AND *IN VIVO*

Introduction

Few studies have specifically addressed the mechanoresponsiveness of MKs. The primary findings have elucidated that mechanically stimulating MKs enhances their adhesion to different extracellular matrix substrates (74,75) and can also trigger the formation of platelets (76,77). Several limitations to these studies exist, namely that they have only been conducted in culture conditions, and the models of mechanical stimulation are not well-controlled. In one model of "turbulence", MKs were "mixed gently, i.e. five times up and down" as a means of applying force (75). Another study stimulated cells by "[agitation] in an environmental shaker at 50 rpm" (76). Furthermore, there has been no consideration that the response of these cells to mechanical cues may have some impact on their potent interactions with bone-lineage cells. In an effort to address this, we set out to establish both well-controlled *in vitro* and *in vivo* models of mechanical stimulation of MKs.

Models of mechanical stimulation in vitro

Numerous *in vitro* systems have been developed to characterize cellular response to applied physical force, including the application of strain by seeding cells on a deformable substrate (78), subjecting cells to hydrostatic pressure (79), or shear through a parallel plate flow chamber (80). Previously in our lab, devices have been custom-built to impart each of these forces independently on cells in culture. Based on the likely forces generated within the marrow cavity as described earlier, fluid shear and hydrostatic pressure would be the most likely physiologically relevant forces for marrow-derived cells.

Though a variety of genes are differentially expressed in the presence of load, these studies will focus on a few commonly utilized markers of a so-called "mechanoresponse". C-fos, a critical transcription factor in the AP-1 pathway, has been shown to be upregulated in various systems, including bone-lineage cells *in vitro* (81-83) and *in vivo* (7,84) in response to physical stimuli. Osteoblastic and osteocytic cell lines exposed to fluid shear also demonstrate increases in expression of cyclooxygenase-2 (cox-2), a key component in the synthesis of prostaglandin (82,85,86).

Models of mechanical adaptation in vivo

Several models have also been developed to assess effects of mechanical stimulation on long bones. One of the most common and perhaps best characterized is by axial loading of the ulna (2,87). Because of the natural curvature of the ulna, applying axial loads leads to bone bending, thus generating both tensile and compressive forces in the lateral and medial aspects, respectively (2). The adaptive response in this model is restricted to the periosteal regions where new bone formation is predominantly observed (2,88).

Similar devices have been developed to apply axial compression to tibiae as well. These models demonstrate a similar anabolic effect in response to applied physical stimuli, however, unlike the ulnar loading model, they also elicit changes in trabecular architecture in addition to cortical adaptation. Fritton, et al. demonstrated a modest increase in both bone volume fraction and mineral content in tibiae subject to axial loads generating 800 με relative to contralateral, non-loaded controls (89). Data from the same group suggests that tibiae exposed to 1200 με have a much more robust response in trabecular and mid-diaphyseal cortical parameters (90,91). DeSouza, et al. importantly demonstrated the age dependence on the tibial response to applied axial loads. Though there were increases in trabecular morphologic parameters in loaded compared to non-loaded tibiae in 8 wk animals, the same loading conditions engendered decreases in these same values in 12 and 20 wk animals (92).

Based on the intramedullary response historically noted in this model, we chose to develop a tibial loading model in order to assess whether cells within the marrow cavity,

namely MKs, respond to mechanical stimulation in a similar manner as "known" mechanoresponders, such as osteocytes.

Methods

Cell Culture

Two separate megakaryocytic cell lines were studied – the Meg-01 megakaryoblastic cell line and the K562 erythromyeloblastic progenitor cell line differentiated to mature megakaryocytes by treatment with phorbol 12-myristate 13-acetate (PMA). Meg-01 cells (ATCC; Manassas, VA) were maintained in RPMI + 10% fetal bovine serum + 1% Penicillin-Streptomycin. K562 cells (a kind gift from Dr. Laurie McCauley) were grown in IMDM + 10% fetal bovine serum + 1% Penicillin-Streptomycin. To induce cells down a megakaryocytic lineage, K562 cells were cultured in the presence of 10 nM PMA (Sigma-Aldrich; St. Louis, MO) for 3 days prior to utilization in fluid shear experiments.

Hydrostatic pressure

35 mm tissue culture plates were coated with 0.1% gelatin (Sigma-Aldrich; St. Louis, MO) for 1h at room temperature and subsequently rinsed in PBS and DMEM. Meg-01 cells were plated at a density of 750,00 cells/plate in DMEM + 10% fetal bovine serum + 1% Penicillin-Streptomycin. After 24 h in culture, the media was changed to serum-free conditions for approximately 16 hours. Plates were inserted into a custom-made device (Figure 2.1a) described previously (93). Chambers were connected to a compressed air source and controlled pressures of 5 or 10 psi were imparted by control of

a custom-written LabView (National Instruments; Austin, TX) program for 30, 60, or 90 minutes. Parallel plates were also harvested untouched, or placed into the chambers for equivalent times to assess handling effects of plates (termed chamber controls). Each condition was run in duplicate for each timepoint.

Preparation of Culture Plates for Fluid Shear

All fluid shear protocols and devices were based on work previously established in our laboratory (93). Glass slides were washed sequentially in 20% sulfuric acid, tap water, and 0.1M sodium hydroxide. After rinsing in ethanol, slides were exposed to 2% γ-aminopropyltriethoxysilane followed by an incubation in 0.25% gluteraldehyde. Cast silicone chambers coated with an adhesive sealant were pressed onto the covalently modified slides, creating a sealed well to allow cells seeded on the slide to be cultured until ready to load. For Meg-01 cells, plates were coated with 0.1% gelatin (Sigma-Aldrich; St. Louis, MO) for 1 h at room temperature. For K562 cells, slides were incubated with 5 $\mu g/cm^2$ fibronectin (Sigma-Aldrich; St. Louis, MO) in a sodium-bicarbonate solution for 3 h at room temperature. Following substrate coating, plates were rinsed with PBS and serum-free media, and cells were then seeded at a density of 1 x 10^6 cells/plate in DMEM + 10% fetal bovine serum + 1% Penicillin-Streptomycin. After 24 h in culture, the media was changed to serum-free conditions for approximately 16 hours.

Fluid Shear Loading

Silicone chambers were removed from the plate seeded with cells and the plates were inserted into parallel plate flow chambers (Figure 2.1b). Teflon lines connected the chambers to media-filled syringes that were attached to a motor-controlled linear slide. Custom-written computer programs controlled motor movement and three separate flow rates were chosen to engender three different magnitudes of shear stress, 0.5, 1, or 2 Pa based on the equation describing laminar flow between parallel plates, $\tau = \frac{6\mu Q}{bh^2}$ where τ = shear stress [Pa], μ = media viscosity [Pa *s], Q = flow rate [cm^3/s], b = channel width [cm], and h = channel height [cm]. Untouched (UT) samples were also harvested, as well as sham controls, which were inserted and immediately removed from the chambers and allowed to sit in the incubator unsheared for 30 minutes.

RNA extraction, Reverse transcription and PCR

Immediately following treatment, cells were rinsed with PBS and lysed in Buffer RLT (Qiagen; Valencia, CA) + β-mercaptoethanol, homogenized using Qiashredder columns, and stored at -70° C until further processing. RNA was isolated using the RNeasy kit (Qiagen; Valencia, CA) according to the manufacturer's instructions. RNA was quantified and 0.5 -1 μg of RNA was reverse transcribed using Superscript III reverse transcriptase and primed by random hexamers. For a given experiment, the same amount of RNA was reverse transcribed across all groups. Real-time PCR was performed and amplification of gene products was determined by the incorporation of SYBR Green fluorescent nucleic acid stain (Invitrogen; Carlsbad, CA). 18s rRNA was chosen as an internal control based on its common use as an control in *in vitro* (94) and *in*

vivo (95) loading studies. Normalized changes in expression of c-fos and cox-2 in response to load relative to untouched controls were calculated using the ΔΔc(t) method (96). All primer sequences are reported in Table 1. Data is expressed in terms of mean ± SD values from four (Meg-01) or two (K562) independent experiments and samples of similar treatments were run in duplicate (Meg-01) or triplicate (K562).

Tibial loading model

A model for application of axial compressive load on a mouse tibia was developed based on previous studies (89,92). The tibia was confined between a platen machined to accommodate the foot and a cup to apply load directly through the knee (Figure 2.2). This cup was attached to a cantilever beam which in turn was attached to a motor-controlled linear slide. The motor was driven by a feedback signal from a strain gauge affixed to the cantilever beam and calibrated such that known amounts of force applied to the end of the beam corresponded with known voltages from the strain gauge.

Strain gauging

In order to determine the amount of force needed to elicit peak physiologic strain of approximately 2000 με (97), strain gauges were affixed to the medial aspect of the mid-shaft of six tibiae from four 8-wk C57Bl6 male mice. The surface of the bone was gently scraped to remove the periosteum, and the surface cleaned with acetone and 100% ethanol. The bone was treated with Catalyst-C (Vishay; Malvern, PA) and strain gauge (#EA-06-015DJ-120) attached with M-bond 200 adhesive (Vishay; Malvern, PA). Data was acquired using LabView (National Instruments; Austin, TX).

In vivo loading

The right tibia of 8-week-old male C57Bl6 mice from a colony maintained in-house was subject to axial loading for 10 minutes at a frequency of 4 Hz and peak load of approximately 9N, corresponding to roughly 2000 με from strain gauging data (Figure 2.3). Animals were euthanized either 30 (n=5) or 60 (n=5) minutes following the completion of load. These times were selected based on studies demonstrating maximal increase in c-fos expression in osteocytes in response to applied mechanical stimulation *in vivo* (84,98).

Tissue Processing and Histology

Loaded tibiae, along with their non-loaded contralateral control, were harvested and decalcified in 20% EDTA in RNase-free water for 2 days at 4°C. Specimens were rinsed in RNase-free water and subsequently fixed in methacarn, a fixative composed of 60% methanol, 30% chloroform, and 10% acetic acid. These processing conditions were based on previously published work on techniques for processing bone in preparation for laser capture microdissection (99) as well as preliminary studies conducted to confirm that RNA integrity was optimally preserved when tissue was fixed following decalcification (data not shown). Following fixation, specimens were rinsed in 100% ethanol and cryopreserved in 30% sucrose in PBS at 4°C overnight prior to embedding in Tissue-Tek OCT (Sakura Finetek; Torrance, CA). Blocks were frozen by placing them on an aluminum block super-cooled in liquid nitrogen and stored at -70°C until sectioned.

Cryosectioning was performed in a Hacker-Bright OTF cryostat. Blocks were placed in the cryostat approximately 30 minutes prior to sectioning to allow them to equilibrate to the chamber temperature of -20° C. Sections were cut using a tungsten carbide blade and mounted onto a PEN Membrane Glass Slide (Molecular Devices; Sunnyvale, CA) and stored at -70° C until needed. Slides were stained using the HistoGene Staining Kit (Molecular Devices; Sunnyvale, CA) according to the manufacturer's protocol. Special care was taken to use RNAse-free reagents when staining slides. Following dehydration in xylenes, slides were air-dried and taken directly to be microdissected.

Laser Capture Microdissection

Microdissection was performed using an Arcturus Veritas system (Molecular Devices; Sunnyvale, CA). In brief, a CapSure Macro LCM cap (Molecular Devices; Sunnyvale, CA) for osteocytes or a CapSure HS LCM cap for MKs coated with a thin "transfer film" was placed above a given region of interest. A UV cutting laser was utilized to trace the region, be it areas of bone encompassing primarily osteocytes or individual MKs. An infrared laser was then pulsed through the cap, melting the transfer film onto the cells of interest, thereby bonding the cells to the cap. The cap was directly visualized to confirm the completeness of the capture. In the event that extraneous material was captured onto the cap, it was removed from the cap by ablating the material with the cutting laser, or else carefully removed using a Post-it™ note (3M; St. Paul, MN). For osteocytes, regions of cortical bone encompassing approximately 2500 cells from the metaphyseal region were captured across two serial slides from a given limb.

One hundred MKs, selected based on their unique morphology (Figure 2.4a), were captured from two serial slides from a given limb. Individual cells were captured with relatively little excess material (Figure 2.4b). MKs were only captured from four animals harvested 30 minutes following loading. Following capture, either 10 μl (for MKs) or 50 μl (for osteocytes) of Extraction Buffer (Molecular Devices; Sunnyvale, CA) was added directly to the surface of the cap and incubated at 42° C for 30 minutes. The caps were then centrifuged at 800 x g for 2 minutes to collect cell lysate, and samples were then stored at -70° C until further processing.

RNA extraction, Reverse transcription and PCR

RNA was extracted using the PicoPure Extraction Kit (Molecular Devices; Sunnyvale, CA) based on the manufacturer's protocol. Following RNA elution, 9.5 μl of RNA was reverse transcribed using Superscript III reverse transcriptase and primed by random hexamers. In order to assess the quality of the captured RNA, 2 μl of extracted RNA was also analyzed on an Agilent Bioanalyzer 2100 (Agilent; Santa Clara, CA) with assistance from the University of Michgian Microarray Core Facility. Real-time PCR was performed and amplification of gene products was determined by the incorporation of SYBR Green fluorescent nucleic acid stain (Invitrogen; Carlsbad, CA). Beta-2-microglobulin (β2m) was chosen as an internal control based on evidence that it also serves as a reliable control for *in vivo* mechanical stimulation studies (100). Normalized changes in expression c-fos response to β2m were calculated using the ΔΔc(t) method (96). To ensure that we were able to isolate individual cell types and differentiate between tissue types, regions of bone and marrow were also isolated from sections and

expression of DMP1, an osteocyte specific gene, was measured. All primer sequences are reported in Table 2.

Statistics

For gene expression studies in cell culture experiments, a one-way ANOVA with a Tukey's test post-hoc was used to determine statistical significance across groups. For *in vivo* loading studies, a Student's t-test was performed to compare changes in loaded vs. non-loaded gene expression for a given cell type. In both cases, statistical significance was determined as $p < 0.05$.

Results

In vitro studies

Meg-01 cells subject to 5 psi or 10 psi hydrostatic pressure for 30, 60, or 90 minutes demonstrated no significant changes in c-fos or cox-2 expression relative to untouched or chamber controls (Figure 2.5). In the presence of fluid shear, however, Meg-01 display a robust response after 30 minutes of shear in terms of changes in c-fos expression relative to 18s rRNA (Figure 2.6a). The increase in c-fos expression when subject to 0.5 Pa is similar to the baseline effects of mechanical perturbation as evidenced by the sham control. However, in both 1 Pa or 2 Pa shear, there is a statistically significant ($p < 0.05$) increase in c-fos expression relative to both UT and sham-treated control. Meg-01 exposed to 1 Pa or 2 Pa fluid shear stress also demonstrate significantly higher expression of cox-2 relative to UT controls, but not significantly higher than sham-treated baseline controls (Figure 2.6b).

In addition to qualitative morphologic confirmation that PMA was driving the undifferentiated K562 cell-line down a megakaryocyte lineage, we assessed levels of CD61, an integrin specific to megakaryocytes and platelets. We detected 170-fold increase in CD61 relative to 18s rRNA in PMA-treated K562 cells relative to non-treated cells (Figure 2.7). C-fos expression is enhanced with fluid shear in all shear stress conditions compared to the UT control, but not significantly elevated relative to sham-treatment (Figure 2.8a). Only cells exposed to 0.5 Pa display a statistically significant increase in c-fos expression compared to sham-treated baseline controls. Cells exposed to 0.5 or 2 Pa fluid shear stress demonstrate significantly greater expression of cox-2 relative to 18s rRNA when compared to UT controls, but not statistically different from sham treated controls (Figure 2.8b).

In vivo studies

We confirmed that populations of cells from cortical bone express DMP1 at significantly higher levels than cells from regions of bone marrow (Figure 2.9). In tibiae harvested 30 minutes following one bout of loading, c-fos expression normalized to β2m is upregulated approximately 2.8-fold in osteocytes from loaded bones relative to non-loaded contralateral controls (Figure 2.10). This response is attenuated in tibiae harvested 60 minutes following load, in which c-fos expression is only 1.9-fold higher in loaded relative to non-loaded limbs. A load-response was also confirmed in MKs captured from bones harvested 30 minutes following load. C-fos in this cell population was upregulated approximately 3.1-fold in loaded relative to non-loaded tibiae.

Discussion

In vitro studies

The results presented here demonstrate that megakaryocytes respond to physical stimuli both in culture conditions as well as in an *in vivo* context, namely as evidenced by changes in expression of the mechanoresponsive gene, c-fos. Interestingly, Meg-01 cells did not respond to hydrostatic pressure, a factor they are likely subject to physiologically. However, previous studies using this device also determined that other cells, specifically MC3T3 pre-osteoblasts, did not respond to this loading modality in the absence of other cytokines such as IL-1 (93). Therefore, though the lack of response may be indicative of a true lack of mechanoresponse to hydrostatic pressure, it also calls to question the efficacy of this particular *in vitro* loading device.

The magnitude of this mechanoresponse in culture, as determined by changes in gene expression, appears to depend on the differentiation state of the cell. K562 cells treated with PMA, a model of more mature megakaryocytes than Meg-01 megakaryoblastic cells, demonstrate increases in c-fos in response to fluid shear, but the magnitude of this response is markedly diminished compared to the response of Meg-01 cells. Interestingly, undifferentiated K562 cells also respond much more robustly than cells treated with PMA (data not shown). This may indicate that immature megakaryocytes are more sensitive to mechanical cues than mature cells.

Not only does the magnitude of response vary across cell types but the trend in response to increasing shear stress differs as well. In Meg-01 cells, there is an increasing trend in c-fos expression with increasing shear stress. (The large standard deviation in

the 1 Pa treated samples was a result of one outliar in this group, thus masking a cleaner dose-response, as seen in cox-2 expression). However, the maximum increase in c-fos expression is stimulated by 0.5 Pa in K562 cells, with decreases in c-fos expression as shear stress increases. This same trend was observed in undifferentiated K562 cells as well (data not shown). This implies some difference inherent in how this particular cell line responds to shear. Studies by Mardikar, et al. have demonstrated that K562 cells exposed to 1 Pa shear stress in a viscometer display signs of "mechanical damage" (i.e. papillation, as qualitatively assessed by microscopy) as a result of this stimulus (101). There is no direct comparison with Meg-01 cells to discern whether or not similar effects are seen in these cells under similar conditions, however it is certainly an important consideration in the interpretation of this data.

Our results also demonstrate that cox-2 expression in megakaryocytes is less affected by shear than expression of c-fos. The magnitude of changes in cox-2 expression in Meg-01 cells is significantly less than the robust changes we detected in c-fos expression. In PMA-treated K562 cells, cox-2 levels are minimally affected by load, and predominantly influenced simply by handling of the plates as seen in the sham control. In contrast, osteoblasts subject to fluid shear for 30 minutes demonstrate roughly equivalent increases in c-fos and cox-2 relative to untouched baseline controls (82,102). One possible explanation for the apparent lack of cox-2 response might be the relatively short time course. Though 30 minutes of fluid shear was enough to induce a significant increase in cox-2 in MLO-Y4 osteocyte-like cells in response to fluid shear (85), other studies suggest that cox-2 is maximally upregulated following 1 to 4 hours in other

osteoblastic cell lines (82,86). Alternatively, cox-2 might not be mechanically regulated in MKs as it is in osteoblast lineage cells.

In vivo studies

Our strain gauging data is corroborated by other studies which have demonstrated similar relationships between applied force and resultant tissue-level strains (89). We have also demonstrated that, in response to 10 minutes of tibial axial compression, osteocytes from the metaphyseal region of the loaded limb express roughly 2.8-fold increase in c-fos in the loaded relative to non-loaded limb after 30 minutes and 1.9-fold increase after 60 minutes. The magnitude of this response is diminished compared to a comparable study by Inaoka, et al., which showed a maximum 4-fold induction in expression of c-fos normalized to actin following 1 hour of vertebral loading (98).

In an effort to specifically address the mechanoresponsiveness of MKs *in vivo*, we isolated individual MKs from loaded and non-loaded limbs using laser capture microdissection solely from bones harvested 30 minutes post-load, given the maximal response in osteocytes from this group. We determined that MK expression of c-fos was elevated approximately 3.1-fold in loaded relative to non-loaded limbs, comparable to the levels of expression of osteocytes. This difference was statistically significant compared to the non-loaded control limbs. This is the first study to our knowledge that has assessed the response of these cells to an applied physical stimulus *in vivo*.

The large standard deviations in gene expression data can likely be attributed to the varying degree to which effects of processing and laser capture can have on RNA integrity, compounded with the natural variability that is inherent in *in vivo* studies.

Though great efforts were taken to optimize processing techniques to preserve RNA integrity as well as to treat all samples as consistently as possible, there was still significant variability in the quality of RNA from captured samples as indicated by Agilent Bioanalyzer results.

We have shown that laser capture microdissection is a powerful tool that can be utilized to detect changes in gene expression in bone as a result of applied physical stimulus. This technology has previously been used to isolate specific cell populations within bone (99,103,104) as well as to assess changes in mechanically-induced gene expression in other cell types, such as endothelial cells (105) and skeletal muscle (106). However, this is the first study to utilize this technique to assess cellular mechanosensitivity in bone *in vivo*. Though we have only assessed changes in one particular target gene, this could be expanded to address a plethora of other questions with this model, such as comparison of changes in gene expression at different sites throughout the bone, as well as the possibility of incorporation of microarrays to detect other genes mechanically up- or down-regulated in osteocytes, MKs, or other specific cell types.

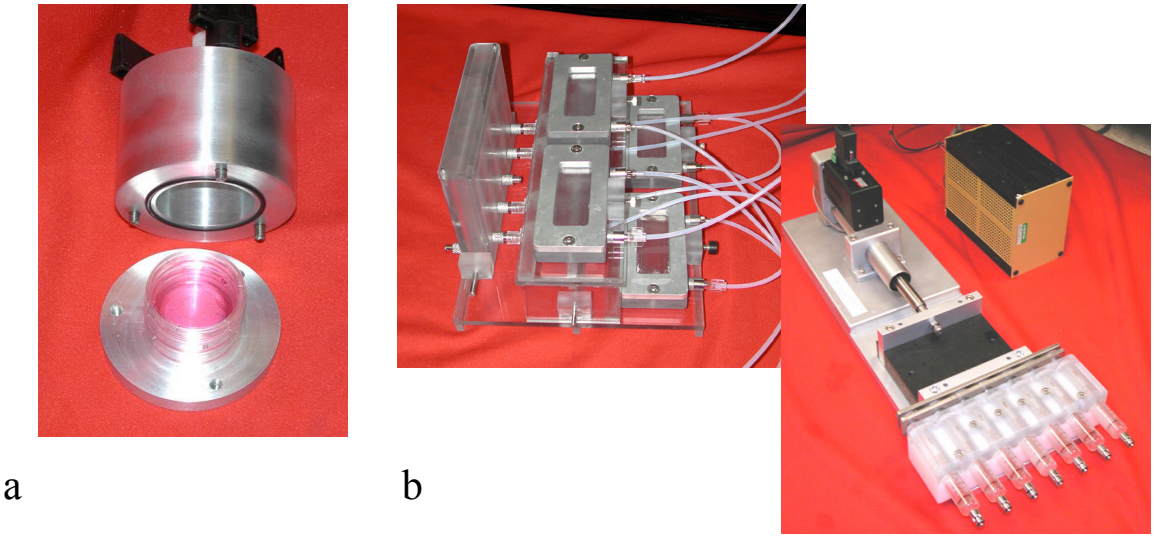

Figure 2.1: Cell culture loading modalities. (a) Hydrostatic pressure system. (b) Fluid shear device. Cells are seeded on glass slides and inserted into parallel plate flow chambers, with tubing leading both to a media reservoir and a syringe pump system. Media is pumped through syringes attached to programmable servo-motor via a linear actuator. (Images courtesy of M. Ominsky)

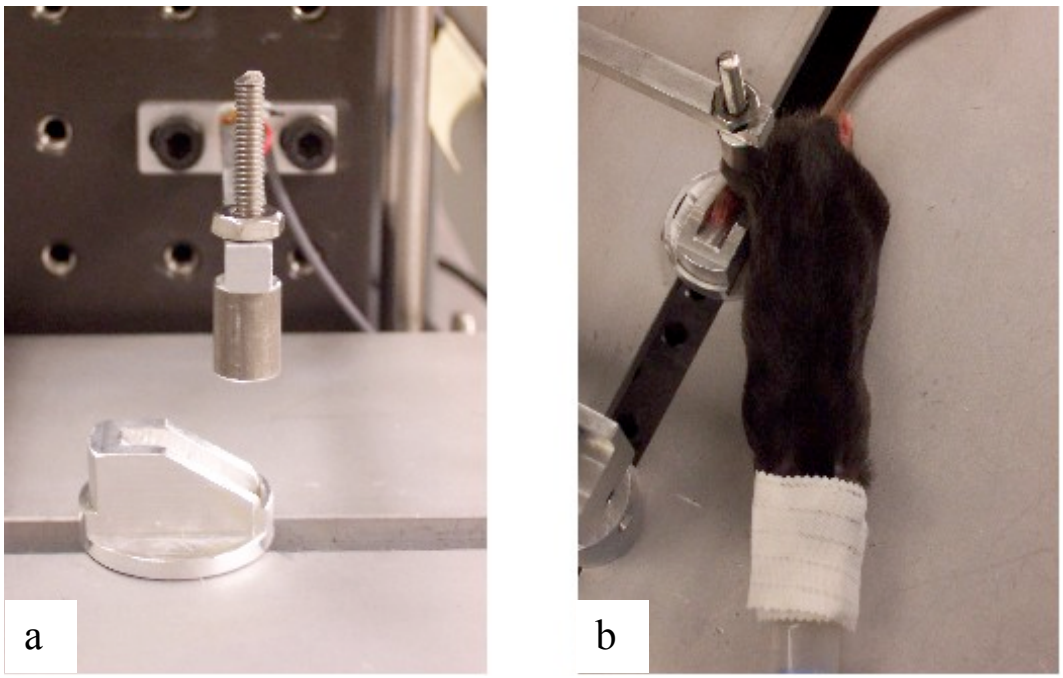

Figure 2.2 – Tibial loading apparatus. (a) The custom-machined platen and loading cup and (b) demonstration of anaesthetized mouse in position for loading.

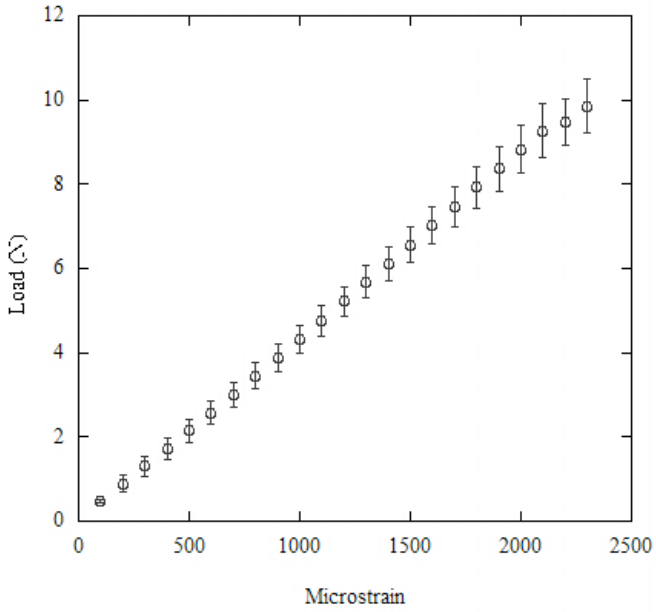

Figure 2.3 – Force-strain relationship for wild-type C56Bl6 mice. Tibiae were strain gauged and voltage readings corresponding to strain and applied force were acquired using LabView. Data represents average values from six limbs from four 8-week male mice (mean ± SD).

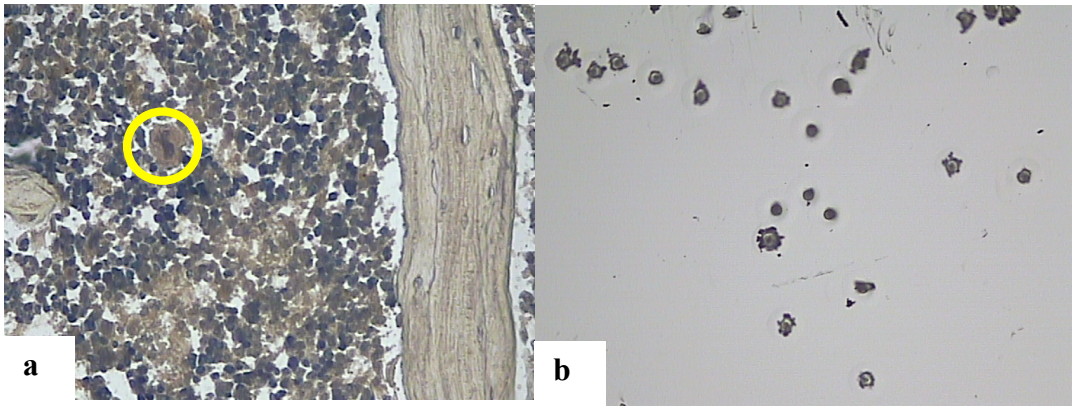

Figure 2.4 – Laser capture microdissection of MKs. (a) MKs were identified by their unique morphologic characteristics, namely large size and multi-lobed nucleus. (b) Individual cells were captured with relatively small amounts of extraneous material.

Table 2.1: Primer sequences for human-derived cell lines Meg-01 and K562.

Gene (human)	Forward	Reverse
c-fos	cgttgtgaagaccatgacag	tccgcttggagtgtatcagt
cox-2	caccctctatcactggcatc	aacattcctaccaccagcaa
18s rRNA	ctcaacacgggaaacctcac	atgccagagtctcgttcgtt

Table 2.2: Primer sequences for laser capture microdissected samples from murine tibiae.

Gene (mouse)	Forward	Reverse
c-fos (osteocytes)	ggggacagcctttcctacta	tggggataaagttggcacta
c-fos (MKs)	ggggacagcctttcctacta	gacagatctgcgcaaaagtc
DMP1	gactccacagacaccacaca	cgctgttcctcactctcact
b2m	ctggtctttctggtgcttgt	cgttcttcagcatttggatt

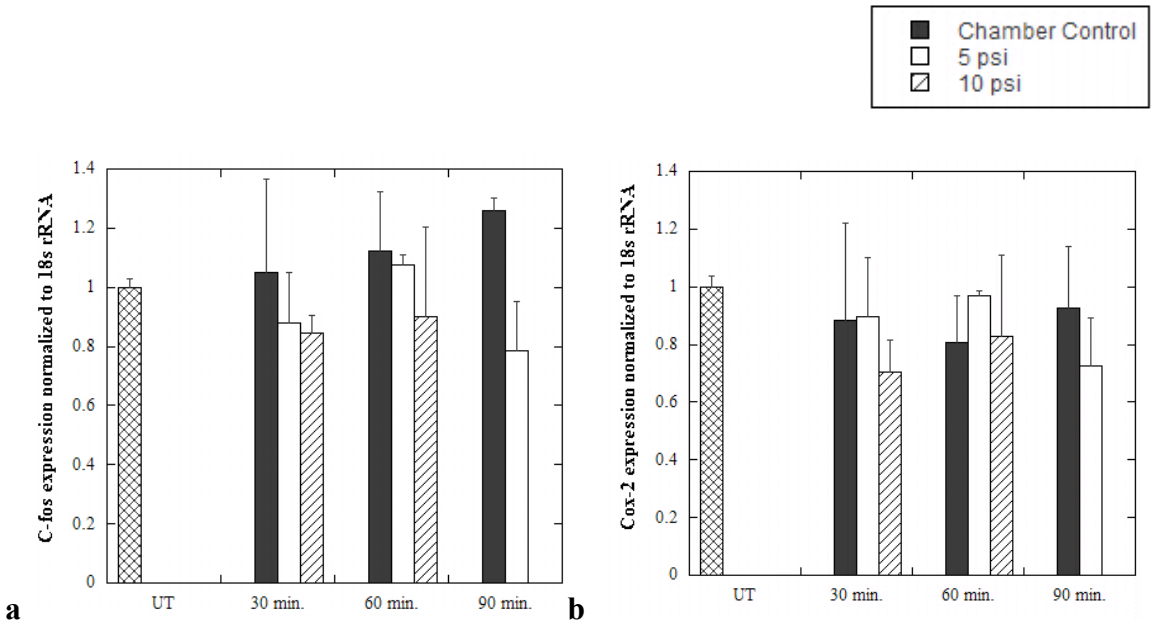

Figure 2.5 – Meg-01 cells in response to hydrostatic pressure. RT-PCR was performed to detect changes in (a) c-fos and (b) cox-2 expression relative to 18s rRNA. Data represents mean ± SD for each treatment (n=2).

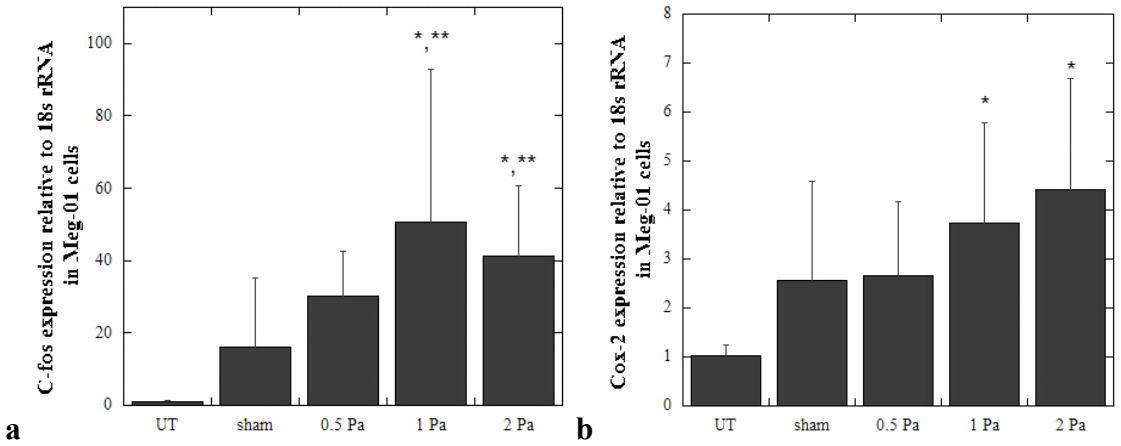

Figure 2.6 – Meg-01 cells in response to fluid shear stress. RT-PCR was performed to detect changes in (a) c-fos and (b) cox-2 expression relative to 18s rRNA. Each treatment was performed in duplicate and data represents four independent experiments (mean ± SD). *p<0.05 relative to untouched, **p<0.05 relative to sham treatment.

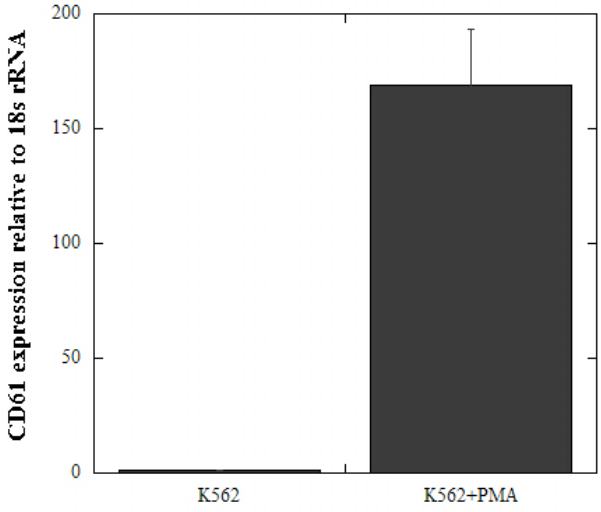

Figure 2.7– Validation of differentiation state of K562 cells treated with PMA. K562 cells were cultured in the presence of PMA for 3 days. Expression of CD61, an integrin found specifically on MKs and platelets, as assessed by RT-PCR was normalized to 18s rRNA.

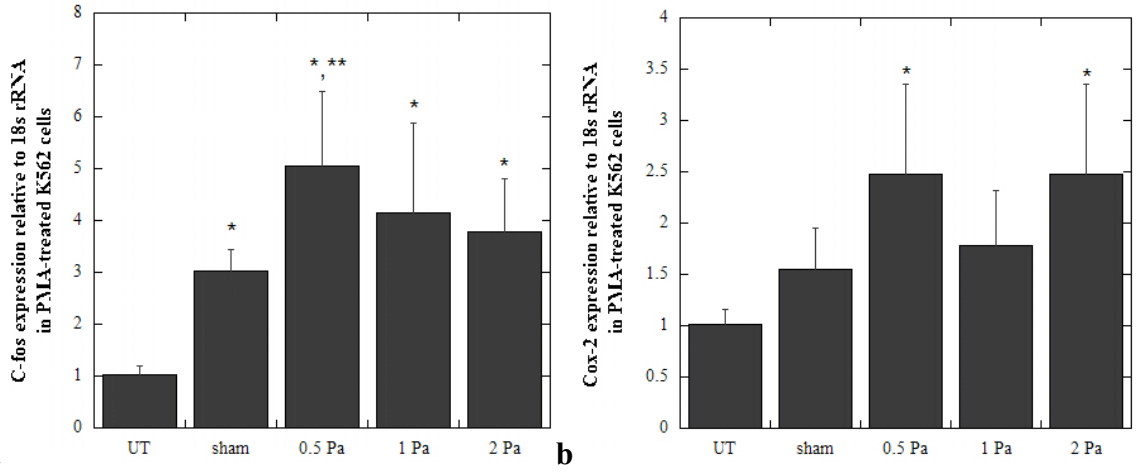

Figure 2.8 – PMA-treated K562 cells in response to fluid shear stress. RT-PCR was performed to detect changes in (a) c-fos and (b) cox-2 expression relative to 18s rRNA. Each treatment was performed in triplicate and data represents two independent experiments (mean ± SD). *p<0.05 relative to UT, **p<0.05 relative to sham

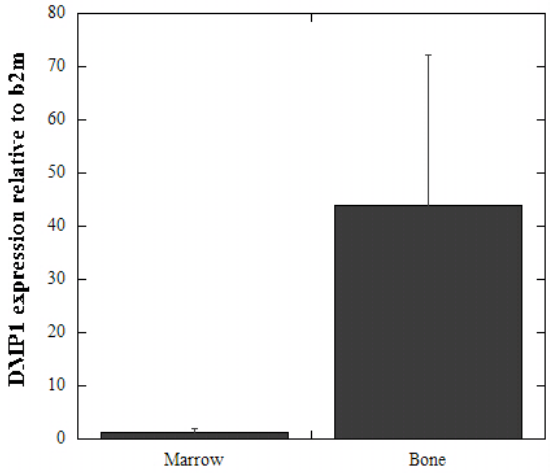

Figure 2.9 – Confirmation of tissue specificity of laser capture. Regions of bone and marrow were captured from mouse tibia. Expression of DMP1, assessed by RT-PCR, was normalized to levels of β2m. Data represents mean ± SD for each tissue type (n=2).

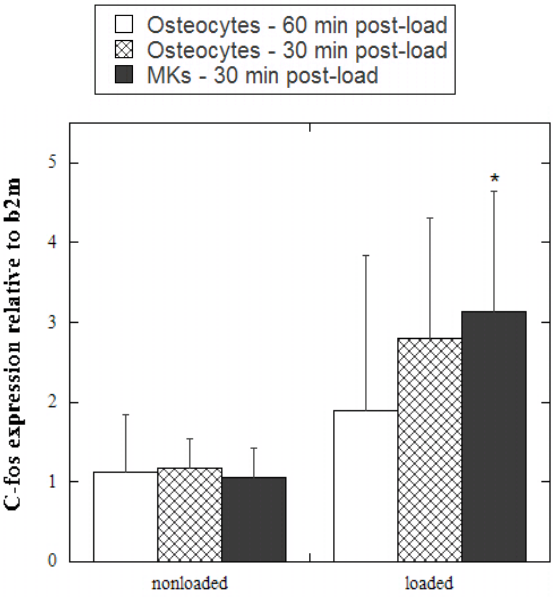

Figure 2.10 – C-fos expression normalized to β2m in cells from loaded and non-loaded tibiae. Data represents mean ± SD from n=5 (osteocytes) or n=4 (MKs) specimens. *p<0.05 relative to non-loaded values

CHAPTER III

FUNCTIONAL CONSEQUENCES OF MEGAKARYOCYTE MECHANORESPONSIVENESS: IMPLICATIONS FOR LONG-TERM ADAPTATION TO MECHANICAL STIMULUS

Introduction

Various mouse models with elevated numbers of MKs have elucidated the potent effects that these cells can have on bone homeostasis. Our studies have focused both on mice that have increased MK numbers due to genetic alterations (i.e. GATA-1^{low} mice) as well as those that can be induced by pharmacologic means by injections with thrombopoietin.

GATA-1^{low} mice

GATA-1 is a transcription factor critical for the maturation of many cells in the hematopoietic lineage, including megakaryocytes. Since it is also required for the formation of red blood cells, complete knock-out of the GATA-1 gene results in embryonic lethality. To specifically address the role of GATA-1 in MK development, a mouse model was developed in which a targeted mutation within one of the regulatory elements of the GATA-1 gene leads to a megakaryocyte-specific loss of gene expression (107,108). Selective loss of this gene in MKs highlights the importance of this

transcription factor in the maturation of MKs and the subsequent formation of platelets. At 1 month of age, these mice have approximately 7 times the number of MKs than their wild-type littermates (109), but the cells that are present in the GATA-1^{low} mice are notably arrested in maturation as evidenced by ultrastructural analysis (107). The number of platelets in these mice is also dramatically reduced (110). By 6 months of age, the marrow cavity is characterized by the presence of diffuse reticular fibers and, by 12 months, the marrow and spleen are severely myelofibrotic (109). These mice also become severely osteosclerotic. Phenotyping studies by Kacena, et al. demonstrated nearly complete occlusion of the marrow cavity with trabecular bone by 9 months of age (55).

Effects of Thrombopoietin

Thrombopoietin (TPO) is a potent inducer of megakaryocyte proliferation, differentiation and platelet formation. Seminal work in the purification of this protein demonstrated increases in numbers of MK progenitors, the numbers of MKs present in bone marrow, and numbers of platelets as a result of 5-7 days TPO injection (111,112). In addition to having profound effects on cell number when administered *in vivo*, TPO also increases the size and ploidy of MKs present (113,114). Recombinant protein is commonly administered to expand MK populations *in vivo* prior to marrow harvests to obtain primary MKs (70,115,116).

The skeletal phenotype of mice exposed to high levels of TPO parallels that of the GATA-1^{low} mice. Mice that overexpress TPO either by implantation with bone marrow infected with retrovirus expressing TPO (117,118) or constitutive expression of TPO in

the marrow and spleen (119) also develop myelofibrotic and osteosclerotic phenotypes with time.

To address whether mice with elevated numbers of MKs would have an altered skeletal response to load, we utilized the tibial loading model previously described to impart repetitive loads to young (6 wk) GATA-1^{low} mice, before the osteosclerotic phenotype develops, or their wild-type littermates. Similarly, wild-type C57Bl6 mice injected with either TPO or vehicle were subject to tibial loading to assess whether a pharmacological means of elevating MK number would also have an effect on mechanically mediated bone adaptation.

Methods

Characterization of GATA-1^{low} mice

GATA-1^{low} breeders were a kind gift from Dr. Laurie McCauley and were obtained with permission from Dr. Stuart Orkin. To assess baseline variations in skeletal phenotype prior to initiation of loading, tibiae from 6 wk male wild-type (n=7) and GATA-1^{low} (n=5) mice were harvested and fixed in 70% ethanol prior to analysis by μCT. Femurs to be tested in four-point bending were isolated and stored in PBS-soaked gauze at -20º C.

Strain gauging, as described in Chapter 2, was also carried out on 6-wk wild-type (n=2) and GATA-1^{low} (n=2) mice to determine what forces were necessary to elicit the target strain of 2000 με at the tibial mid-shaft. Figure 3.1 demonstrates the striking differences between the force-strain relationships of wild-type and GATA-1^{low} mice. Approximately 10 N results in 2000 με at the tibial mid-shaft in wild-type 6 wk mice,

whereas the same strains only require approximately 5 N of compressive force in the GATA-1^{low} mice.

In vivo loading of GATA-1^{low} mice

The right tibiae of 6-week-old male GATA-1^{low} mice (n=9) or wild-type littermates (n=18) were subject to 4 Hz cyclic loading for 10 minutes a day, 5 days per week for 2 weeks. Because of the dramatic difference in estimated forces needed generate 2000 με between GATA-1^{low} and wild-type mice, wild-type mice were exposed to one of two conditions – either a load that would generate the same estimated strains (2000 με) as the GATA-1^{low} mice, termed strain-matched or WT-SM (n=9) or the same load applied to GATA-1^{low} mice, termed load-matched or WT-LM (n=9). Three days following the last day of loading, both tibiae were harvested and immediately stored in 70% Ethanol.

Micro-Computed Tomography (μCT)

All bones were scanned on an eXplore Locus SP μCT scanner (GE Medical, Waukesha, WI) at a resolution of 18 μm per voxel. Two regions along the length of the tibia were isolated for analysis – the metaphyseal region, spanning 10% of the length of the tibia just distal to the growth plate, and the diaphyseal region, centered at 50% the length of the tibia and spanning 2.5% of the total length. In the metaphyseal region, the trabecular compartment was isolated using a spline ROI and analyzed for trabecular morphometric parameters. This region was then "blanked" and the morphometric parameters were also calculated for the resulting cortical shell. At the mid-diaphysis, the

cortical bone was selected using the cortical ROI tool, and morphologic parameters were calculated. For femurs, a cortical ROI at the mid-diaphysis was selected for geometric parameters of this region.

Mechanical Testing

Following μCT analysis, femurs from 6 week GATA-1^{low} and wild-type mice subsequently tested in four-point bending using a custom-built apparatus driven by a Mini Bionix II servohydraulic system (MTS; Eden Prairie, MN) (120). Femurs were loaded in the anterior-posterior direction, such that posterior was in tension and anterior in compression. Bones were loaded at a constant displacement rate of 0.1 mm/s.

Histomorphometry

Following μCT analysis, tibiae (n=5 from each group) were dehydrated in a graded series of ethanols and embedded in polymethylmethacrylate. Specimens were sectioned at 500 μm increments using an Exakt 300 bandsaw (Exakt Technologies, Oklahoma City, OK) then ground and polished to 100 μm using silicone sandpaper (1200 and 2400 grit) on an Exakt 300 microgrinding device (Exakt Technologies, Oklahoma City, OK). Two sections per bone, one from the metaphyseal region and one from the mid-diaphyseal region, were analyzed.

Calcein and alizarin labels were traced manually using Bioquant software. From these measurements, standard histomorphometric parameters (MS/BS, MAR, and BFR) were calculated (121).

TPO administration

To determine the proper dosing regimen, a pilot study was conducted to observe the effects of long-term TPO administration based on flow cytometric analysis as well as histologic observation. For this study, 16 mice received daily injections of 200ng recombinant mouse TPO (Peprotech; Rocky Hill, NJ) in 0.1% mouse serum albumin (Sigma-Aldrich; St. Louis, MO) in PBS for 7 days and were euthanized at days 0 (pre-injection), 3, 7, 10, and 14 (n=4 for all time points). Immediately following sacrifice, tibiae were fixed in NBF and decalcified in formic acid buffered in sodium citrate and processed for paraffin sectioning and stained with hematoxylin and eosin. Prior to embedding, bones were analyzed by μCT to assess any morphologic changes as a result of TPO injections. Femurs were also harvested for flow cytometric analysis of the marrow to determine the percentage of cells expressing CD41, an integrin found on the surface of megakaryocytes and platelets.

Flow Cytometry

Immediately following harvest of femurs, marrow was flushed into PBS + 5% fetal bovine serum. Red blood cells were lysed with ACK lysis buffer (Lonza; Basel, Switzerland), and cell suspensions rinsed in PBS, resuspended in wash buffer (PBS + 5% fetal bovine serum + 0.1% sodium azide) and filtered through a 70 μm cell strainer. Cells were counted using a hemocytometer and were separated into 4 individual tubes of 1 x 10^6 cells per tube from each animal. After centrifugation, cells were resuspended in wash buffer and duplicate samples from each animal were incubated for 30 minutes either in the presence or absence of a FITC-conjugated anti-CD41 antibody (Abcam; Cambridge,

MA) at 4 ºC. Following three sequential washes, cells were resuspended in PBS + 1% PFA and stored at 4 ºC in the dark until analysis. Samples were run on a FACSCalibur machine (BD Biosciences; San Jose, CA) with the assistance of the University of Michigan Flow Cytometry Core Facility.

In vivo loading of TPO-treated mice

Male C57Bl6 mice were purchased from Jackson Laboratories (Bar Harbor, ME). At 8 weeks of age, mice began a course of daily injections for 12 days with either 200ng TPO (Peprotech; Rocky Hill, NJ) in 0.1% mouse serum albumin (Sigma-Aldrich; St. Louis, MO) in PBS or vehicle. Injections began 3 days prior to the initiation of load to initially elevate the population of MKs present within the marrow. The right tibia of 8-week-old male C57Bl6 mice was subject to 4 Hz cyclic loading for 10 minutes a day, 5 days per week for 2 weeks. The peak load applied was determined from previously acquired strain gauge data from wild-type C57Bl6 mice (Chapter 2). Three days following the last day of loading, both tibiae were harvested and immediately stored in 70% ethanol. All tibiae were scanned using the same μCT parameters and sectioned for dynamic histomorphometry as described above.

Statistics

For all μCT analysis of loaded vs. non-loaded tibiae, statistical significance was determined by a Student's paired t-test with a significance level of $p < 0.05$. For characterization of tibiae during the time course of TPO injections, a one-way ANOVA

($p < 0.05$) was performed across each timepoint with a Tukey's test post-hoc to identify specific differences between groups.

Results

At 6 weeks of age, GATA-1^{low} mice demonstrate reduced morphologic parameters compared to their wild-type littermates (Table 3.1). Within the trabecular compartment, GATA-1^{low} mice are characterized by lower BV/TV and Tb.N. as well as increased Tb.Sp., as highlighted in Figure 3.2a-c, though these differences were not statistically significant. The average cortical area within the metaphyseal region was significantly lower in GATA-1^{low} relative to wild-type mice (Figure 3.2d). There are no discernable differences, however, in cortical parameters at the mid-diaphysis (Table 3.1, Figure 3.2d).

The stiffness, as determined from four-point bending of femurs, was reduced in GATA-1^{low} compared to wild-type littermates (Figure 3.3a), consistent with the implications from strain gauge data in Figure 3.1. Similarly, the moment of inertia in the direction of loading (Iyy) was reduced in GATA-1^{low} compared to wild-type littermates (Figure 3.3b). A predicted elastic modulus was calculated, based on the equation $E = \frac{S(3ab^2 - 4b^3)}{12I}$ where S represents stiffness, I the moment of inertia, and a and b are the dimensions between spans of the four-point bending device (120). This was calculated to be 4244 ± 595 for GATA-1^{low} mice and 4236 ± 839 for wild-type mice, suggesting that the differences observed in stiffness are likely explained by geometric differences between the two genotypes and not due to inherent differences in material

properties. This is also supported by the finding that TMD is not significantly different between the two genotypes (Table 3.1).

The length of loaded tibia, as measured as distance from the growth plate to the distal-most part of the tibia on μCT, was decreased relative to non-loaded controls (Table 3.2). This difference was statistically significant in the WT-SM group in which there was on average a 1.5% decrease in tibial length in loaded compared to non-loaded bones. There was a 0.37% and 0.46% decrease in length with load in GATA-1^{low} and WT-LM respectively, though these differences were not statistically significant.

Surprisingly, the application of axial tibial load in both GATA-1^{low} and WT mice subject to both loading magnitudes led to decreases in trabecular geometric parameters (Table 3.3). Tb.N. was significantly diminished in all groups (Figure 3.4b). BV/TV also consistently decreased with load, though this did not reach statistical significance in the GATA-1^{low} mice (Figure 3.4a). Tb. Sp. was significantly increased in both WT-SM and WT-LM, and though not significant, was increased in GATA-1^{low} mice as well (Figure 3.4c). BFR was also decreased with load in the WT-LM group, though no apparent differences were detected in the WT-SM or GATA-1^{low} mice in response to load (Figure 3.4e). Due to the large variability in these measurements, however, this change was not statistically significant. The only finding indicative of positive effects of load on trabecular bone was a significant increase in TMD (solely within the WT-SM) group in response to load (Figure 3.4d).

Within the cortical shell of the metaphyseal region, increases in morphometric parameters and TMD were also observed in the WT-SM group (Table 3.4). Cortical area within this region is the only parameter that is differentially regulated by load across

groups, with a significant increase in WT-SM, decrease in WT-LM, and no change in GATA-1low mice with load (Figure 3.5a). Representative slices from μCT analysis of the metaphyseal region demonstrate this cortical response is primarily localized to the posterior aspect of the tibia (Figure 3.6). As in the trabecular compartment, TMD in the WT-SM group is also significantly enhanced with load (Figure 3.5b).

The geometric properties at the mid-diaphysis were largely unchanged (Table 3.5). The only significant effects of load were seen in WT-LM mice in which the outer perimeter and cortical area decreased in loaded compared to non-loaded limbs (Figure 3.7a,b). At the mid-diaphysis, contrary to the other regions analyzed, the TMD decreases with load in the WT-SM group while remaining unchanged with load in the other groups (Figure 3.7c). The endosteal BFR appears to be diminished in response to load in all groups (Figure 3.7d), whereas decreases in periosteal BFR seem to be restricted to the WT-LM group (Figure 3.7e). Once again, large variability in this measurement precludes any statistically significant differences.

The pilot study conducted to assess the temporal effects of long-term TPO administration on MK number confirmed that MK number was enhanced over the course of the 7 day injection by both histologic observation (Figure 3.8) as well as numbers of CD41-positive cells present in the marrow (Figure 3.9). Qualitatively the MKs present also appeared larger from histologic assessment, as would be expected from our understanding of the effects of TPO from the literature. The effects of TPO on MK number, as determined by FACS analysis of CD41+ cells, were transient. By 3 days following the last injection, the numbers of MKs had already fallen to 50% of the original

number and 1 week following the last injection, MK numbers had returned to baseline levels (Figure 3.9).

μCT assessment of tibiae from all timepoints confirms no significant changes in bone geometric properties either in the trabecular bone or cortical bone of the metaphyseal or diaphyseal regions with 7 days of TPO administration (Table 3.6).

Based on the transient effects of TPO, we extended the course of injections to 12 days in order to ensure the persistence of enhanced numbers of MKs throughout the 2-week time course for loading. Both TPO- and vehicle-treated animals demonstrated similar changes in tibial length (Table 3.7) and morphologic parameters (Tables 3.8-3.10) as a result of load compared with WT-SM groups from the previous study. As with the GATA-1^{low} mice, load consistently led to a decrease in BV/TV and Tb. N. and an increase in Tb. Sp. (Figure 3.10a-c). Similarly, BFR within trabecular bone does not change (Figure 3.10e). However, unlike the GATA-1^{low} study, TMD is reduced in response to load (Figure 3.10d), though this does not reach statistical significance in the TPO-treated group.

Again, the only potentially anabolic effects of load are observed in the cortical shell of the metaphyseal region, where a significant increase in cortical area (Figure 3.11a) and TMD (Figure 3.11b) were seen in both TPO- and vehicle-treated animals. And also consistent with results from the GATA-1^{low} study, cortical area at the mid-diaphyseal region was significantly decreased in both groups in response to load (Figure 3.12a), with no concomitant change in TMD (Figure 3.12b). There is a trend toward a decrease in periosteal BFR in response to load (Figure 3.12d), though, again, not statistically significant given the high degree of variability.

Discussion

The effects of load from our tibial compression device are quite surprising and contradictory to what we had expected based on results from other similar experimental models. Given that other published studies have demonstrated an increase in trabecular parameters in similar aged mice in response to comparable loads (89,92), the robust decreases seen in BV/TV with load were unanticipated. Several pilot studies were conducted during the development of this system, and this phenomenon was consistently observed regardless of animal age, loading magnitude, and cycle number (data not shown).

The explanation for the differences seen between our results and those from other groups remains elusive. Though the tibial loading device is designed to impart repeated, controlled loads, it is possible that inherent differences in apparatus design or experimental protocol might have some effects on response to load. For instance, variations in the placement of the tibia within the cup, the curvature of the cup itself, or even the presence or absence of padding within the cup, may alter the points of contact and therefore the resulting load distribution through the tibia. The thickening of the proximal cortex in the metaphysis might imply that the direction of the resultant force through the knee may be slightly off-axis, thereby leading to an anabolic adaptive response in this region as opposed to directly below the knee through the trabecular region.

The differences observed in tibial length as a result of load also indicates damage may be accumulating at the growth plate. In a rat model of ulnar loading, cyclic loading

with a peak force eliciting a strain of 3500 με at the mid-shaft led to significant cracking within the growth plate, as well as impaired capillary invasion (122). This may also account for the resulting decreases in trabecular parameters. However a more rigorous assessment of events at the growth plate, specifically through histologic observations, would be necessary to draw such conclusions.

This change in tibial length may also be explained by the fact that directly applying compressive loads on the growth plate has been shown to have inhibitory effects on long bone growth. This principle, commonly referred to as the Hueter-Volkmann law, is clinically employed by orthopaedic surgeons to correct growth deformities in the growing skeleton. Therefore, it is also highly plausible that direct compressive load gives rise to deleterious effects on the tibial growth of a rapidly growing animal.

It is also critically important to highlight the inherent limitations in strain gauging, and therefore the potential inconsistencies between load-strain relationships across studies. Specifically in mouse limbs, where the dimensions of the strain gauges are roughly equivalent to the width of the bone, slight variations in placement are inevitable and even minor differences in the amount of adhesive used to attach the gauges can result in errors associated with this technique. Even publications from the same group demonstrate drastic variations in strain gauging results – Fritton, et al. reported that 5 N of force engendered approximately 1250 με (89), however the same group later determined that 11.5 N of load was necessary to induce this same strain. De Souza, et al., also found similar correlations to Fritton's original publication, with 5 N leading to approximately 1000 με at the lateral face of the tibia but a lower strain (~700 με) on the medial aspect. A load of 13 N was reported to be sufficient to elicit 2000 με at the lateral

surface and 1500 με at medial surface. Though our load-strain relationship corresponds closely with Fritton's original reported values, it is still highly probable that the loads we are imparting may not be generating the magnitude of strains we predict.

The baseline phenotype of GATA-1^{low} mice was also somewhat surprising. We chose to start loading mice at 6 weeks of age based on findings from the literature that this would be sufficiently early enough to ensure the skeletal phenotype had not yet presented in these mice. In a few cases we saw the appearance of trabeculae forming within the mid-diaphysis of the tibiae by 8 weeks. However, the overall reduction in trabecular and cortical parameters in GATA-1^{low} compared to wild-type mice at 6 weeks implies some alteration in bone formation prior to the onset of the dramatic skeletal phenotype observed at later times. Previously published work has confirmed that osteoblasts derived from GATA-1^{low} mice have similar proliferative and mineralization characteristics as cells from their wild-type littermates (55), thus eliminating the possibility that there may be some defect in osteoblast behavior. Nevertheless, baseline differences in the morphologic parameters implies some fundamental difference in skeletal development that precedes the striking increase in bone mass that develops with age.

This difference also manifests itself in whole bone stiffness, as determined from four-point bending tests of the femurs. The decreased stiffness in the transgenic mice is likely explained by decreases in geometric properties (i.e. moment of inertia) rather than inherent material differences. However, we have not completely ruled out the possibility of differences in local material properties. To adequately address this, techniques such as nanoindentation could be utilized to assess material differences at the local level.

Alternatively, Raman spectroscopy could be employed to identify any potential differences inherent in the mineralized matrix.

The only significant difference between the load response from different groups was found in the change in cortical area within the metaphysis. Wild-type mice loaded at approximately 10 N (~2000 με) had significant bone apposition, specifically on the posterior aspect of the tibia, in response to load. There was also a concomitant increase in TMD within this compartment as well. Interestingly, cortical area was unchanged in GATA-1^{low} mice and decreased in wild-type load-matched controls. The difference between the response in the two wild-type groups indicates some dependence on loading magnitude. This is consistent with results from De Souza, et al., demonstrating a dose-dependent increase in total interlabel area in the metaphyseal region (92). However at loads of 8.7 - 10 N (loads sufficient to initiate a cortical expansion in our model), there were no changes in detected in interlabel area at the metaphyseal region. This was only significantly increased in loaded compared to non-loaded limbs with 12 N (or higher) loads. Though this does suggest lower loads may not initiate the same response as higher loads in this model, it is also surprising that loads that generated significant changes in our model were not anabolic in a comparable model.

The lack of change in metaphyseal cortical area in the GATA-1^{low} animals could either be interpreted as a diminished response of the bone at 2000 με (compared to WT-SM) or a protection against the catabolic response seen under 5 N load (compared to WT-LM). The baseline μCT data also demonstrates that cortical area is decreased in 6wk GATA-1^{low} mice compared to wild-type littermates (Figure 3.2d) but, interestingly, over the 2-week course of loading, the cortical area of non-loaded control limbs from GATA-

1^{low} mice eventually reaches that of wild-type mice (Figure 3.4d). It is possible, therefore, that any changes due to elevated MK numbers are outweighed by the morphometric changes as a result of growth. This is a complication from using growing animals in a model of adaptation, however given the dramatic skeletal phenotype that develops with time in the GATA-1^{low} mice, experiments using older animals would present ever more challenges in comparisons to wild-type controls.

The minimal change (or decrease) in cortical area at the mid-diaphysis is not necessarily surprising based on the literature, which has demonstrated contradictory results as well. Fritton, et al. reported no change at the mid-diaphysis in maximum cross-sectional moment of inertia and only a minor increase in mineral content, two metrics that were significantly enhanced in the metaphyseal region in response to axial tibial loading (89). However, work from the same group also demonstrated robust increases in cross-sectional area at this site when the magnitude of load was increased (123). De Souza, et al. also showed significant increases in interlabel area at both endosteal and periosteal surfaces at the mid-diaphysis. Importantly, though, these increases were most significant at higher loads than those imparted in this study (12-13 N). At loads comparable to those used in this study, this parameter was decreased at 8.7 N and remained unchanged with 10 N of load, thus further supporting our findings at these approximate loads.

Changes in BFR, though not statistically significant given the high degree of variability, generally reflect the geometric trends seen from μCT results at the mid-diaphysis. The WT-LM group is the only group which demonstrates decreases in BFR both at the endosteal and periosteal surface in response to load. This corresponds to a

reduced cortical area with load, likely explained by these decreases in the rate at which bone is formed at both surfaces in the presence of load. Both GATA-1^{low} and WT-SM groups also demonstrate relative decreases in endosteal BFR with load, however, no significant changes in geometric properties were detected.

We initially performed a pilot study to ensure that our TPO administration regimen would have the predicted effects on MK number as reported in the literature. We were not certain, however, how long the elevated numbers of MKs would persist following cessation of TPO injections. Though similar dosing regimens have been reported (112), the assessment of MK number as a result of these treatments has been performed immediately following the time course of injections. Arnold, et al. demonstrated the temporal nature of changes in MK frequency and ploidy following a single dose of pegylated form of recombinant human MGDF (the N-terminal receptor-binding domain of TPO) with peak changes 4-6 days following injection. However, extrapolating these findings to the current work may not be relevant, since doses were much higher than those used in our study, and the polyethylene glycol moiety enhances the biological activity of the cytokine (124). We therefore decided to investigate a previously reported dosing regimen that was consistent with other studies (personal communication with X. Li).

The decision, then, to extend the course of injections for the tibial loading study was made with the assumption that the additional 5 days of TPO injections would have consistent effects on MK number and bone morphology. Ideally the baseline experiment would be repeated to confirm that, indeed, MK number would persist as expected throughout the course of injection and that there would be no other deleterious effects on

the bone tissue as a result of TPO treatment. However, evidence from the literature suggests that mice continuously exposed to TPO *in vivo* take several weeks to develop an altered skeletal phenotype. TPO-overexpressing mice demonstrate severe myelofibrosis and osteosclerosis 10 weeks following transplantation with retrovirally-transfected bone marrow. Another model of TPO-overexpression by retrovirus demonstrates that, though myelofibrosis and osteosclerosis are predominant in the marrow cavity 7 months post-implantation, these phenotypes are not present in the marrow of mice 2 months following implantation, though occasionally trabecular spicules were observed in the medullary space (118). Furthermore, transgenic mice constitutively expressing TPO are found to have no signs of myelofibrosis or osteosclerosis at 3 months of age (119). Therefore, it seems plausible that the extension of TPO injection from 7 to 12 days should not dramatically affect bone architecture.

Results for both vehicle- and TPO-treated mice in response to applied loads generally mirror those from the WT-SM group of the previous study. There are also no apparent differences between vehicle- and TPO-treated mice subject to tibial loading, suggesting that the pharmacologically-induced numbers of MKs had no effect on the animals' response to tibial loading. This could suggest that there is no advantageous effect of elevated MK numbers in adaptation to applied loads. However, as discussed above, this model of axial tibial load may also not be optimal for detecting intramedullary changes in response to load. Anabolic response that might be stimulated by load could be masked by the apparent catabolic response that arises, potentially as a result of deleterious effects of applied load to the growth plate.

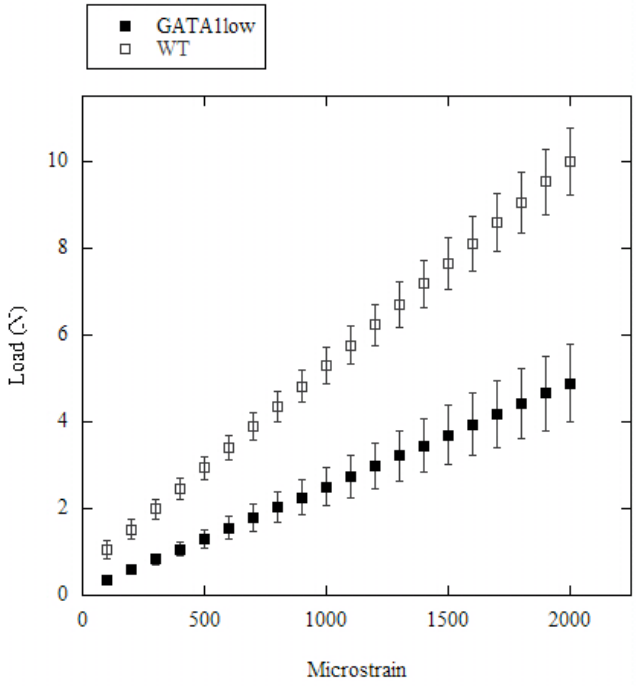

Figure 3.1 – Force-strain relationship for GATA-1^{low} and wild-type littermates. Tibiae were strain gauged and voltage readings corresponding to strain and applied force were acquired using LabView. Data represents average values from three limbs from two mice per genotype (mean ± SD).

Table 3.1: µCT results from 6wk GATA-1^{low} and wild-type mice. Data represents mean ± SD from n=7 (wild-type) or n=5 (GATA-1^{low}) mice. *p<0.05 between WT and GATA-1^{low} mice

	GATA-1^{low}	WT
Trabecular Parameters		
BV/TV	0.076 ± 0.027	0.091 ± 0.024
BS/BV	70.73 ± 7.00	68.24 ± 5.29
Tb.Th.	0.029 ± 0.003	0.030 ± 0.002
Tb.N.	2.611 ± 0.763	3.069 ± 0.660
Tb.Sp.	0.397 ± 0.170	0.314 ± 0.090
TMD (mg/cc)	468.37 ± 18.33	472.25 ± 15.86
Cortical Parameters - Metaphyseal Region		
Inner Perimeter (mm)	6.009 ± 0.295	6.060 ± 0.429
Outer Perimeter (mm)	6.729 ± 0.389	6.979 ± 0.444
Marrow Area (mm^2)	2.047 ± 0.196	2.055 ± 0.286
Cortical Area (mm^2)	0.413 ± 0.076	0.480 ± 0.052 *
TMD (mg/cc)	713.06 ± 24.53	724.99 ± 16.16
Cortical Parameters - Diaphyseal Region		
Inner Perimeter (mm)	2.177 ± 0.072	2.195 ± 0.105
Outer Perimeter (mm)	3.302 ± 0.146	3.366 ± 0.182
Marrow Area (mm^2)	0.351 ± 0.024	0.361 ± 0.036
Cortical Area (mm^2)	0.472 ± 0.054	0.496 ± 0.058
TMD (mg/cc)	977.31 ± 26.70	976.95 ± 27.09

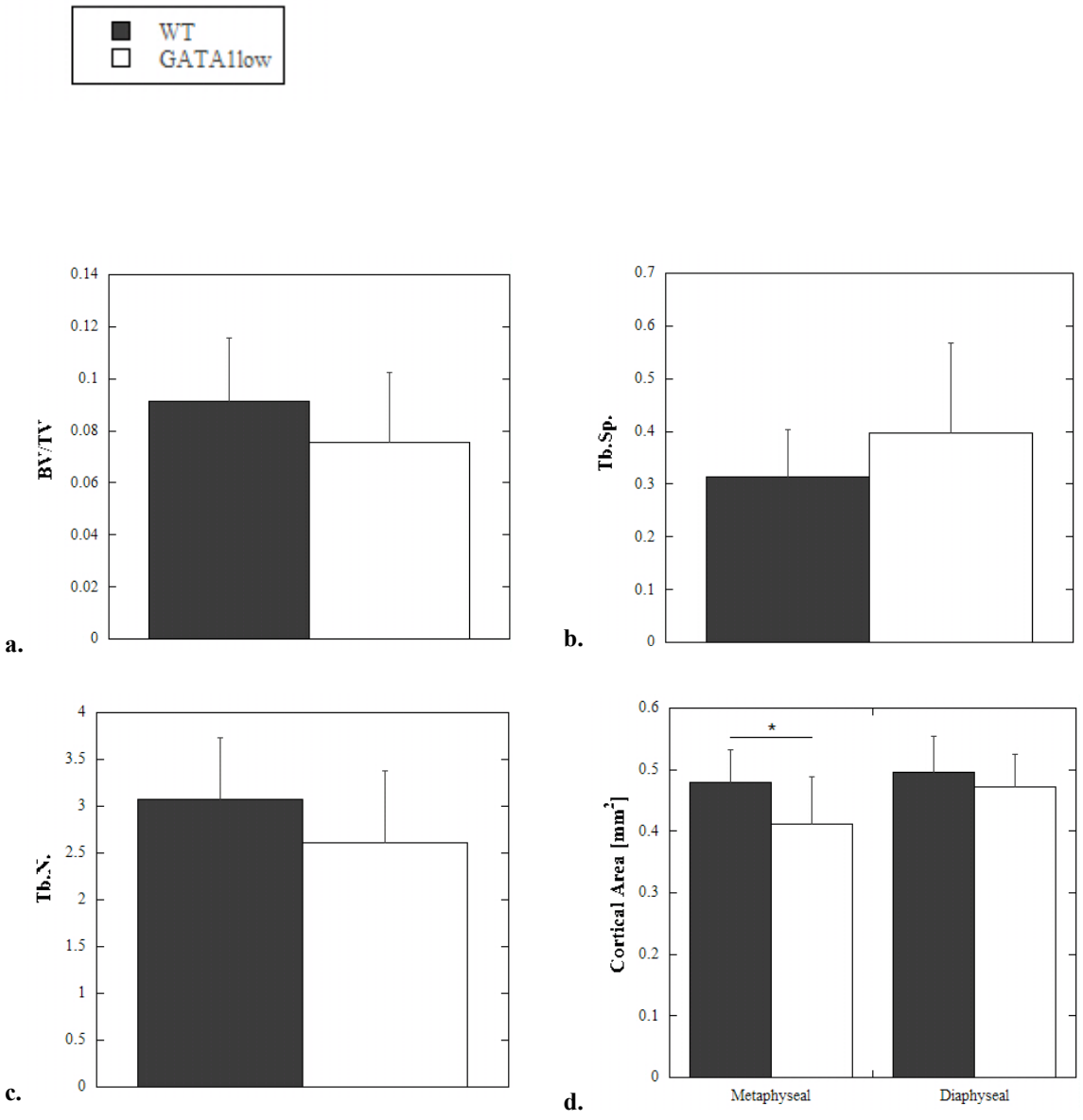

Figure 3.2: Graphical representation of μCT results highlighting differences between 6wk GATA-1^{low} mice and wild-type littermates. Prominent differences were observed in (a) BV/TV, (b) Tb. Sp., (c) Tb.N. and (d) cortical area. *$p<0.05$ between WT and GATA-1^{low} mice.

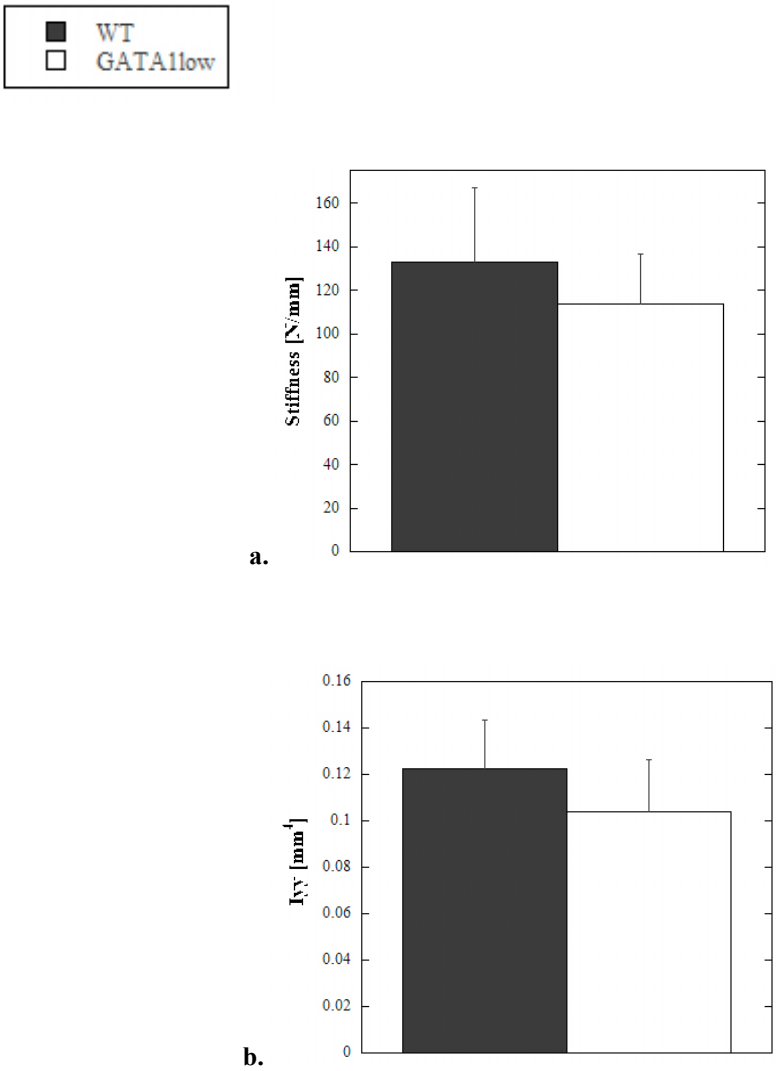

Figure 3.3: Mechanical and geometric properties from femurs of 6 wk GATA-1^{low} and wild-type mice. (a) Stiffness was determined from four-point bending tests and (b) moment of inertia (Iyy) by μCT analysis. Data represents mean ± SD from n=7 (wild-type) or n=5 (GATA-1^{low}) mice.

Table 3.2: Tibial length as determined from μCT images of GATA-1^{low} or wild-type mice subject to 2 weeks of tibial loading.

		GATA-1^{low}	WT - SM	WT - LM
Length (mm)	Non-loaded	15.67 ± 0.22	15.42 ± 0.38	15.40 ± 0.34
	Loaded	15.61 ± 0.22	15.18 ± 0.42 *	15.33 ± 0.31

WT mice were either strain-matched (WT-SM; n=9) or load-matched (WT-LM; n=9) to GATA-1^{low} (n=9) loading conditions. Data represents mean ± SD. *$p < 0.05$ in loaded compared to non-loaded limbs within a group.

Table 3.3: Trabecular parameters of GATA-1^{low} and wild-type mice subject to two weeks of tibial loading.

		GATA-1^{low}	WT - SM	WT - LM
BV/TV	Non-loaded	0.080 ± 0.032	0.096 ± 0.046	0.111 ± 0.048
	Loaded	0.054 ± 0.031	0.069 ± 0.024 *	0.084 ± 0.038 *
BS/BV	Non-loaded	54.67 ± 12.51	65.48 ± 10.48	62.66 ± 8.92
	Loaded	62.11 ± 8.13	61.16 ± 6.58	68.08 ± 10.87 *
Tb.Th.	Non-loaded	0.040 ± 0.017	0.031 ± 0.006	0.033 ± 0.005
	Loaded	0.033 ± 0.004	0.033 ± 0.004	0.030 ± 0.005 *
Tb.N.	Non-loaded	2.060 ± 0.604	2.958 ± 0.856	3.282 ± 0.924
	Loaded	1.583 ± 0.723 *	2.076 ± 0.606 *	2.685 ± 0.808 *
Tb.Sp.	Non-loaded	0.480 ± 0.132	0.330 ± 0.100	0.294 ± 0.094
	Loaded	0.780 ± 0.521	0.481 ± 0.128 *	0.375 ± 0.130 *
TMD (mg/cc)	Non-loaded	531.60 ± 62.83	507.24 ± 28.61	505.51 ± 27.68
	Loaded	502.52 ± 34.91	525.22 ± 25.50 *	495.34 ± 34.16
MS/BS (%)	Non-loaded	17.67 ± 7.88	19.17 ± 9.95	28.04 ± 16.13
	Loaded	16.57 ± 3.97	21.81 ± 4.75	16.60 ± 11.83
MAR (μm/d)	Non-loaded	1.55 ± 0.56	1.63 ± 0.99	1.39 ± 0.64
	Loaded	1.77 ± 0.72	1.70 ± 0.58	1.14 ± 0.74
BFR ($\mu m^3/\mu m^2/d$)	Non-loaded	0.301 ± 0.195	0.368 ± 0.259	0.350 ± 0.191
	Loaded	0.299 ± 0.144	0.379 ± 0.158	0.220 ± 0.143

WT mice were either strain-matched (WT-SM; n=9) or load-matched (WT-LM; n=9) to GATA-1^{low} (n=9) loading conditions. Histomorphometric analysis was performed on n=5 specimens per group. Data represents mean ± SD. *$p < 0.05$ in loaded compared to non-loaded limbs within a group.

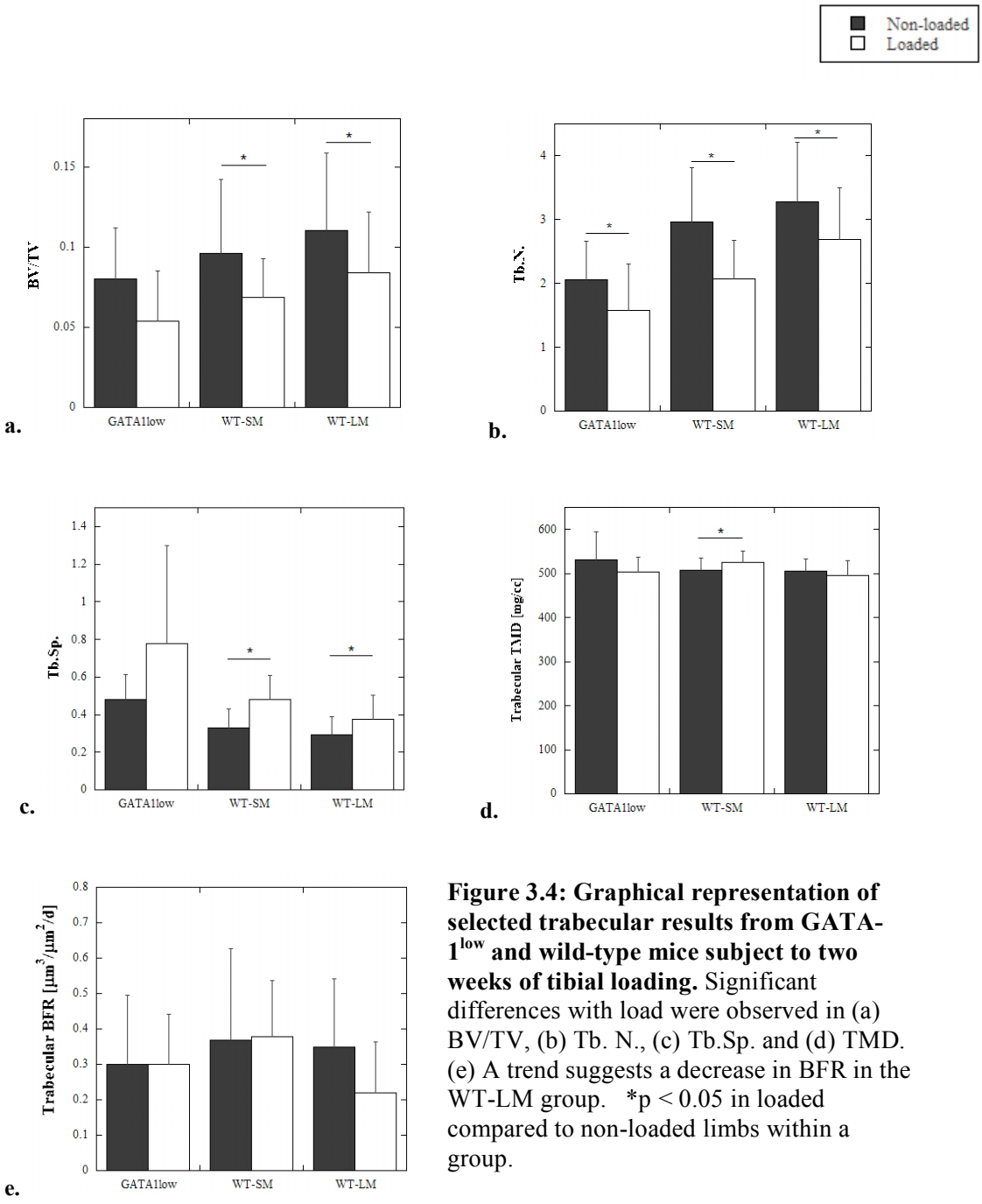

Figure 3.4: Graphical representation of selected trabecular results from GATA-1^{low} and wild-type mice subject to two weeks of tibial loading. Significant differences with load were observed in (a) BV/TV, (b) Tb. N., (c) Tb.Sp. and (d) TMD. (e) A trend suggests a decrease in BFR in the WT-LM group. *$p < 0.05$ in loaded compared to non-loaded limbs within a group.

Table 3.4: Cortical parameters within the metaphyseal region of GATA-1^{low} and wild-type mice subject to two weeks of tibial loading.

		GATA-1^{low}	WT - SM	WT - LM
Inner Perimeter (mm)	Non-loaded	5.609 ± 0.219	5.588 ± 0.249	5.568 ± 0.167
	Loaded	5.607 ± 0.217	5.634 ± 0.367	5.664 ± 0.167 *
Outer Perimeter (mm)	Non-loaded	6.955 ± 0.221	6.904 ± 0.371	6.881± 0.317
	Loaded	6.843 ± 0.337	7.029 ± 0.361	6.766 ± 0.285 *
Marrow Area (mm^2)	Non-loaded	1.846 ± 0.175	1.796 ± 0.173	1.798 ± 0.067
	Loaded	1.867 ± 0.177	1.818 ± 0.217	1.867 ± 0.099 *
Cortical Area (mm^2)	Non-loaded	0.671 ± 0.083	0.625 ± 0.117	0.629 ± 0.059
	Loaded	0.665 ± 0.113	0.734 ± 0.092 *	0.589 ± 0.063 *
TMD (mg/cc)	Non-loaded	785.69 ± 21.29	822.74 ± 40.75	806.12 ± 29.34
	Loaded	795.27 ± 36.81	847.53 ± 29.16 *	790.87 ± 24.97

WT mice were either strain-matched (WT-SM; n=9) or load-matched (WT-LM; n=9) to GATA-1^{low} (n=9) loading conditions. Data represents mean ± SD. *$p < 0.05$ in loaded compared to non-loaded limbs within a group.

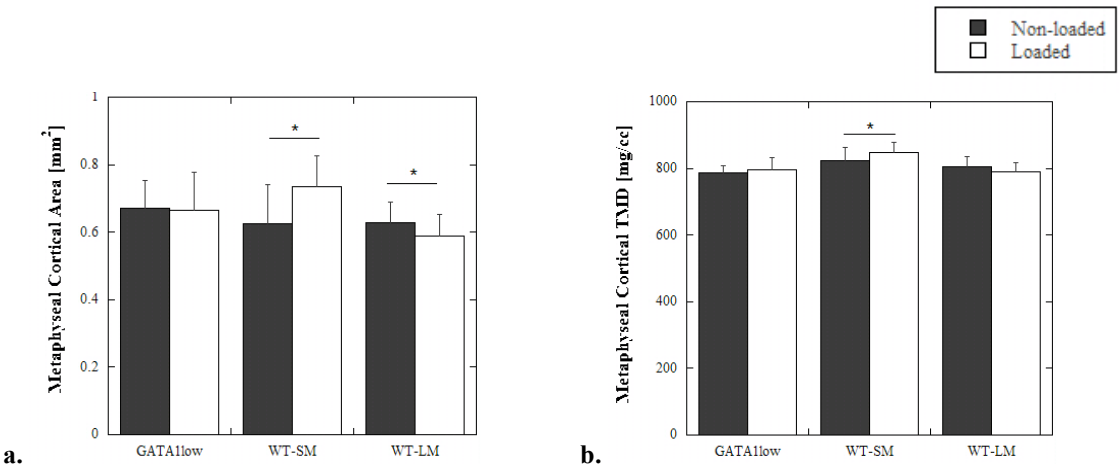

Figure 3.5: Graphical representation of selected metaphyseal cortical results from GATA-1^{low} and wild-type mice subject to two weeks of tibial loading. Significant differences were observed in (a) metaphyseal cortical area and (b) TMD in the WT-SM group. *$p < 0.05$ in loaded compared to non-loaded limbs within a group.

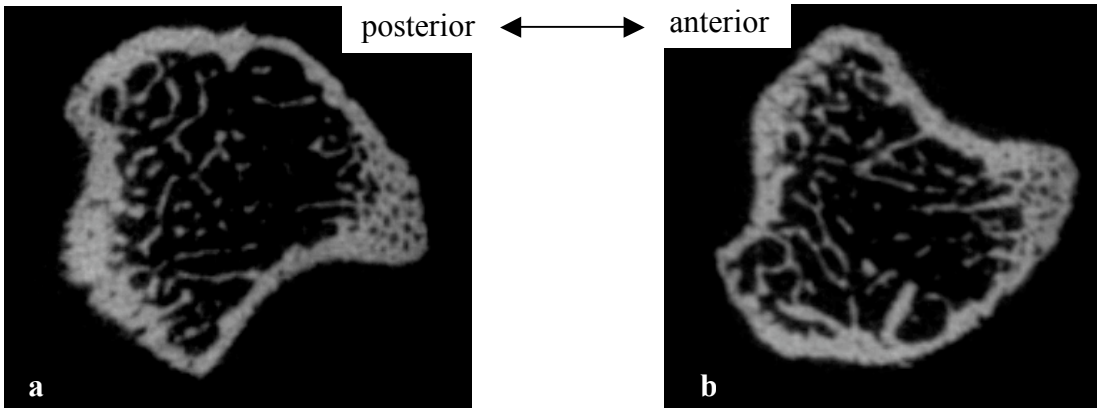

Figure 3.6: Representative μCT images of metaphyseal regions of tibiae from the WT-SM group. A thickening of the posterior cortex and reduction in BV/TV is qualitatively observable in (a) loaded compared to (b) non-loaded tibiae.

Table 3.5: Cortical parameters within the diaphyseal region of GATA-1^{low} and wild-type mice subject to two weeks of tibial loading.

		GATA-1^{low}	WT - SM	WT - LM
Inner Perimeter (mm)	Non-loaded	2.203 ± 0.079	2.183 ± 0.089	2.180 ± 0.076
	Loaded	2.226 ± 0.057	2.158 ± 0.138	2.159 ± 0.075
Outer Perimeter (mm)	Non-loaded	3.690 ± 0.196	3.656 ± 0.295	3.581 ± 0.117
	Loaded	3.677 ± 0.229	3.587 ± 0.305	3.533 ± 0.146 *
Marrow Area (mm^2)	Non-loaded	0.360 ± 0.028	0.631 ± 0.131	0.355 ± 0.026
	Loaded	0.366 ± 0.026	0.610 ± 0.144	0.347 ± 0.024
Cortical Area (mm^2)	Non-loaded	0.649 ± 0.096	0.632 ± 0.131	0.605 ± 0.047
	Loaded	0.643 ± 0.110	0.611 ± 0.144	0.585 ± 0.057 *
TMD (mg/cc)	Non-loaded	1036.16 ± 19.02	1066.16 ± 26.69	1056.34 ± 22.67
	Loaded	1035.25 ± 26.98	1050.93 ± 27.51 *	1048.28 ± 25.82
Periosteal MS/BS (%)	Non-loaded	70.85 ± 22.48	56.97 ± 13.65	72.32 ± 21.18
	Loaded	68.88 ± 23.16	58.28 ± 19.90	49.01 ± 8.19
Periosteal MAR (μm/d)	Non-loaded	1.855 ± 0.823	1.021 ± 1.291	1.827 ± 0.335
	Loaded	1.541 ± 0.808	1.244 ± 1.389	1.212 ± 0.759
Periosteal BFR ($\mu m^3/\mu m^2/d$)	Non-loaded	1.371 ± 0.962	0.713 ± 1.065	1.363 ± 0.597
	Loaded	1.193 ± 0.947	0.915 ± 1.268	0.607 ± 0.378
Endosteal MS/BS (%)	Non-loaded	47.17 ± 16.20	53.11 ± 18.12	71.31 ± 16.52
	Loaded	47.52 ± 18.94	61.97 ± 15.19	53.12 ± 9.62
Endosteal MAR (μm/d)	Non-loaded	0.809 ± 0.373	0.558 ± 0.702	0.832 ± 0.308
	Loaded	0.488 ± 0.566	0.076 ± 0.133	0.472 ± 0.543
Endosteal BFR ($\mu m^3/\mu m^2/d$)	Non-loaded	0.400 ± 0.248	0.236 ± 0.281	0.630 ± 0.327
	Loaded	0.198 ± 0.228	0.053 ± 0.097	0.286 ± 0.349

WT mice were either strain-matched (WT-SM; n=9) or load-matched (WT-LM; n=9) to GATA-1^{low} (n=9) loading conditions. Histomorphometric analysis was performed on n=5 specimens per group. Data represents mean ± SD. *$p < 0.05$ in loaded compared to non-loaded limbs within a group.

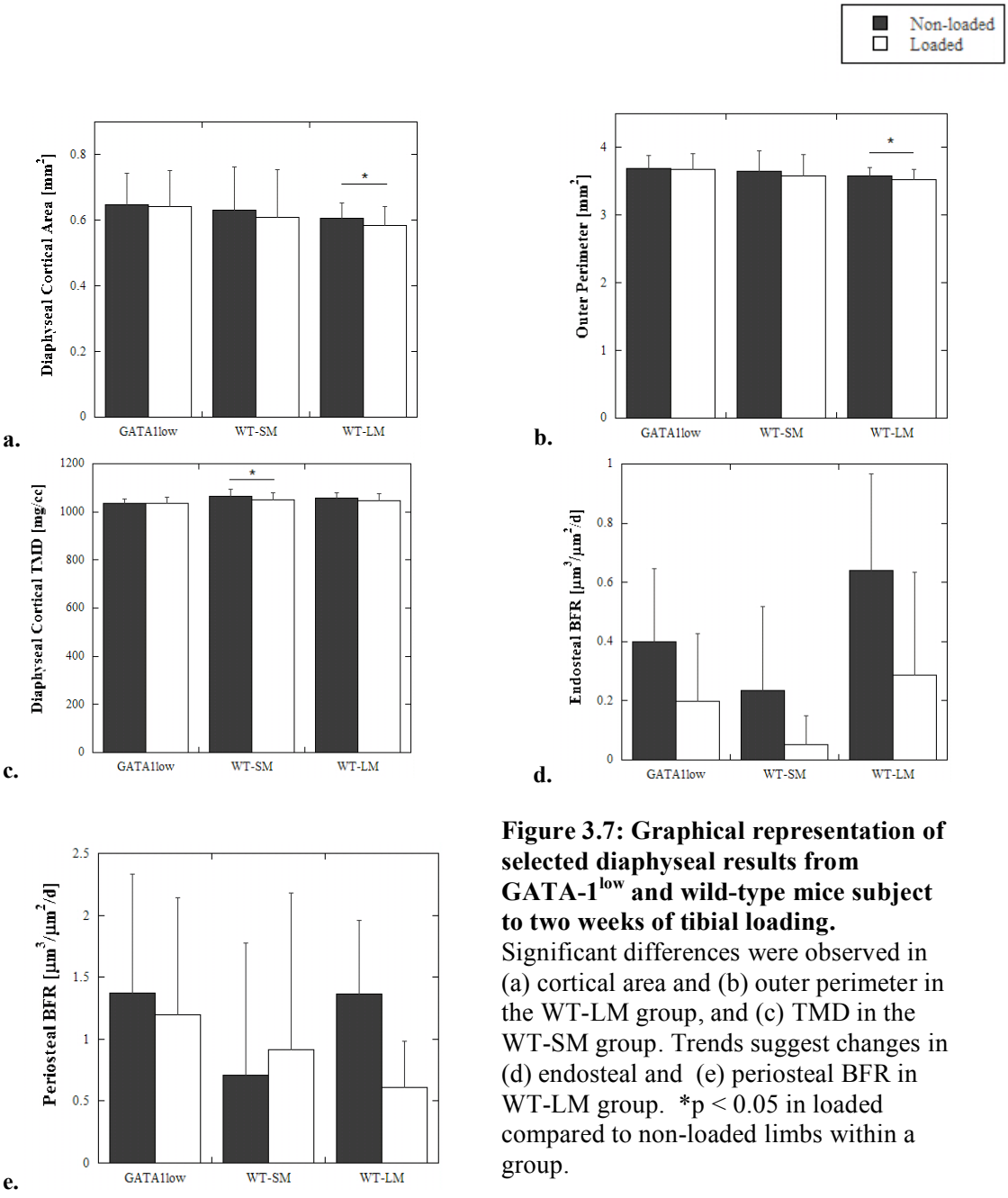

Figure 3.7: Graphical representation of selected diaphyseal results from GATA-1^{low} and wild-type mice subject to two weeks of tibial loading. Significant differences were observed in (a) cortical area and (b) outer perimeter in the WT-LM group, and (c) TMD in the WT-SM group. Trends suggest changes in (d) endosteal and (e) periosteal BFR in WT-LM group. *$p < 0.05$ in loaded compared to non-loaded limbs within a group.

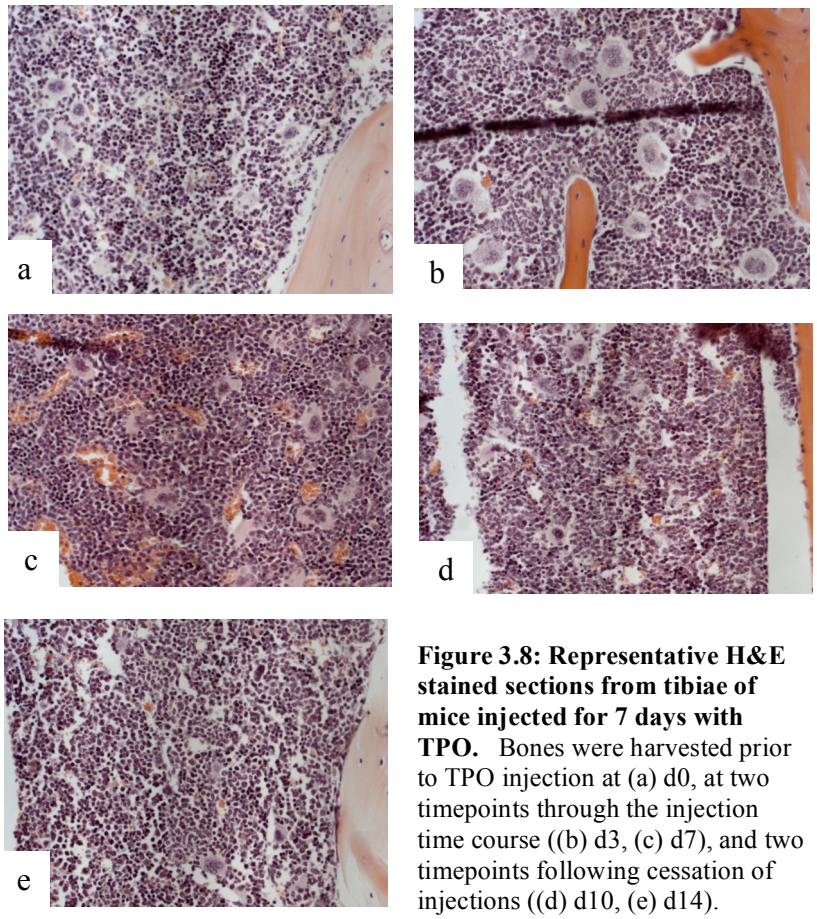

Figure 3.8: Representative H&E stained sections from tibiae of mice injected for 7 days with TPO. Bones were harvested prior to TPO injection at (a) d0, at two timepoints through the injection time course ((b) d3, (c) d7), and two timepoints following cessation of injections ((d) d10, (e) d14).

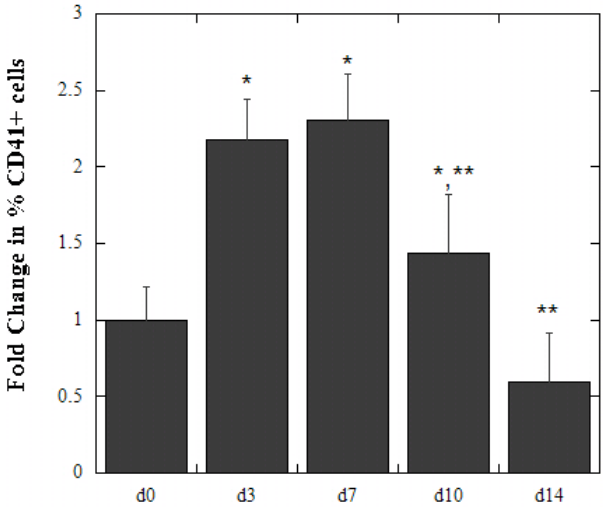

Figure 3.9 – FACS analysis of CD41+ cells from mice injected for 7d with TPO. Marrow was flushed from four animals per group and duplicate samples per animal were assessed for percentage of CD41+ cells. *p<0.05 rel to d0, **p<0.05 rel to d3

Table 3.6: µCT analysis of tibiae from mice injected for 7d with TPO.

	d0	d3	d7	d10	d14
Trabecular Parameters					
BV/TV	0.211 ± 0.041	0.202 ± 0.037	0.204 ± 0.026	0.227 ± 0.018	0.205 ± 0.082
BS/BV	50.220 ± 5.275	52.436 ± 5.280	50.741 ± 4.326	47.949 ± 3.229	50.275 ± 9.428
Tb.Th.	0.040 ± 0.004	0.038 ± 0.004	0.040 ± 0.003	0.042 ± 0.003	0.041 ± 0.008
Tb.N.	5.224 ± 0.627	5.228 ± 0.527	5.127 ± 0.398	5.410 ± 0.127	4.889 ± 1.034
Tb.Sp.	0.154 ± 0.028	0.154 ± 0.022	0.156 ± 0.017	0.143 ± 0.006	0.170 ± 0.048
Cortical Parameters - Metaphyseal Region					
Inner Perimeter (mm)	5.378 ± 0.163	5.418 ± 0.194	5.311 ± 0.150	5.570 ± 0.156	5.295 ± 0.159
Outer Perimeter (mm)	7.5444 ± 0.5032	7.406 ± 0.266	7.293 ± 0.212	7.759 ± 0.329	7.339 ± 0.505
Marrow Area (mm^2)	1.5598 ± 0.0667	1.622 ± 0.052	1.548 ± 0.067	1.696 ± 0.114	1.599 ± 0.107
Cortical Area (mm^2)	0.8005 ± 0.0713	0.771 ± 0.090	0.797 ± 0.059	0.874 ± 0.064	0.846 ± 0.128
Cortical Parameters - Diaphyseal Region					
Inner Perimeter (mm)	2.2770 ± 0.07662	2.263 ± 0.107	2.310 ± 0.112	2.326 ± 0.140	2.322 ± 0.124
Outer Perimeter (mm)	3.9614 ± 0.1771	3.9506 ± 0.2164	3.926 ± 0.162	4.072 ± 0.280	3.978 ± 0.221
Marrow Area (mm^2)	0.3799 ± 0.0223	0.3759 ± 0.0293	0.396 ± 0.034	0.400 ± 0.053	0.399 ± 0.040
Cortical Area (mm^2)	0.7871 ± 0.0764	0.740 ± 0.061	0.753 ± 0.059	0.833 ± 0.116	0.781 ± 0.089

Bones (n=4 per group) were harvested prior to TPO injection (d0), at two timepoints through the injection time course (d3, d7), and two timepoints following cessation of injections (d10, d14). Data represents mean ± SD.

Table 3.7: Tibial length as determined from μCT images of TPO and vehicle treated mice subject to two weeks of tibial loading.

		VEH	TPO
Length (mm)	Non-loaded	16.045 ± 0.288	15.916 ± 0.345
	Loaded	15.742 ± 0.244 *	15.626 ± 0.320 *

Data represents mean ± SD for vehicle (n=6) or TPO-treated (n=5) mice. *$p < 0.05$ in loaded compared to non-loaded limbs within a group.

Table 3.8: Trabecular parameters of TPO and vehicle treated mice subject to two weeks of tibial loading.

		VEH	TPO
BV/TV	Non-loaded	0.175 ± 0.053	0.146 ± 0.049
	Loaded	0.122 ± 0.040 *	0.097 ± 0.027 *
BS/BV	Non-loaded	56.679 ± 8.114	59.127 ± 8.836
	Loaded	61.159 ± 7.920 *	62.578 ± 4.974
Tb.Th.	Non-loaded	0.036 ± 0.005	0.035 ± 0.006
	Loaded	0.033 ± 0.005 *	0.032 ± 0.003
Tb.N.	Non-loaded	4.793 ± 0.729	4.152 ± 0.697
	Loaded	3.612 ± 0.687 *	2.988 ± 0.642 *
Tb.Sp.	Non-loaded	0.177 ± 0.038	0.212 ± 0.047
	Loaded	0.252 ± 0.059 *	0.314 ± 0.072 *
TMD (mg/cc)	Non-loaded	543.90 ± 19.73	535.96 ± 21.40
	Loaded	527.40 ± 16.75 *	528.57 ± 10.73
MS/BS (%)	Non-loaded	24.65 ± 6.17	19.37 ± 11.30
	Loaded	25.03 ± 8.56	17.26 ± 7.38
MAR (μm/d)	Non-loaded	1.478 ± 0.382	1.257 ± 0.876
	Loaded	1.572 ± 0.199	1.088 ± 0.681
BFR ($\mu m^3/\mu m^2/d$)	Non-loaded	0.368 ± 0.142	0.181 ± 0.147
	Loaded	0.382 ± 0.102	0.200 ± 0.206

Data represents mean ± SD for vehicle (n=6) or TPO-treated (n=5) mice. Histomorphometric analysis was performed on n=5 specimens per group. *$p < 0.05$ in loaded compared to non-loaded limbs within a group.

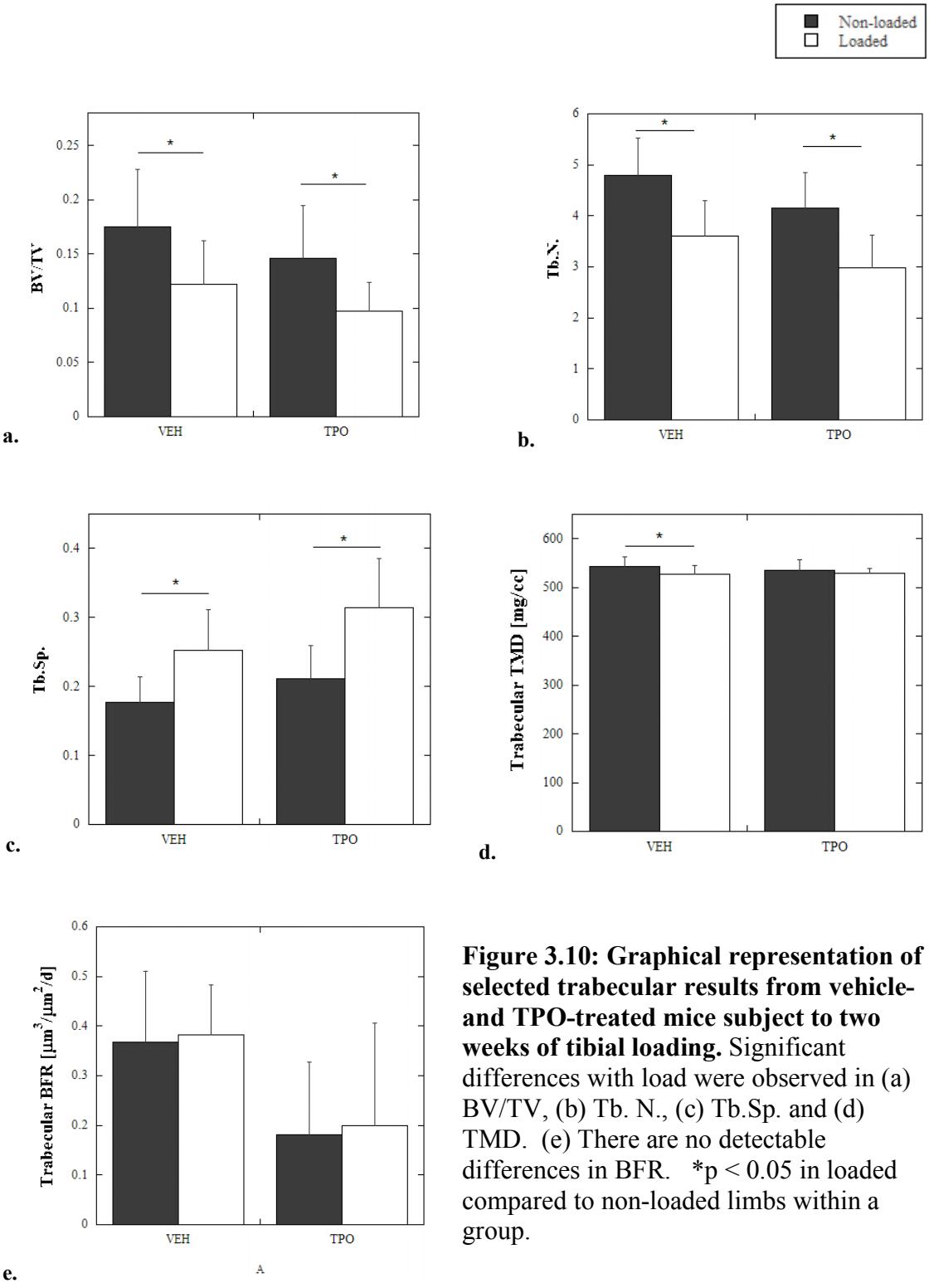

Figure 3.10: Graphical representation of selected trabecular results from vehicle- and TPO-treated mice subject to two weeks of tibial loading. Significant differences with load were observed in (a) BV/TV, (b) Tb. N., (c) Tb.Sp. and (d) TMD. (e) There are no detectable differences in BFR. *$p < 0.05$ in loaded compared to non-loaded limbs within a group.

Table 3.9: Cortical parameters within the metaphyseal region of TPO and vehicle treated mice subject to two weeks of tibial loading.

		VEH	TPO
Inner Perimeter (mm)	Non-loaded	5.533 ± 0.142	5.420 ± 0.208
	Loaded	5.424 ± 0.120	5.327 ± 0.179
Outer Perimeter (mm)	Non-loaded	7.044 ± 0.286	6.772 ± 0.322
	Loaded	6.947 ± 0.187	6.769 ± 0.308
Marrow Area (mm^2)	Non-loaded	1.724 ± 0.095	1.676 ± 0.137
	Loaded	1.654 ± 0.080	1.617 ± 0.098
Cortical Area (mm^2)	Non-loaded	0.691 ± 0.094	0.671 ± 0.077
	Loaded	0.737 ± 0.078 *	0.742 ± 0.068 *
TMD (mg/cc)	Non-loaded	840.89 ± 17.49	841.41 ± 6.63
	Loaded	860.67 ± 15.83 *	876.80 ± 21.09 *

Data represents mean ± SD for vehicle (n=6) or TPO-treated (n=5) mice. *$p < 0.05$ in loaded compared to non-loaded limbs within a group.

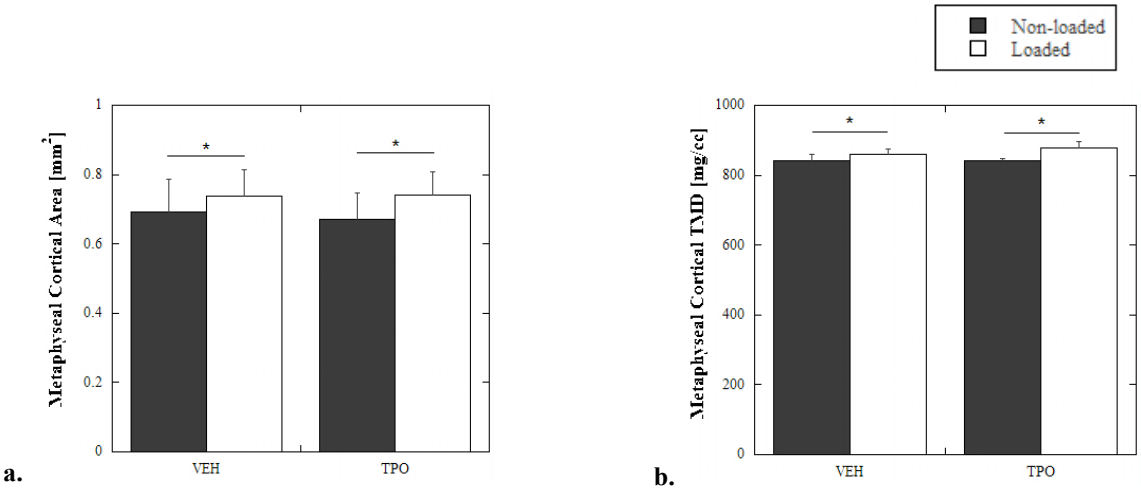

Figure 3.11: Graphical representation of selected metaphyseal cortical results from vehicle- and TPO-treated mice subject to two weeks of tibial loading.
(a) Metaphyseal cortical area and (b) TMD increased significantly with load in both groups. *$p < 0.05$ in loaded compared to non-loaded limbs within a group.

Table 3.10: Cortical parameters within the diaphyseal region of TPO and vehicle treated mice subject to two weeks of tibial loading.

		VEH	TPO
Inner Perimeter (mm)	Non-loaded	2.159 ± 0.056	2.160 ± 0.124
	Loaded	2.131 ± 0.098	2.158 ± 0.071
Outer Perimeter (mm)	Non-loaded	3.682 ± 0.182	3.685 ± 0.219
	Loaded	3.596 ± 0.197	3.606 ± 0.225
Marrow Area (mm^2)	Non-loaded	0.347 ± 0.017	0.348 ± 0.039
	Loaded	0.340 ± 0.029	0.347 ± 0.026
Cortical Area (mm^2)	Non-loaded	0.677 ± 0.085	0.672 ± 0.086
	Loaded	0.634 ± 0.097 *	0.639 ± 0.084 *
TMD (mg/cc)	Non-loaded	1087.32 ± 14.21	1078.50 ± 7.58
	Loaded	1083.90 ± 8.65	1072.64 ± 18.28
Periosteal MS/BS (%)	Non-loaded	64.24 ± 22.77	70.24 ± 19.52
	Loaded	67.39 ± 15.23	58.39 ± 23.92 *
Periosteal MAR (μm/d)	Non-loaded	1.255 ± 0.928	1.421 ± 1.380
	Loaded	0.820 ± 0.297	0.894 ± 0.848
Periosteal BFR ($\mu m^3/ \mu m^2/d$)	Non-loaded	0.934 ± 0.885	1.092 ± 1.062
	Loaded	0.543 ± 0.247	0.609 ± 0.558
Endosteal MS/BS (%)	Non-loaded	42.61 ± 13.67	51.71 ± 12.24
	Loaded	50.64 ± 12.18	40.25 ± 7.92
Endosteal MAR (μm/d)	Non-loaded	0.483 ± 0.595	0.495 ± 0.240
	Loaded	0.713 ± 0.465	0.535 ± 0.522
Endosteal BFR ($\mu m^3/ \mu m^2/d$)	Non-loaded	0.261 ± 0.351	0.255 ± 0.132
	Loaded	0.394 ± 0.280	0.193 ± 0.172

Data represents mean ± SD for vehicle (n=6) or TPO-treated (n=5) mice. Histomorphometric analysis was performed on n=5 specimens per group. *$p < 0.05$ in loaded compared to non-loaded limbs within a group.

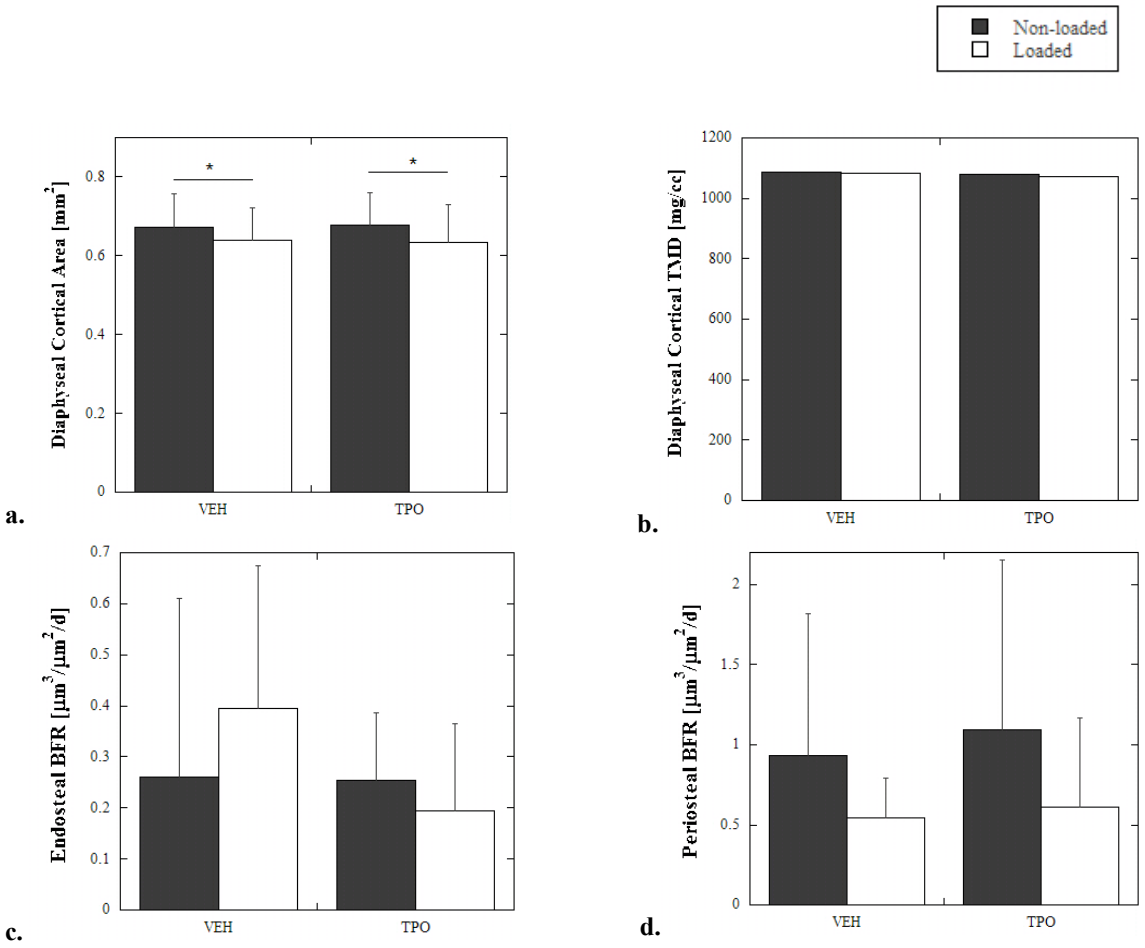

Figure 3.12: Graphical representation of selected diaphyseal results from vehicle- and TPO-treated mice subject to two weeks of tibial loading. (a) Cortical area decreases in both groups, while (b) TMD is unchanged. (c) BFR at the endosteal surface is minimally affected by load, whereas (d) BFR at the periosteal surface appears to decrease with load. *$p < 0.05$ in loaded compared to non-loaded limbs within a group.

CHAPTER IV

FUNCTIONAL CONSEQUENCES OF MEGAKARYOCYTE MECHANORESPONSIVENESS: EFFECTS OF MECHANICAL STIMULUS ON MEGAKARYOCYTE/OSTEOBLAST INTERACTIONS

Introduction

Studies of MK in culture have highlighted the robust effects these cells can have on osteoblasts and their progenitor cells. When cultured in the presence of MKs, osteoblasts demonstrate an enhanced proliferative capacity compared with cells in the absence of MKs (55). This phenomenon was shown to be dependent upon cell-cell contact and was not observed when osteoblasts were solely cultured in conditioned media from MKs. Mesenchymal stem cells (MSCs) cultured in the presence of CD61-positive cells (i.e. MKs) form more colonies by CFU-f assay, and specifically more alkaline phosphatase-positive colonies than cells cultured with the CD61-negative fraction of marrow aspirates (57).

Though MKs enhance the proliferation of osteoblasts when co-cultured, their effects on osteoblast differentiation are not as well-documented. Bord, et al. demonstrated that osteoblasts cultured in the presences of MKs for 24 hours express elevated levels of type I collagen in the presence of MKs compared with cells cultured

alone (125). In contrast, Ciovacco, et al. found that, after 14 days of culture in differentiation medium, osteoblasts cultured with MK demonstrate significant decreases in expression of alkaline phosphatase, osteocalcin, and type I collagen, as well as decrease in calcium deposition, compared with osteoblasts alone (56).

In the final set of experiments, we sought to address whether mechanical stimulation of MK in culture would have any impact on these cells' effects on osteoblast proliferation and differentiation.

Methods

Cell Culture

Meg-01 cells (ATCC; Manassas, VA) were maintained in RPMI + 10% fetal bovine serum + 1% Penicillin-Streptomycin. To prepare for fluid shear, slides were washed sequentially in 20% sulfuric acid, tap water, and 0.1M sodium hydroxide. After rinsing in ethanol, slides were exposed to 2% γ-aminopropyltriethoxysilane followed by an incubation in 0.25% gluteraldehyde. Cast silicone chambers coated with an adhesive sealant were pressed onto the covalently modified slides, creating a sealed well to allow cells seeded on the slide to be cultured until ready to load.

Plates were coated with 0.1% gelatin (Sigma-Aldrich; St. Louis, MO) for 1 h at room temperature. Following substrate coating, plates were rinsed with PBS and serum-free media, and cells were then plated in DMEM + 10% fetal bovine serum + 1% Penicillin-Streptomycin. Cells were seeded either at a density of 100,000 cells/plate (for UT condition) or 250,000 cells/plate (for sham and 1 Pa conditions). These were determined to yield approximately 50,000 cells remaining adherent to the plate following

their respective treatment (data not shown). After 24 h in culture, the media was changed to serum-free conditions for approximately 16 hours.

Fluid Shear Loading

Silicone chambers were removed from the plate seeded with cells and the plates were inserted into parallel plate flow chambers as described in Chapter 2. Only one condition, a flow rate generating 1 Pa shear stress for 30 minutes, was selected since it still elicited a robust mechanoresponse (as shown in Chapter 2) but resulted in fewer cells shearing off the plate than the 2 Pa condition. Plates were also subject to sham treatment or harvested untouched as before. Conditioned media from each treatment group was also harvested for proliferation studies. Media was centrifuged to remove cellular debris, and fetal bovine serum and Penicillin + streptomycin were added and sterile filtered using a 0.22 μm syringe filter. 50,000 MC3T3 were then resuspended in conditioned media and plated in 6-well dishes.

Immediately following treatment, slides were placed in a sterile 10 cm dish and 1 mL of a 50,000 cells/mL suspension MC3T3-E1 clone 4 pre-osteoblastic cells in DMEM + 10% fetal bovine serum + 1% Penicillin-Streptomycin were added directly to the slide. After approximately 16 hours, 12 mL fresh media was added. For plates to be used in mineralization studies, co-cultures were maintained with antiobiotic-antimycotic in lieu of penicillin-streptomycin to minimize fungal contamination that was prone to develop in handled plates.

Assessment of proliferation

In order to specifically quantify proliferation of MC3T3 within co-culture plates, we took advantage of the fact that these cell lines are derived from different species – MC3T3 from mouse and Meg-01 from human. Therefore we used PCR using species-specific markers to amplify genomic DNA as a surrogate measure for cell number. After 3 days in culture, plates were rinsed with sterile PBS and stored at -80 °C. Cells were harvested in 200 μL PBS and genomic DNA extracted using the DNeasy Blood & Tissue kit (Qiagen; Valencia, CA) according to the manufacturer's instructions. PCR was performed on the resulting genomic DNA using species-specific primers for cox-1 (126). We confirmed that, in fact, mouse primers did specifically amplify MC3T3 cells, and also that a linear relationship exists between c(t) value and $\log_2$(DNA content) from serial dilutions of known quantities of DNA (Figure 4.1). Data reflects three independent experiments with 2-4 plates per condition for each experiment.

Mineralization studies

After 3 days in culture, the media was replaced with differentiation media containing 10mM β-glycerophosphate (BGP) (Sigma-Aldrich; St. Louis, MO) and 50μg/mL L-ascorbic acid (Sigma-Aldrich; St. Louis, MO). Media was replaced every three days, with fresh BGP and ascorbic acid being added fresh each time.

RNA extraction, Reverse transcription and PCR

Plates were harvested at days 0 (prior to addition of differentiation media), 4, 9, and 14 following addition of differentiation media to assess changes in gene expression

representative of osteoblast maturation. At the indicated day of harvest, cells were rinsed with PBS and stored at -70° C until further processing. Samples were lysed in Buffer RLT (Qiagen; Valencia, CA) + β-mercaptoethanol and homogenized using Qiashredder columns. RNA was isolated using the RNeasy kit (Qiagen; Valencia, CA) according to the manufacturer's instructions. RNA was quantified and 1 μg of RNA was reverse transcribed using Superscript III reverse transcriptase and primed by random hexamers. Real-time PCR was performed and amplification of gene products was determined by the incorporation of SYBR Green fluorescent nucleic acid stain (Invitrogen; Carlsbad, CA). Expression of Runx2, osterix, osteocalcin, and bone sialoprotein were all normalized to β-actin. Primer sequences for gene expression studies (Table 4.1) were selected based on previously published work (127). We also confirmed that these primers specifically detected gene expression from mouse-derived MC3T3 and not the human-derived Meg-01 cells (data not shown). Data represents two independent experiments with 2-4 plates per condition per timepoint for each experiment.

Alizarin Red S staining

At 21days, plates were rinsed with sterile PBS and allowed to air dry. 50% ethanol was then added for 3 minutes, aspirated, and Alizarin Red S stain added for 5 minutes. Plates were rinsed several times with ddH2O to remove excess stain and allowed to air dry before scanning.

Calcium assay

Cell layers from 18- or 21-day cultures were scraped directly into 1.5 mL tubes and incubated in 0.5M HCl for 1 hr at room temperature. Samples were centrifuged for 10 min. at 6,000 x g and supernatant removed and stored at -20 °C until assayed. Calcium content was determined using a QuantiChrom™ calcium assay kit (BioAssay systems; Hayward, CA) and optical densities from the colorimetric assay were read at 612 nm on a SpectraMax5 spectrophotometer (Molecular Devices; Sunnyvale, CA).

Statistics

To determine statistical significance, one-way ANOVA was used to assess differences across groups. For proliferation studies, MC3T3 cultured in the presence of Meg-01 directly or conditioned media were compared to MC3T3 only control to assess effect of treatment of MK on the resulting osteoblast proliferation. For gene expression studies, a one-way ANOVA was conducted across different treatment groups at the same timepoint to assess effect of MK treatment on osteoblast mineralization potential. In all experiments, statistical significance was determined at $p < 0.05$.

Results

MC3T3 cells cultured in the presence of Meg-01 cells, but not conditioned media from these cells, demonstrate pronounced increase in proliferation relative to MC3T3-only controls after 3 days in culture (Figure 4.2). However, there is no significant effect of mechanical stimulation of MKs on their resultant effects on MC3T3 proliferation. The fold-change in mouse genomic DNA content in UT Meg-01 and sham treated Meg-01

containing co-cultures are significantly higher than MC3T3 only controls ($p<0.05$). However, the corresponding quantity in 1Pa-treated Meg-01 containing co-cultures was not statistically significant over MC3T3 only plates (though still greatly enhanced). This suggests a trend in a decreased effect on proliferation from Meg-01 cells exposed to fluid shear compared to UT or sham treated cells.

To assess effects of Meg-01 on MC3T3 differentiation, we looked at expression of several markers of osteoblastic maturation. Runx2 and osterix are transcription factors that are critical in the early stages of osteoblast differentiation (128,129). Osteocalcin and bone sialoprotein are extracellular matrix proteins that are expressed later in the differentiation cascade (130,131). We utilized RT-PCR to detect changes in the expression of these genes normalized to levels of β-actin over 14 days in the presence of differentiation media. Figure 4.3 demonstrates the results for MC3T3 cultured in the presence of UT, sham-treated, or 1 Pa sheared Meg-01 cells. Globally, expression of all markers of osteoblast differentiation increase over the course of the 14-day experiment, as expected. The data suggests that the expression of each of these markers is diminished in MC3T3 cultured in the presence of 1 Pa treated Meg-01 cells compared to those cultured in the presence of UT or sham-treated Meg-01, though only a few comparisons across treatment groups for a given timepoint are statistically significant. Only osteocalcin expression at d4 and BSP expression at d4 and d14 were found to be significantly lower in co-cultures with 1 Pa treated Meg-01 compared to those with sham-treated Meg-01 cells.

Qualitative assessment of Alizarin Red S stained co-cultures, however, indicate enhanced mineralization of MC3T3 in the presence of mechanically-perturbed (i.e. either

sham or 1 Pa treated) Meg-01 cells compared with co-cultures containing UT Meg-01 (Figure 4.4). However, variation in the amount of Alizarin-staining nodules across two independent experiments also highlights the variability in the extent of mineralization in this co-culture system.

Results from calcium assays quantitatively confirm the observations from Alizarin experiments (Figure 4.5). Co-cultures of MC3T3 with both sham-treated Meg-01 and Meg-01 exposed to 1 Pa shear contain significantly higher amounts of matrix-bound calcium than co-cultures with UT Meg-01.

Discussion

We have developed a system to address the hypothesis that mechanical stimulation of MKs will impact the effects these cells have on osteoblast behavior. We have confirmed that, as reported in the literature, we see a substantial effect of the presence of MKs on osteoblast proliferation when in co-culture, but not when osteoblasts are cultured in the presence of MK-conditioned media. However there is no dramatic effect of mechanical stimulation on MKs on their resultant proliferative-inducing effects on MC3T3. Our data suggests a small but non-significant decrease in MC3T3 cell number, as determined by quantity of genomic DNA, in the co-cultures in the presence of 1Pa-stimulated Meg-01 compared with UT or sham-treated Meg-01.

An understanding of what proliferative factors may be differentially regulated in response to load would necessitate further exploration of the specific mechanism by which MKs impact osteoblast proliferation in static culture, which is not well-documented. MKs secrete various growth factors, such as basic fibroblast growth factor

(bFGF), transforming growth factor β (TGF β) and platelet derived growth factor (PDGF), which are all potent inducers of osteoblast proliferation (132-134). It is thought that TGF-β is a key regulator of the myelofibrosis and osteosclerosis seen in a TPO-overexpression model. Irradiated mice transplanted with marrow from TGF β-/- mice retrovirally expressing TPO demonstrated no signs of myelofibrosis or osteosclerosis, unlike recipients with TGF β+/+ marrow (135). However, in contrast, MKs isolated from GATA-1^{low} mice express lower levels of PDGF and TGF-β than those from wild-type mice (109). Therefore, the increase in bone formation is not necessarily a product simply of elevated growth factor expression, but still may be an important regulator in the effects MKs have on osteoblasts.

Importantly, this phenomenon, as we and others have shown, necessitates direct cell-cell contact. In reference back to the physiological context of these cells as outlined in Chapter 1, it seems more plausible that MKs, should they have any significant effects on the behavior of osteoblasts or their progenitor cells, would have these effects before they have fully matured and migrated to bone marrow vasculature. This conceptually provides more evidence that direct effects of MKs *in vivo* would more likely arise from immature megakaryocytes located in close proximity to osteoblasts and MSC rather than mature cells residing near sinusoids.

The effect of mechanical stimulation of MKs on the differentiation of co-cultured MC3T3 is somewhat perplexing. Alizarin Red staining qualitatively suggests an increase in mineralization of co-cultures with mechanically stimulated Meg-01 cells (either by shear stress, or simply by handling as evidenced by the sham treated condition). Importantly, this observation is corroborated by quantitative findings that there is more

calcium present (and therefore enhanced mineral formation) in these mechanically-stimulated co-cultures. However, this is contradicted by gene expression studies which suggest an impaired, or delayed, differentiation of MC3T3 cultured in the presence of 1 Pa-treated Meg-01 compared with sham-treated controls. These results are not statistically significant due to the large variability across experiments, with the exception of OCN expression at d4 and BSP at d4 and d14. However, strong trends were also noted for changes in runx2 expression at d9 ($p=0.06$), BSP at d9 ($p=0.1$), Osx at d14 ($p=0.16$), and OCN at both d9 ($p=0.13$) and d14 ($p=0.15$) in co-cultures with1Pa-treated Meg-01 compared to those with sham-treated cells.

A definitive explanation to account for these two apparently contradictory findings remains elusive. Generally, increases in mineral formation in culture are accompanied by increases in expression of markers associated with osteoblast maturity. The apparent increase in mineralization in mechanically-perturbed cultures combined with concommittant decreases in the expression of genes indicative of osteoblast maturation in these same cultures may indicate that MKs could have other direct effects on formation of mineralized nodules independent of osteoblast maturation. We observed that, oftentimes, there were more mineralized nodules formed in regions of the plate heavily occupied by MKs, whereas in other areas of the plate with fewer MKs present, there were fewer mineralized nodules present (Figure 4.6). It is important to recall that MKs themselves express various bone matrix proteins, such as osteonectin (62) and osteocalcin (63), as well as crosslinking proteins such as factor XIII (64). Though it is not clear what implications this might have on direct matrix formation, it highlights the potential complexity of the role of MKs on mineralization.

The variability seen in results from these co-culture experiments can undoubtedly by largely attributed to inherent limitations in the experimental system. Though we attempted to optimize conditions and cell-seeding densities to ensure that, following the handling of these plates, the same numbers of MKs would remain adherent, there are still inherent variations in the resulting numbers of cells. Furthermore, even when approximately the same numbers of cells remain adherent to the plate, it is impossible to control the spatial distribution of the resulting cells. This is an inherent complication by using the parallel-plate flow chamber for these studies. Recently an enclosed spinning disk shear device specifically for studying co-culture was developed by Taylor, et al., which would limit some of these complications (136). This device would also eliminate direct handling of cell-seeded plates which poses a major challenge for cell maintenance and experimental variability.

A more controlled method of mechanical stimulation, or rather one in which cell loss is minimized, would be critically important for a more robust assessment of effects of fluid shear on MKs and their impacts on co-cultured osteoblasts. Our results indicate some differences may be present, namely a reduction in osteoblast proliferation and enhancement of osteoblast mineralization. Further studies are necessary, however, to thoroughly investigate the mechanism driving this phenomenon.

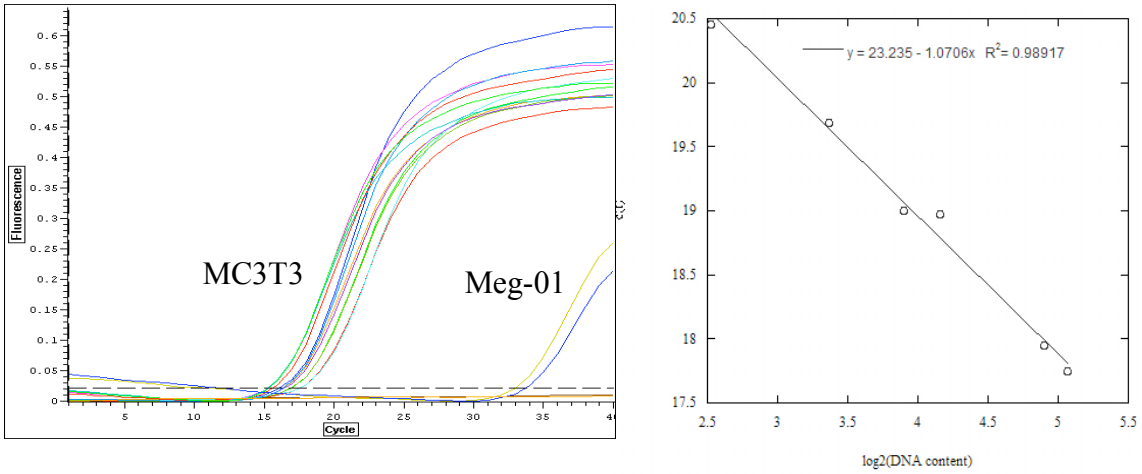

a. b.

Figure 4.1 – Validation of a technique using PCR to detect changes in mouse genomic DNA content as a surrogate measure of cell number. We confirmed that (a) PCR using mouse cox-1 primers on genomic DNA specifically amplifies product from MC3T3 and not Meg-01 cells, and (b) a linear relationship exists between c(t) value and $\log_2$(DNA content) for known dilutions of DNA, confirming that a change in c(t) value of 1 corresponds to a doubling in DNA quantity.

Table 4.1: Primer sequences for osteoblast differentiation gene expression studies

Gene	Forward	Reverse
Runx2	gtcagcaaagcttcttttcg	ttgttgctgttgctgttgtt
Osterix	tctctccatctgcctgactc	gtcagcgtatggcttctttg
Osteocalcin	cgctctgtctctctgacctc	tcacaagcagggttaagctc
Bone sialoprotein	ttccatcgaagaatcaaagc	tcgcagtctccattttcttc
β-actin	aagagctatgagctgcctga	tggcatagaggtctttacgg

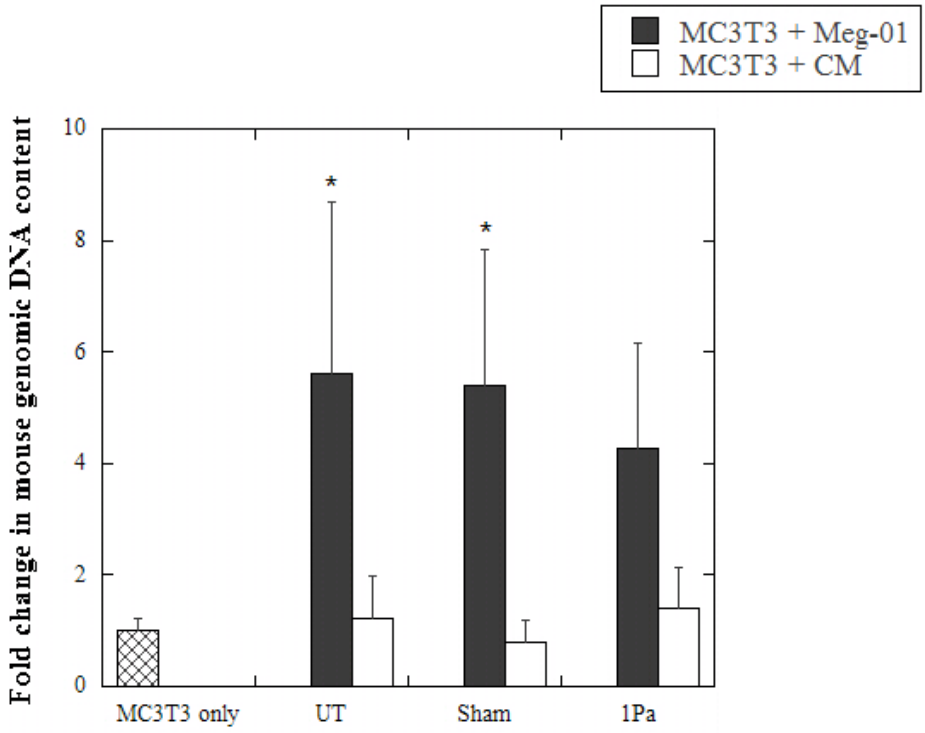

Figure 4.2 – Effects of mechanical stimulation of Meg-01 on MC3T3 proliferation. Cells or conditioned media (CM) from UT, sham, or 1Pa treated Meg-01 were cultured with MC3T3. Fold change in mouse genomic DNA content relative to MC3T3 only controls after 3 days in culture. Experiment was repeated three times in duplicate. Data represents mean ± SD. *$p<0.05$ compared to MC3T3 only control

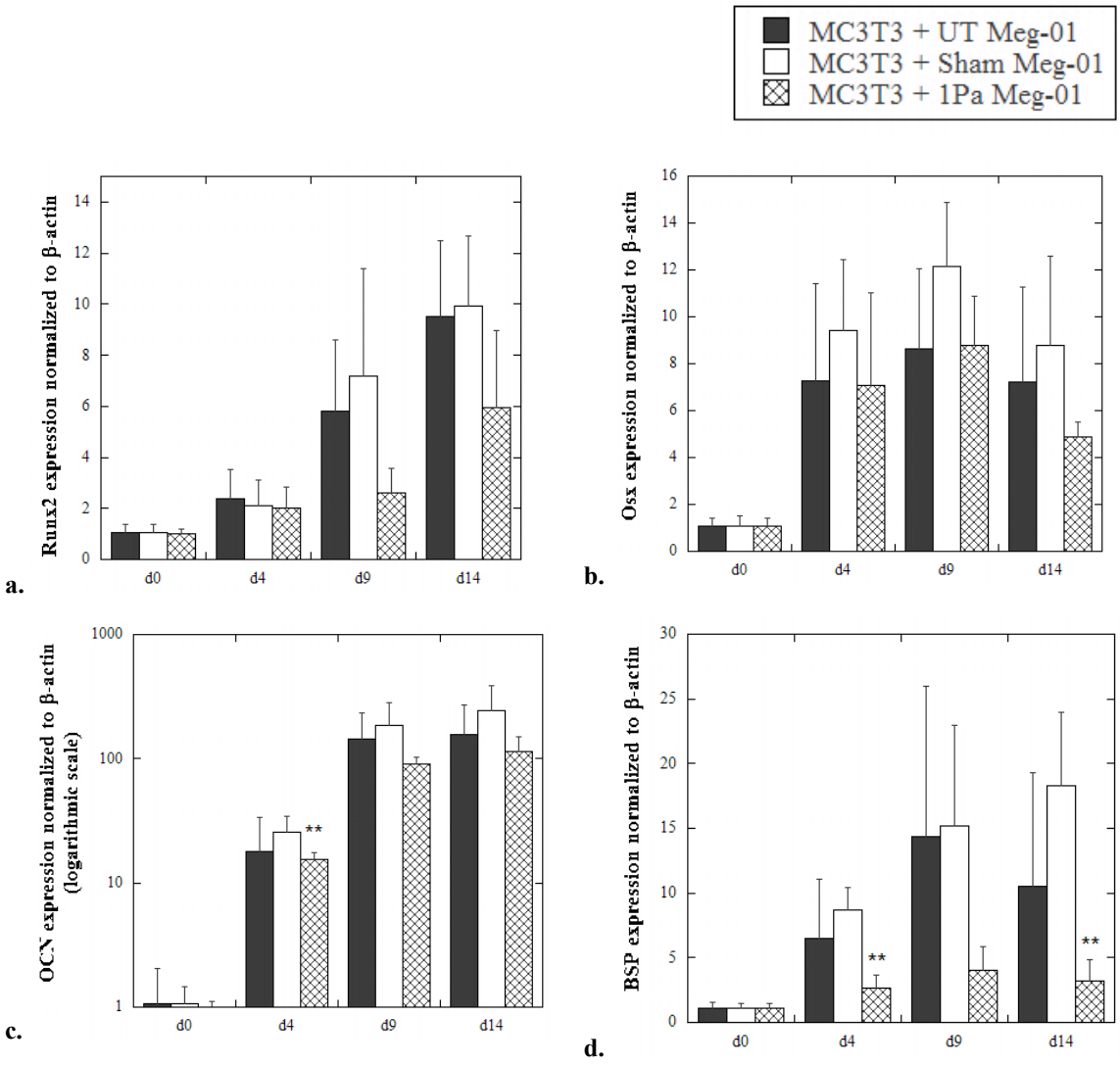

Figure 4.3 – Effects of mechanical stimulation of Meg-01 on consequent MC3T3 expression of osteoblastic differentiation markers. Expression of (a) Runx2, (b) osterix, (c) osteocalcin, and (d) bone sialoprotein were normalized to β-actin. Results for each treatment at a given timepoint are expressed relative to baseline expression for that treatment at d0. Data represents mean ± SD from two independent experiments with 2-4 samples per timepoint per experiment. **$p<0.05$ compared to MC3T3 + sham-treated Meg-01

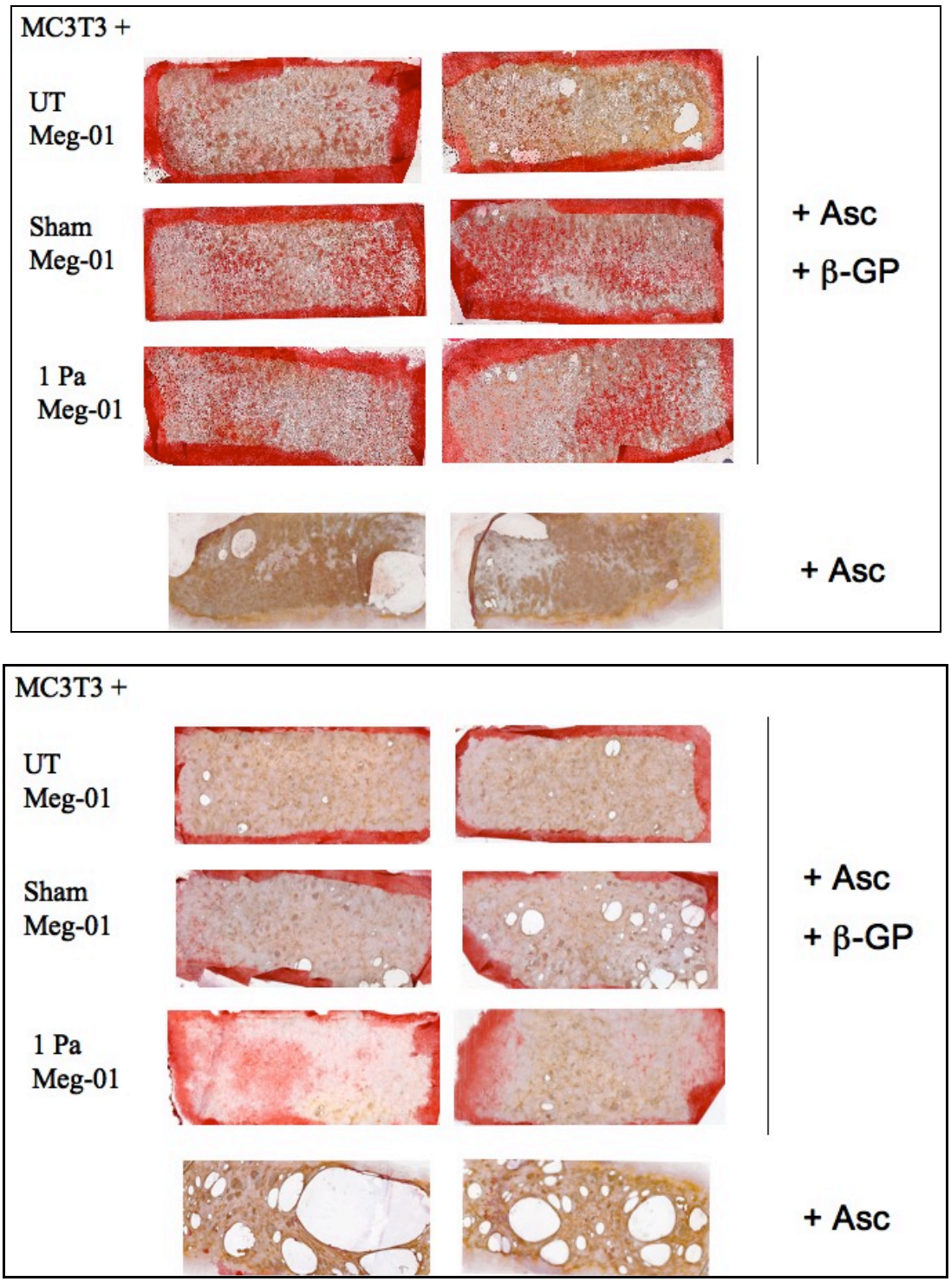

Figure 4.4 – Alizarin Red S staining of co-cultures of MC3T3 with UT, sham-, or 1Pa treated Meg-01 cells.

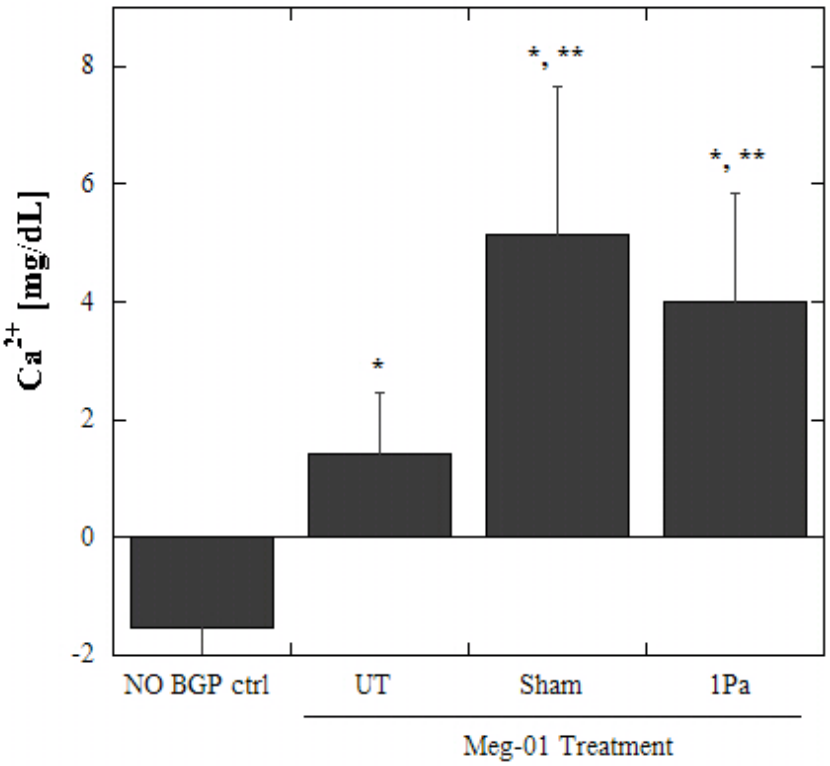

Figure 4.5 – Calcium content of MC3T3 co-cultured with UT, sham-, or 1Pa treated Meg-01 cells. Data represents mean ± SD from three independent experiments, with 2-5 plates for a given treatment per experiment. *$p<0.05$ relative to No BGP treated control. **$p<0.05$ relative to UT.

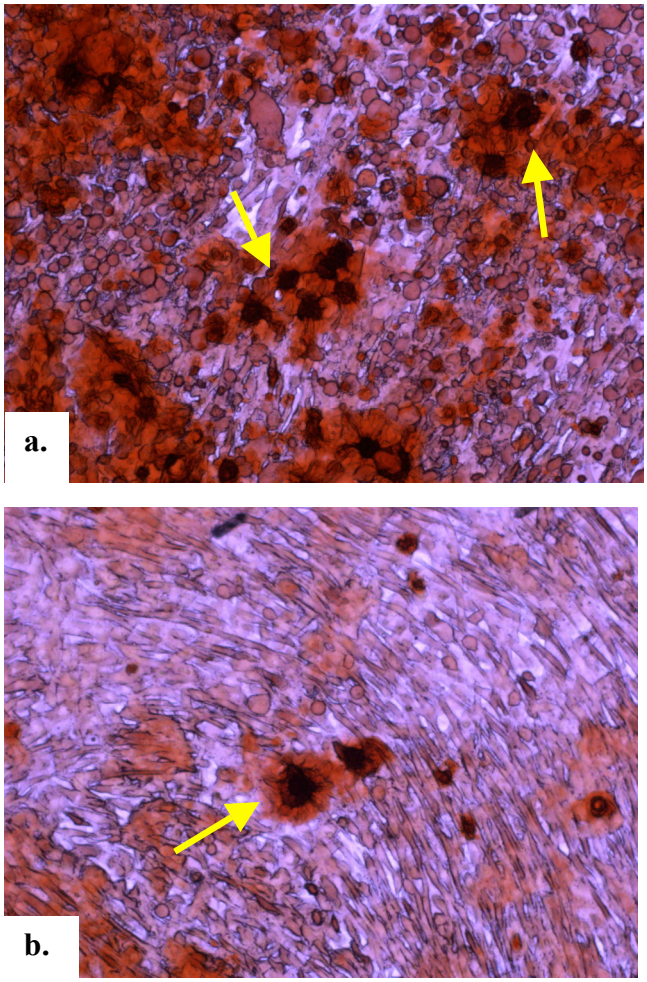

Figure 4.6 – Location of mineralized nodules in Meg-01/MC3T3 co-cultures.
Alizarin Red-positive nodules (arrows) tend to be more prominent in regions where more Meg-01 cells remain adherent (a) compared to regions less occupied by Meg-01 cells (b).

CHAPTER V

CONCLUSION

In this dissertation, we have set out to address a novel hypothesis that would broaden the discussion within the field about which cells may play a role in sensing and responding to applied loads in bone. MKs have been studied extensively in the hematology literature but have only recently gained the attention of bone biologists for their capacity to dramatically modulate the activity of osteoblasts, MSCs, and osteoclasts. Though there is evidence to suggest that MKs demonstrate some altered behavior when subject to mechanical perturbation *in vitro*, their mechanoresponse has not been well-characterized in a controlled environment, nor has it been assessed in an *in vivo* model of mechanical stimulation. Furthermore, the question of whether or not this mechanoresponse has any functional implications for their influences on bone cells has never been addressed.

In an effort to test our hypothesis we developed both *in vitro* and *in vivo* systems to address cellular mechanoresponsiveness as monitored by changes in gene expression. We adapted a parallel plate flow chamber previously developed in our lab to expose these cells to controlled fluid shear forces. Though the cell lines used can adhere to a matrix-coated substrate, they are not generally adherent cells and therefore the adhesion is transient and not robust. Our choice of substrate coatings, gelatin (denatured collagen) for

Meg-01 cells and fibronectin for PMA-treated K562 cells, were found to optimally enhance adhesion of these cells when exposed to fluid shear forces but are also constituents of the stromal matrix and therefore likely candidates for interactions *in vivo*. However, the physiologic matrix is much more complex, composed of various matrix proteins and, perhaps more importantly, would be a much more compliant structure than a hard glass surface. Perhaps encapsulating these cells in a 3-dimensional matrix and subjecting them to fluid flow in a bioreactor would be a more accurate representation of the cells' native mechanical environment.

We also developed a device, based on previously reported models, to apply controlled mechanical stimulus to the mouse tibia. Though we were able to detect changes in gene expression of a key mechanosensitive gene, c-fos, as a result of applied force, this model may not be the most appropriate means of determining long-term adaptive effects of load on bone. Given the surprising results in Chapter 3, combined with inconsistent results found in other similar studies in the literature, another model may be more appropriate for assessing changes within the intramedullary space. Specifically, the model developed by Qin, et al., in which quadriceps stimulation has been shown to both increase intramedullary pressure and subsequently generate an anabolic response in the metaphyseal region, may be more suited to our purposes (21). This would allow us to assess intramedullary phenomena without the potential complication of damage to the growth plate, which may be responsible for some of the deleterious effects seen in our model in response to applied loads.

Though the limitations in the experimental system confounded our ability to fully explore our hypothesis in these experiments, the contribution from the results of our tibial

loading should not be underestimated. Though other groups have utilized this tibial loading system as a model for the anabolic actions of mechanical stimulus, the model as a whole is potentially not as well-characterized as the orthopaedic community assumes it to be. The understanding of the local mechanical effects due to this axial load would be greatly enhanced by the incorporation of finite element models to more accurately map the strains that develop throughout the length of the tibia as a result of these forces. Strain gauging only provides a snapshot of events at a small region that is easily accessible to the investigator. Clearly, however, there may be significant differences in the strain distributions at other regions of the bone. Computational models would also allow us to assess how sensitive changes in force distribution are to slight variations in tibial placement within the device.

In spite of these experimental limitations, we have demonstrated some critical findings. We demonstrated that MKs respond to controlled fluid shear forces in culture. We investigated two culture models of MK, the Meg-01 megakaryoblast cell line and K562 leukemic cells differentiated down an MK lineage by treatment with PMA. Both cell types demonstrate an upregulation of c-fos and, to a lesser extent, cox-2 in response to fluid shear. In addition, we observed that the extent to which MKs respond to fluid shear may depend on their maturation state. To more thoroughly investigate this observation, further studies could be conducted on the same cell line at various stages of MK development. Though we did observe differences between undifferentiated and differentiated K562 cells, this cell line is classified as a "pluripotent hematopoietic progenitor cell" line (137) and therefore might not be as directly applicable as a model of committed MK behavior. Ideally primary cells would also be incorporated into this

model as well to confirm effects seen in cell lines are comparable to those directly from marrow harvests. This was attempted several times for the purpose of this study, however the low yields obtained from primary MK harvests in conjunction with the high numbers of cells needed for fluid shear experiments prohibited this as a viable option.

We also confirmed that MKs, like osteocytes, respond to physical stimuli *in vivo* utilizing laser capture microdissection. This is the first study to our knowledge that has assessed the mechanoresponsiveness of these cells in a physiologic context, as well as the first study to utilize this technology to investigate mechanically-induced changes in gene expression in response to applied loads in bone. One area for future study would be to further discriminate between classes of MKs to determine if, in fact, cells at different stages in maturity demonstrate differences in response to mechanical loads. MKs in the current study were isolated based on their morphology, thus likely biasing the population toward more mature, easily identifiable cells. In addition, sections could be stained with an MK specific marker, such as CD41, CD61, or von Willebrand factor to help identify cells committed to the MK lineage but are not as easily distinguishable morphologically on tissue sections as large, polyploid mature MKs.

The results from our co-culture experiments suggest that mechanical stimulus may alter the influence that MKs can exert on osteoblasts. Specifically, MC3T3 appear to demonstrate reduced proliferation and enhanced mineralization, as evidenced by Alizarin Red S staining and calcium content, in the presence of mechanically-stimulated Meg-01 cells. Studies are ongoing in an effort to improve the reproducibility of our results, though design of a new device might be the best alternative to addressing this hypothesis while eliminating the inherent challenges faced with this system.

Though these findings are still preliminary, this could have dramatic implications for the orthopaedic community at various levels. Fundamentally, this work highlights the potential complexity of the mechanical regulation of bone. Hopefully we have set the stage for other investigators to consider the notion that mechanotransduction in bone may not solely be a single cell phenomenon, but perhaps a more complex series of events involving the communication between accessory cells, such as MKs, and their effector cells that can directly influence bone homeostasis. Furthermore, this may also broaden the perspective within the field of what cells may play a role in adaptation to mechanical stimulus. Though there is a significant amount of literature to support the dogma that osteocytes are the primary mechanoresponders in bone, there are other cells within bone that may be subject to mechanical cues and have some influence on bone adaptation as well.

Though clinical implications are far more distant, this work may also plant the seed for new directions in the development of therapeutics for treating bone metabolic diseases as well as enhanced techniques for bone regeneration and repair. The current state of the art in the development of orthopaedic therapeutics is to specifically target cells that are directly responsible for formation or resorption of bone. However, if we develop a deeper understanding of the mechanism by which accessory cells, such as MKs, act on these bone metabolic processes, our perspective of potential therapeutic targets may be broadened.

REFERENCES

1. Guldberg RE, Caldwell NJ, Guo XE, Goulet RW, Hollister SJ, Goldstein SA 1997 Mechanical stimulation of tissue repair in the hydraulic bone chamber. J Bone Miner Res **12**(8)**:**1295-302.

2. Torrance AG, Mosley JR, Suswillo RF, Lanyon LE 1994 Noninvasive loading of the rat ulna in vivo induces a strain-related modeling response uncomplicated by trauma or periostal pressure. Calcif Tissue Int **54**(3)**:**241-7.

3. Turner CH, Akhter MP, Raab DM, Kimmel DB, Recker RR 1991 A noninvasive, in vivo model for studying strain adaptive bone modeling. Bone **12**(2)**:**73-9.

4. Rubin CT, Lanyon LE 1985 Regulation of bone mass by mechanical strain magnitude. Calcif Tissue Int **37**(4)**:**411-7.

5. Gross TS, Srinivasan S, Liu CC, Clemens TL, Bain SD 2002 Noninvasive loading of the murine tibia: an in vivo model for the study of mechanotransduction. J Bone Miner Res **17**(3)**:**493-501.

6. Klein-Nulend J, van der Plas A, Semeins CM, Ajubi NE, Frangos JA, Nijweide PJ, Burger EH 1995 Sensitivity of osteocytes to biomechanical stress in vitro. FASEB J **9**(5)**:**441-5.

7. Kawata A, Mikuni-Takagaki Y 1998 Mechanotransduction in stretched osteocytes--temporal expression of immediate early and other genes. Biochem Biophys Res Commun **246**(2)**:**404-8.

8. Yellowley CE, Li Z, Zhou Z, Jacobs CR, Donahue HJ 2000 Functional gap junctions between osteocytic and osteoblastic cells. J Bone Miner Res **15**(2)**:**209-17.

9. Hoffler C 2003 In Pursuit of Accurate Structural and Mechanical Osteocyte Mechanotransduction Models Mechanical Engineering, vol. PhD. University of Michigan, Ann Arbor.

10. Tatsumi S, Ishii K, Amizuka N, Li M, Kobayashi T, Kohno K, Ito M, Takeshita S, Ikeda K 2007 Targeted ablation of osteocytes induces osteoporosis with defective mechanotransduction. Cell Metab **5**(6)**:**464-75.

11. Boutahar N, Guignandon A, Vico L, Lafage-Proust MH 2004 Mechanical strain on osteoblasts activates autophosphorylation of focal adhesion kinase and proline-rich tyrosine kinase 2 tyrosine sites involved in ERK activation. J Biol Chem **279**(29)**:**30588-99.

12. Saunders MM, You J, Zhou Z, Li Z, Yellowley CE, Kunze EL, Jacobs CR, Donahue HJ 2003 Fluid flow-induced prostaglandin E2 response of osteoblastic ROS 17/2.8 cells is gap junction-mediated and independent of cytosolic calcium. Bone **32**(4)**:**350-6.

13. Donahue TL, Haut TR, Yellowley CE, Donahue HJ, Jacobs CR 2003 Mechanosensitivity of bone cells to oscillating fluid flow induced shear stress may be modulated by chemotransport. J Biomech **36**(9)**:**1363-71.

14. Nagatomi J, Arulanandam BP, Metzger DW, Meunier A, Bizios R 2003 Cyclic pressure affects osteoblast functions pertinent to osteogenesis. Ann Biomed Eng **31**(8)**:**917-23.

15. Wilkes CH, Visscher MB 1975 Some physiological aspects of bone marrow pressure. J Bone Joint Surg Am **57**(1)**:**49-57.

16. Bryant JD 1983 The effect of impact on the marrow pressure of long bones in vitro. J Biomech **16**(8)**:**659-65.

17. Bryant JD 1988 On the mechanical function of marrow in long bones. Eng Med **17**(2)**:**55-8.

18. Liu ZJ, Herring SW 2000 Bone surface strains and internal bony pressures at the jaw joint of the miniature pig during masticatory muscle contraction. Arch Oral Biol **45**(2)**:**95-112.

19. Zhang P, Su M, Liu Y, Hsu A, Yokota H 2007 Knee loading dynamically alters intramedullary pressure in mouse femora. Bone **40**(2)**:**538-43.

20. Qin YX, Kaplan T, Saldanha A, Rubin C 2003 Fluid pressure gradients, arising from oscillations in intramedullary pressure, is correlated with the formation of bone and inhibition of intracortical porosity. J Biomech **36**(10)**:**1427-37.

21. Qin YX, Lam H 2009 Intramedullary pressure and matrix strain induced by oscillatory skeletal muscle stimulation and its potential in adaptation. J Biomech **42**(2)**:**140-5.

22. Kelly P, Bronk J 1990 Venous Pressure and Bone Formation. Microvascular Research **39:**364-375.

23. Bergula AP, Huang W, Frangos JA 1999 Femoral vein ligation increases bone mass in the hindlimb suspended rat. Bone **24**(3)**:**171-7.

24. Gross P, Heistad D, Marcus M 1979 Neurohumoral regulation of blood flow to bones and marrow. American Journal of Physiology **237**(4)**:**H440-8.

25. Tavassoli M, Yoffey J 1983 Bone Marrow: Structure and Function. Alan R. Liss, Inc.

26. Tondevold E, Bulow J 1983 Bone Blood Flow in Conscious Dogs at Rest and During Exercise. Acta Orthop. Scan. **54**(1)**:**53-57.

27. Dickerson DA, Sander EA, Nauman EA 2008 Modeling the mechanical consequences of vibratory loading in the vertebral body: microscale effects. Biomech Model Mechanobiol **7**(3)**:**191-202.

28. Moalli MR, Wang S, Caldwell NJ, Patil PV, Maynard CR 2001 Mechanical stimulation induces pp125(FAK) and pp60(src) activity in an in vivo model of trabecular bone formation. J Appl Physiol **91**(2)**:**912-8.

29. Pagedas C, Caldwell N, Goldstein S, McCreadie B The potential mechanosensory role of marrow stromal cells in regenerating trabecular bone Trans. Ortho. Res. Soc., vol. 49, New Orleans, LA, pp 396.

30. Keila S, Pitaru S, Grosskopf A, Weinreb M 1994 Bone marrow from mechanically unloaded rat bones expresses reduced osteogenic capacity in vitro. J Bone Miner Res **9**(3)**:**321-7.

31. Machwate M, Zerath E, Holy X, Hott M, Modrowski D, Malouvier A, Marie PJ 1993 Skeletal unloading in rat decreases proliferation of rat bone and marrow-derived osteoblastic cells. Am J Physiol **264**(5 Pt 1)**:**E790-9.

32. Li YJ, Batra NN, You L, Meier SC, Coe IA, Yellowley CE, Jacobs CR 2004 Oscillatory fluid flow affects human marrow stromal cell proliferation and differentiation. J Orthop Res **22**(6)**:**1283-9.

33. Riddle RC, Taylor AF, Genetos DC, Donahue HJ 2006 MAP kinase and calcium signaling mediate fluid flow-induced human mesenchymal stem cell proliferation. Am J Physiol Cell Physiol **290**(3)**:**C776-84.

34. Rubin J, Murphy T, Nanes MS, Fan X 2000 Mechanical strain inhibits expression of osteoclast differentiation factor by murine stromal cells. Am J Physiol Cell Physiol **278**(6)**:**C1126-32.

35. Zhang Q, Liang X, Zhu B, Dong Q, Xu L, Xia L, Hu J, Fu J, Liu M 2006 Effects of fluid shear stress on mRNA expression of carbonic anhydrase II in polarized rat osteoclasts. Cell Biol Int **30**(9)**:**714-20.

36. McAllister TN, Du T, Frangos JA 2000 Fluid shear stress stimulates prostaglandin and nitric oxide release in bone marrow-derived preosteoclast-like cells. Biochem Biophys Res Commun **270**(2)**:**643-8.

37. Anderson GJ, Roswit WT, Holtzman MJ, Hogg JC, Van Eeden SF 2001 Effect of mechanical deformation of neutrophils on their CD18/ICAM-1-dependent adhesion. J Appl Physiol **91**(3)**:**1084-90.

38. Ashida N, Takechi H, Kita T, Arai H 2003 Vortex-mediated mechanical stress induces integrin-dependent cell adhesion mediated by inositol 1,4,5-trisphosphate-sensitive Ca2+ release in THP-1 cells. J Biol Chem **278**(11)**:**9327-31.

39. Hentzen E, McDonough D, McIntire L, Smith CW, Goldsmith HL, Simon SI 2002 Hydrodynamic shear and tethering through E-selectin signals phosphorylation of p38 MAP kinase and adhesion of human neutrophils. Ann Biomed Eng **30**(8)**:**987-1001.

40. Gigant C, Latger-Cannard V, Bensoussan D, Fawzi S, Feugier P, Bordigoni P, Stoltz JF 2003 CD34+ cells homing: quantitative expression of adhesion molecules and adhesion of CD34+ cells to endothelial cells exposed to shear stress. Biorheology **40**(1-3)**:**189-95.

41. Taichman R, Reilly M, Verma R, Ehrenman K, Emerson S 2001 Hepatocyte growth factor is secreted by osteoblasts and cooperatively permits the survival of haematopoietic progenitors. Br J Haematol **112**(2)**:**438-48.

42. Taichman RS, Emerson SG 1994 Human osteoblasts support hematopoiesis through the production of granulocyte colony-stimulating factor. J Exp Med **179**(5)**:**1677-82.

43. Aubin JE 1999 Osteoprogenitor cell frequency in rat bone marrow stromal populations: role for heterotypic cell-cell interactions in osteoblast differentiation. J Cell Biochem **72**(3)**:**396-410.

44. Rickard DJ, Kazhdan I, Leboy PS 1995 Importance of 1,25-dihydroxyvitamin D3 and the nonadherent cells of marrow for osteoblast differentiation from rat marrow stromal cells. Bone **16**(6)**:**671-8.

45. Eipers PG, Kale S, Taichman RS, Pipia GG, Swords NA, Mann KG, Long MW 2000 Bone marrow accessory cells regulate human bone precursor cell development. Exp Hematol **28**(7)**:**815-25.

46. Thiele J, Fischer R 1991 Megakaryocytopoiesis in haematological disorders: diagnostic features of bone marrow biopsies. An overview. Virchows Arch A Pathol Anat Histopathol **418**(2)**:**87-97.

47. Kimura A, Katoh O, Hyodo H, Kuramoto A 1989 Transforming growth factor-beta regulates growth as well as collagen and fibronectin synthesis of human marrow fibroblasts. Br J Haematol **72**(4)**:**486-91.

48. Schmitz B, Thiele J, Kaufmann R, Witte O, Wickenhauser C, Kuhn-Regnier F, Fischer R 1995 Megakaryocytes and fibroblasts--interactions as determined in normal human bone marrow specimens. Leuk Res **19**(9)**:**629-37.

49. Schmitz B, Thiele J, Otto F, Farahmand P, Henze F, Frimpong S, Wickenhauser C, Fischer R 1998 Evidence for integrin receptor involvement in megakaryocyte-fibroblast interaction: a possible pathomechanism for the evolution of myelofibrosis. J Cell Physiol **176**(3)**:**445-55.

50. Avraham H, Scadden DT, Chi S, Broudy VC, Zsebo KM, Groopman JE 1992 Interaction of human bone marrow fibroblasts with megakaryocytes: role of the c-kit ligand. Blood **80**(7)**:**1679-84.

51. Chagraoui H, Sabri S, Capron C, Villeval JL, Vainchenker W, Wendling F 2003 Expression of osteoprotegerin mRNA and protein in murine megakaryocytes. Exp Hematol **31**(11)**:**1081-8.

52. Wakikawa T, Shioi A, Hino M, Inaba M, Nishizawa Y, Tatsumi N, Morii H, Otani S 1997 Thrombopoietin inhibits in vitro osteoclastogenesis from murine bone marrow cells. Endocrinology **138**(10)**:**4160-6.

53. Beeton CA, Bord S, Ireland D, Compston JE 2006 Osteoclast formation and bone resorption are inhibited by megakaryocytes. Bone **39**(5)**:**985-90.

54. Kacena MA, Nelson T, Clough ME, Lee SK, Lorenzo JA, Gundberg CM, Horowitz MC 2006 Megakaryocyte-mediated inhibition of osteoclast development. Bone **39**(5)**:**991-9.

55. Kacena MA, Shivdasani RA, Wilson K, Xi Y, Troiano N, Nazarian A, Gundberg CM, Bouxsein ML, Lorenzo JA, Horowitz MC 2004 Megakaryocyte-osteoblast interaction revealed in mice deficient in transcription factors GATA-1 and NF-E2. J Bone Miner Res **19**(4)**:**652-60.

56. Ciovacco WA, Goldberg CG, Taylor AF, Lemieux JM, Horowitz MC, Donahue HJ, Kacena MA 2009 The role of gap junctions in megakaryocyte-mediated osteoblast proliferation and differentiation. Bone **44**(1)**:**80-6.

57. Miao D, Murant S, Scutt N, Genever P, Scutt A 2004 Megakaryocyte-bone marrow stromal cell aggregates demonstrate increased colony formation and alkaline phosphatase expression in vitro. Tissue Eng **10**(5-6)**:**807-17.

58. Perry MJ, Samuels A, Bird D, Tobias JH 2000 Effects of high-dose estrogen on murine hematopoietic bone marrow precede those on osteogenesis. Am J Physiol Endocrinol Metab **279**(5)**:**E1159-65.

59. Bord S, Vedi S, Beavan SR, Horner A, Compston JE 2000 Megakaryocyte population in human bone marrow increases with estrogen treatment: a role in bone remodeling? Bone **27**(3)**:**397-401.

60. Harris SE, Bonewald LF, Harris MA, Sabatini M, Dallas S, Feng JQ, Ghosh-Choudhury N, Wozney J, Mundy GR 1994 Effects of transforming growth factor beta on bone nodule formation and expression of bone morphogenetic protein 2, osteocalcin, osteopontin, alkaline phosphatase, and type I collagen mRNA in long-term cultures of fetal rat calvarial osteoblasts. J Bone Miner Res **9**(6)**:**855-63.

61. Sipe JB, Zhang J, Waits C, Skikne B, Garimella R, Anderson HC 2004 Localization of bone morphogenetic proteins (BMPs)-2, -4, and -6 within megakaryocytes and platelets. Bone **35**(6)**:**1316-22.

62. Kelm RJ, Jr., Hair GA, Mann KG, Grant BW 1992 Characterization of human osteoblast and megakaryocyte-derived osteonectin (SPARC). Blood **80**(12)**:**3112-9.

63. Thiede MA, Smock SL, Petersen DN, Grasser WA, Thompson DD, Nishimoto SK 1994 Presence of messenger ribonucleic acid encoding osteocalcin, a marker of bone turnover, in bone marrow megakaryocytes and peripheral blood platelets. Endocrinology **135**(3)**:**929-37.

64. Aeschlimann D, Mosher D, Paulsson M 1996 Tissue transglutaminase and factor XIII in cartilage and bone remodeling. Semin Thromb Hemost **22**(5)**:**437-43.

65. Calvi LM, Adams GB, Weibrecht KW, Weber JM, Olson DP, Knight MC, Martin RP, Schipani E, Divieti P, Bringhurst FR, Milner LA, Kronenberg HM, Scadden DT 2003 Osteoblastic cells regulate the haematopoietic stem cell niche. Nature **425**(6960)**:**841-6.

66. Lichtman MA, Chamberlain JK, Simon W, Santillo PA 1978 Parasinusoidal location of megakaryocytes in marrow: a determinant of platelet release. Am J Hematol **4**(4)**:**303-12.

67. Ponomaryov T, Peled A, Petit I, Taichman RS, Habler L, Sandbank J, Arenzana-Seisdedos F, Magerus A, Caruz A, Fujii N, Nagler A, Lahav M, Szyper-Kravitz M, Zipori D, Lapidot T 2000 Induction of the chemokine stromal-derived factor-1 following DNA damage improves human stem cell function. J Clin Invest **106**(11)**:**1331-9.

68. Riviere C, Subra F, Cohen-Solal K, Cordette-Lagarde V, Letestu R, Auclair C, Vainchenker W, Louache F 1999 Phenotypic and functional evidence for the expression of CXCR4 receptor during megakaryocytopoiesis. Blood **93**(5)**:**1511-23.

69. Zweegman S, Veenhof MA, Huijgens PC, Schuurhuis GJ, Drager AM 2000 Regulation of megakaryocytopoiesis in an in vitro stroma model: preferential adhesion of megakaryocytic progenitors and subsequent inhibition of maturation. Exp Hematol **28**(4)**:**401-10.

70. Larson MK, Watson SP 2006 Regulation of proplatelet formation and platelet release by integrin alpha IIb beta3. Blood **108**(5)**:**1509-14.

71. Fox NE, Kaushansky K 2005 Engagement of integrin alpha4beta1 enhances thrombopoietin-induced megakaryopoiesis. Exp Hematol **33**(1)**:**94-9.

72. Nilsson SK, Debatis ME, Dooner MS, Madri JA, Quesenberry PJ, Becker PS 1998 Immunofluorescence characterization of key extracellular matrix proteins in murine bone marrow in situ. J Histochem Cytochem **46**(3)**:**371-7.

73. Sabri S, Jandrot-Perrus M, Bertoglio J, Farndale RW, Mas VM, Debili N, Vainchenker W 2004 Differential regulation of actin stress fiber assembly and proplatelet formation by alpha2beta1 integrin and GPVI in human megakaryocytes. Blood **104**(10)**:**3117-25.

74. Eldor A, Stromberg RR, Vlodavsky I, Hy-Am E, Koslow AR, Friedman LI, Levine RF 1991 The effect of flow on the interaction of isolated megakaryocytes with subendothelial extracellular matrix. Blood Cells **17**(3)**:**447-63; discussion 464-6.

75. de Bruyn K, Zwartkruis F, de Rooij J, Akkerman J, Bos J 2003 The Small GTPase Rap1 is Activated by Turbulence and Is Involved in Integrin alphaiibbeta3-mediated Cell Adhesion in Human Megakaryocytes. Journal of Biological Chemistry **278**(25)**:**22412-22417.

76. Junt T, Schulze H, Chen Z, Massberg S, Goerge T, Krueger A, Wagner DD, Graf T, Italiano JE, Jr., Shivdasani RA, von Andrian UH 2007 Dynamic visualization of thrombopoiesis within bone marrow. Science **317**(5845)**:**1767-70.

77. Dunois-Larde C, Capron C, Fichelson S, Bauer T, Cramer-Borde E, Baruch D 2009 Exposure of human megakaryocytes to high shear rates accelerates platelet production. Blood **114**(9)**:**1875-83.

78. Gilbert JA, Weinhold PS, Banes AJ, Link GW, Jones GL 1994 Strain profiles for circular cell culture plates containing flexible surfaces employed to mechanically deform cells in vitro. J Biomech **27**(9)**:**1169-77.

79. Klein-Nulend J, Roelofsen J, Semeins CM, Bronckers AL, Burger EH 1997 Mechanical stimulation of osteopontin mRNA expression and synthesis in bone cell cultures. J Cell Physiol **170**(2)**:**174-81.

80. Jacobs CR, Yellowley CE, Davis BR, Zhou Z, Cimbala JM, Donahue HJ 1998 Differential effect of steady versus oscillating flow on bone cells. J Biomech **31**(11)**:**969-76.

81. Peake MA, Cooling LM, Magnay JL, Thomas PB, El Haj AJ 2000 Selected contribution: regulatory pathways involved in mechanical induction of c-fos gene expression in bone cells. J Appl Physiol **89**(6)**:**2498-507.

82. Pavalko FM, Chen NX, Turner CH, Burr DB, Atkinson S, Hsieh YF, Qiu J, Duncan RL 1998 Fluid shear-induced mechanical signaling in MC3T3-E1 osteoblasts requires cytoskeleton-integrin interactions. Am J Physiol **275**(6 Pt 1)**:**C1591-601.

83. Granet C, Vico AG, Alexandre C, Lafage-Proust MH 2002 MAP and src kinases control the induction of AP-1 members in response to changes in mechanical environment in osteoblastic cells. Cell Signal **14**(8)**:**679-88.

84. Lean JM, Mackay AG, Chow JW, Chambers TJ 1996 Osteocytic expression of mRNA for c-fos and IGF-I: an immediate early gene response to an osteogenic stimulus. Am J Physiol **270**(6 Pt 1)**:**E937-45.

85. Cheng B, Kato Y, Zhao S, Luo J, Sprague E, Bonewald LF, Jiang JX 2001 PGE(2) is essential for gap junction-mediated intercellular communication between osteocyte-like MLO-Y4 cells in response to mechanical strain. Endocrinology **142**(8)**:**3464-73.

86. Wadhwa S, Godwin SL, Peterson DR, Epstein MA, Raisz LG, Pilbeam CC 2002 Fluid flow induction of cyclo-oxygenase 2 gene expression in osteoblasts is dependent on an extracellular signal-regulated kinase signaling pathway. J Bone Miner Res **17**(2)**:**266-74.

87. Lee KC, Maxwell A, Lanyon LE 2002 Validation of a technique for studying functional adaptation of the mouse ulna in response to mechanical loading. Bone **31**(3)**:**407-12.

88. Hsieh YF, Turner CH 2001 Effects of loading frequency on mechanically induced bone formation. J Bone Miner Res **16**(5)**:**918-24.

89. Fritton JC, Myers ER, Wright TM, van der Meulen MC 2005 Loading induces site-specific increases in mineral content assessed by microcomputed tomography of the mouse tibia. Bone **36**(6)**:**1030-8.

90. Lynch M, Main R, Walsh D, Wright T, van der Meulen M 2008 Cancellous bone adaptation to non-invasive mechanical loading in the murine tibia Trans. Ortho. Res. Soc., vol. 33, San Francisco, CA, pp 933.

91. Main R, Lynch M, van der Meulen M 2008 Tibial strains decrease following in vivo loading in female not male mice Trans. Ortho. Res. Soc., vol. 33, San Francisco, CA, pp 909.

92. De Souza RL, Matsuura M, Eckstein F, Rawlinson SC, Lanyon LE, Pitsillides AA 2005 Non-invasive axial loading of mouse tibiae increases cortical bone formation and modifies trabecular organization: a new model to study cortical and cancellous compartments in a single loaded element. Bone **37**(6)**:**810-8.

93. Ominsky M 2004 Effects of hydrostatic pressure, biaxial strain, and fluid shear on osteoblastic cells: mechanotransduction via NF-κB, MAP kinase, and AP-1 pathways Biomedical Engineering, vol. PhD. University of Michigan, Ann Arbor.

94. Alford AI, Yellowley CE, Jacobs CR, Donahue HJ 2003 Increases in cytosolic calcium, but not fluid flow, affect aggrecan mRNA levels in articular chondrocytes. J Cell Biochem **90**(5)**:**938-44.

95. Maclean JJ, Lee CR, Alini M, Iatridis JC 2004 Anabolic and catabolic mRNA levels of the intervertebral disc vary with the magnitude and frequency of in vivo dynamic compression. J Orthop Res **22**(6)**:**1193-200.

96. Livak KJ, Schmittgen TD 2001 Analysis of relative gene expression data using real-time quantitative PCR and the 2(-Delta Delta C(T)) Method. Methods **25**(4)**:**402-8.

97. Fritton SP, McLeod KJ, Rubin CT 2000 Quantifying the strain history of bone: spatial uniformity and self-similarity of low-magnitude strains. J Biomech **33**(3)**:**317-25.

98. Inaoka T, Lean JM, Bessho T, Chow JW, Mackay A, Kokubo T, Chambers TJ 1995 Sequential analysis of gene expression after an osteogenic stimulus: c-fos expression is induced in osteocytes. Biochem Biophys Res Commun **217**(1)**:**264-70.

99. Shao YY, Wang L, Hicks DG, Ballock RT 2006 Analysis of gene expression in mineralized skeletal tissues by laser capture microdissection and RT-PCR. Lab Invest **86**(10)**:**1089-95.

100. Xing W, Baylink D, Kesavan C, Hu Y, Kapoor S, Chadwick RB, Mohan S 2005 Global gene expression analysis in the bones reveals involvement of several novel genes and pathways in mediating an anabolic response of mechanical loading in mice. J Cell Biochem **96**(5)**:**1049-60.

101. Mardikar SH, Niranjan K 2000 Observations on the shear damage to different animal cells in a concentric cylinder viscometer. Biotechnol Bioeng **68**(6)**:**697-704.

102. Lee DY, Yeh CR, Chang SF, Lee PL, Chien S, Cheng CK, Chiu JJ 2008 Integrin-mediated expression of bone formation-related genes in osteoblast-like cells in response to fluid shear stress: roles of extracellular matrix, Shc, and mitogen-activated protein kinase. J Bone Miner Res **23**(7)**:**1140-9.

103. Benoyahu D, Akavia UD, Socher R, Shur I 2005 Gene expression in skeletal tissues: application of laser capture microdissection. J Microsc **220**(Pt 1)**:**1-8.

104. Jacquet R, Hillyer J, Landis WJ 2005 Analysis of connective tissues by laser capture microdissection and reverse transcriptase-polymerase chain reaction. Anal Biochem **337**(1)**:**22-34.

105. Kondapalli J, Flozak AS, Albuquerque ML 2004 Laminar shear stress differentially modulates gene expression of p120 catenin, Kaiso transcription factor, and vascular endothelial cadherin in human coronary artery endothelial cells. J Biol Chem **279**(12)**:**11417-24.

106. Milkiewicz M, Haas TL 2005 Effect of mechanical stretch on HIF-1{alpha} and MMP-2 expression in capillaries isolated from overloaded skeletal muscles: laser capture microdissection study. Am J Physiol Heart Circ Physiol **289**(3)**:**H1315-20.

107. Shivdasani RA, Fujiwara Y, McDevitt MA, Orkin SH 1997 A lineage-selective knockout establishes the critical role of transcription factor GATA-1 in megakaryocyte growth and platelet development. EMBO J **16**(13)**:**3965-73.

108. McDevitt MA, Shivdasani RA, Fujiwara Y, Yang H, Orkin SH 1997 A "knockdown" mutation created by cis-element gene targeting reveals the dependence of erythroid cell maturation on the level of transcription factor GATA-1. Proc Natl Acad Sci U S A **94**(13)**:**6781-5.

109. Vannucchi AM, Bianchi L, Cellai C, Paoletti F, Rana RA, Lorenzini R, Migliaccio G, Migliaccio AR 2002 Development of myelofibrosis in mice genetically impaired for GATA-1 expression (GATA-1(low) mice). Blood **100**(4)**:**1123-32.

110. Vyas P, Ault K, Jackson CW, Orkin SH, Shivdasani RA 1999 Consequences of GATA-1 deficiency in megakaryocytes and platelets. Blood **93**(9)**:**2867-75.

111. Lok S, Kaushansky K, Holly RD, Kuijper JL, Lofton-Day CE, Oort PJ, Grant FJ, Heipel MD, Burkhead SK, Kramer JM, et al.. 1994 Cloning and expression of murine thrombopoietin cDNA and stimulation of platelet production in vivo. Nature **369**(6481)**:**565-8.

112. Kaushansky K, Lok S, Holly RD, Broudy VC, Lin N, Bailey MC, Forstrom JW, Buddle MM, Oort PJ, Hagen FS, et al.. 1994 Promotion of megakaryocyte progenitor expansion and differentiation by the c-Mpl ligand thrombopoietin. Nature **369**(6481)**:**568-71.

113. Kaushansky K 1997 Thrombopoietin the primary regulator of platelet production. Trends Endocrinol Metab **8**(2)**:**45-50.

114. Kuter DJ, Beeler DL, Rosenberg RD 1994 The purification of megapoietin: a physiological regulator of megakaryocyte growth and platelet production. Proc Natl Acad Sci U S A **91**(23)**:**11104-8.

115. Rojnuckarin P, Drachman JG, Kaushansky K 1999 Thrombopoietin-induced activation of the mitogen-activated protein kinase (MAPK) pathway in normal megakaryocytes: role in endomitosis. Blood **94**(4)**:**1273-82.

116. Drachman JG, Sabath DF, Fox NE, Kaushansky K 1997 Thrombopoietin signal transduction in purified murine megakaryocytes. Blood **89**(2)**:**483-92.

117. Yan XQ, Lacey D, Fletcher F, Hartley C, McElroy P, Sun Y, Xia M, Mu S, Saris C, Hill D, Hawley RG, McNiece IK 1995 Chronic exposure to retroviral vector encoded MGDF (mpl-ligand) induces lineage-specific growth and differentiation of megakaryocytes in mice. Blood **86**(11)**:**4025-33.

118. Villeval JL, Cohen-Solal K, Tulliez M, Giraudier S, Guichard J, Burstein SA, Cramer EM, Vainchenker W, Wendling F 1997 High thrombopoietin production by hematopoietic cells induces a fatal myeloproliferative syndrome in mice. Blood **90**(11)**:**4369-83.

119. Kakumitsu H, Kamezaki K, Shimoda K, Karube K, Haro T, Numata A, Shide K, Matsuda T, Oshima K, Harada M 2005 Transgenic mice overexpressing murine thrombopoietin develop myelofibrosis and osteosclerosis. Leuk Res **29**(7)**:**761-9.

120. Volkman SK, Galecki AT, Burke DT, Miller RA, Goldstein SA 2004 Quantitative trait loci that modulate femoral mechanical properties in a genetically heterogeneous mouse population. J Bone Miner Res **19**(9)**:**1497-505.

121. Parfitt AM, Drezner MK, Glorieux FH, Kanis JA, Malluche H, Meunier PJ, Ott SM, Recker RR 1987 Bone histomorphometry: standardization of nomenclature, symbols, and units. Report of the ASBMR Histomorphometry Nomenclature Committee. J Bone Miner Res **2**(6)**:**595-610.

122. Ohashi N, Robling AG, Burr DB, Turner CH 2002 The effects of dynamic axial loading on the rat growth plate. J Bone Miner Res **17**(2)**:**284-92.

123. Main RP, Lynch ME, van der Meulen MC 2008 Tibial strains decrease following in vivo loading in female not male mice Trans. Ortho. Res., vol. 33, San Francisco, CA, pp 909.

124. Hokom MM, Lacey D, Kinstler OB, Choi E, Kaufman S, Faust J, Rowan C, Dwyer E, Nichol JL, Grasel T, Wilson J, Steinbrink R, Hecht R, Winters D, Boone T, Hunt P 1995 Pegylated megakaryocyte growth and development factor

abrogates the lethal thrombocytopenia associated with carboplatin and irradiation in mice. Blood **86**(12)**:**4486-92.

125. Bord S, Frith E, Ireland DC, Scott MA, Craig JI, Compston JE 2005 Megakaryocytes modulate osteoblast synthesis of type-l collagen, osteoprotegerin, and RANKL. Bone **36**(5)**:**812-9.

126. Parodi B, Aresu O, Bini D, Lorenzini R, Schena F, Visconti P, Cesaro M, Ferrera D, Andreotti V, Ruzzon T 2002 Species identification and confirmation of human and animal cell lines: a PCR-based method. Biotechniques **32**(2)**:**432-4, 436, 438-40.

127. Alford AI, Terkhorn SP, Reddy AB, Hankenson KD 2009 Thrombospondin-2 regulates matrix mineralization in MC3T3-E1 pre-osteoblasts. Bone.

128. Ducy P, Zhang R, Geoffroy V, Ridall AL, Karsenty G 1997 Osf2/Cbfa1: a transcriptional activator of osteoblast differentiation. Cell **89**(5)**:**747-54.

129. Nakashima K, Zhou X, Kunkel G, Zhang Z, Deng JM, Behringer RR, de Crombrugghe B 2002 The novel zinc finger-containing transcription factor osterix is required for osteoblast differentiation and bone formation. Cell **108**(1)**:**17-29.

130. Hauschka PV, Reid ML 1978 Timed appearance of a calcium-binding protein containing gamma-carboxyglutamic acid in developing chick bone. Dev Biol **65**(2)**:**426-34.

131. Chen J, Shapiro HS, Sodek J 1992 Development expression of bone sialoprotein mRNA in rat mineralized connective tissues. J Bone Miner Res **7**(8)**:**987-97.

132. Canalis E, McCarthy TL, Centrella M 1989 Effects of platelet-derived growth factor on bone formation in vitro. J Cell Physiol **140**(3)**:**530-7.

133. Globus RK, Patterson-Buckendahl P, Gospodarowicz D 1988 Regulation of bovine bone cell proliferation by fibroblast growth factor and transforming growth factor beta. Endocrinology **123**(1)**:**98-105.

134. Kasperk CH, Wergedal JE, Mohan S, Long DL, Lau KH, Baylink DJ 1990 Interactions of growth factors present in bone matrix with bone cells: effects on DNA synthesis and alkaline phosphatase. Growth Factors **3**(2)**:**147-58.

135. Chagraoui H, Komura E, Tulliez M, Giraudier S, Vainchenker W, Wendling F 2002 Prominent role of TGF-beta 1 in thrombopoietin-induced myelofibrosis in mice. Blood **100**(10)**:**3495-503.

136. Taylor AF, Saunders MM, Shingle DL, Cimbala JM, Zhou Z, Donahue HJ 2007 Mechanically stimulated osteocytes regulate osteoblastic activity via gap junctions. Am J Physiol Cell Physiol **292**(1)**:**C545-52.

137. Butler TM, Ziemiecki A, Friis RR 1990 Megakaryocytic differentiation of K562 cells is associated with changes in the cytoskeletal organization and the pattern of chromatographically distinct forms of phosphotyrosyl-specific protein phosphatases. Cancer Res **50**(19)**:**6323-9.